- 26. Heffner, B.L. 1992. Automated measurement of polarization mode dispersion using Jones matrix eigenanalysis. *IEEE Photonics Technology Letters* 4:1066.
- 27. Jones, R.C. 1947. A new calculus for the treatment of optical systems. VI: Experimental determination of the matrix. *Journal of the Optical Society of America*, 37:110-112.
- 28. TIA/EIA FOTP-122, 1996. Polarization-mode dispersion measurement for singlemode optical fibers by Jones matrix eigenanalysis, Washington, DC: Telecommunications Industry Association.
- 29. Heffner, B.L. 1993. Attosecond-resolution measurement of polarization mode dispersion in short sections of optical fiber. *Optics Letters*, 18 (24):2102–2104.

#### The Interferometric PMD Measurement Method

- Mochizuki, K., Y. Namihira, and H. Wakabayashi. 1981. Polarization mode dispersion measurements in long singlemode fibers. *Electronics Letters*, 17:153-154.
- 31. Gisin, N., J-P Von der Weid, and J-P Pellaux. 1991. Polarization mode dispersion of short and long singlemode fibers. *Journal of Lightwave Technology* LT-9:821-827 and references therein.
- 32. Heffner, B.L. 1985. Analysis of interferometric PMD measurements: Relation to principal states model for highly mode-coupled fibers. *Technical Digest—Optical Fibre Measurement Conference*. Liege, Belgium, September.
- Williams, P.A. and P.R. Hernday. 1995. Anomalous relation between time and frequency domain PMD measurements. Technical Digest—Optical Fibre Measurement Conference. Liege, Belgium, September.
- 34. TIA/EIA FOTP-124. Polarization-mode dispersion measurement for singlemode optical fibers by the interferometric method, Telecommunications Industry Association.
- Williams, P.A. 1996. Accuracy issues in comparisons of time- and frequency-domain polarization mode dispersion measurements. *Technical Digest—Symposium on Optical Fiber measure*ments. NIST Special Publication 905: 125-129.
- 36. Namihira, Y., K. Nakajima, and T. Kawazawa. 1993. Electronics Letters, 29:1649.
- 37. Gisin, N., R. Passy, and J.P. Von der Weid. 1994. *IEEE Photonics Technology Letters* 6: 730-732.

# CHAPTER

13

# Characterization of Erbium-Doped Fiber Amplifiers

Douglas M. Baney

#### INTRODUCTION

This chapter presents several commonly used methods for optical amplifier gain and noise figure measurement. The methods are often modified in various ways depending on the instrumentation selected for the testing as well as the specifics of the measurement results obtained. With this in mind, the principle goal of this chapter is to convey enough information about the basic measurement methods so that the reader can make informed decisions on measurement procedures, experimental apparatus, and possible further improvements to the measurement techniques. As characterization methods are optimized, often the physics of the optical amplifier influences the measurement technique. For this reason, a working knowledge of the amplifier is useful to understand the basis for the measurement techniques.

Some of the amplifier properties that affect the communications systems are the optical gain, gain flatness, noise, temporal response, and polarization dependence. <sup>1-5</sup> These characteristics have a bearing on the methods employed for testing optical amplifiers. This chapter will be focused primarily on the erbium-doped fiber amplifier (EDFA), which has had a significant impact on lightwave telecommunications and the field of optics in general. A discussion of the various noise processes caused by optical amplification and interference effects<sup>6,7</sup> is also presented. This will be useful in understanding the origin of the noise figure of an optical amplifier.

The organization of the chapter is as follows. A discussion of basic fiber amplifier characteristics is presented in Section 13.1. Section 13.2 discusses the concept of optical gain. The noise processes that contribute to signal-to-noise ratio (SNR) degradation are introduced in Section 13.3. Noise figure definition is discussed in Section 13.4. Section

13.5 deals with measurement of gain and noise figure using both optical and electrical methods. Section 13.6 discusses other types of optical amplifiers which may impact future telecommunications systems. Section 13.7 highlights the most significant sources of measurement uncertainty in gain and noise figure measurements. Section 13.8 provides useful constants for noise figure calculations, and Section 13.9 provides a brief summary of this chapter.

#### 13.1 FIBER AMPLIFIERS

The history of the rare-earth doped fiber amplifier dates back to the early 1960s with the demonstration of optical gain in neodymium-doped glass fiber at a wavelength of 1.06  $\mu$ m.<sup>8,9</sup> Years later, the convergence of singlemode glass fiber drawing and semiconductor laser technologies set the stage for the 1.55  $\mu$ m fiber optic amplifier. The optical propagation loss in silica glass fiber is lowest at 1.55  $\mu$ m (~0.2 dB/km) making this wavelength region important for long-haul telecommunications. The demonstration, in 1986, of an erbium-doped silica fiber laser, and an EDFA in 1987<sup>10,11</sup> showed the great potential of fiber optic amplifiers. Soon after these initial results, telecommunications laboratories around the world began research and development efforts aimed at applying the EDFA towards optical communications systems.

The EDFA has a number of characteristics which make it an excellent amplifier for optical communications including: polarization-independent gain, low interchannel crosstalk, wide optical bandwidth and low-noise generation. In brief, the EDFA offers a nearly ideal way to compensate for signal propagation losses along high-speed singlemode fiberoptic links.

# 13.1.1 Basic Concepts

The basic *black-box* characteristics of an optical amplifier are shown in Figure 13.1. The incident optical signal is amplified after traversing the optical amplifier. In addition to providing for optical gain, the amplifier also adds other optical powers to the input and output optical fiber. These added optical powers include:

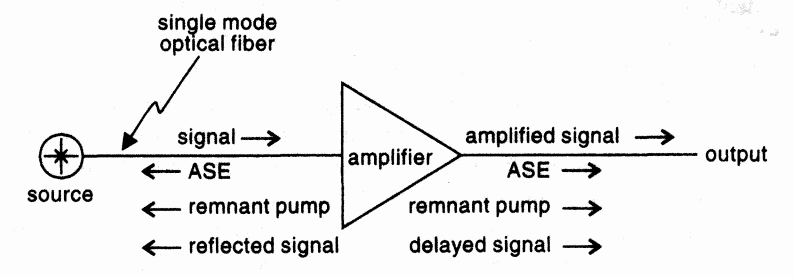


**Figure 13.1** In addition to signal amplification in the forward direction, the amplifier adds other powers to the optical network.

- Amplified spontaneous emission (ASE);
- Remnant power from the pump laser;

Fiber Amplifiers

Sec. 13.1

· Time-delayed scaled-replicas of the signal power.

The degree to which these added powers are significant depends on the design of the EDFA.

The essential components of the EDFA are shown in Figure 13.2. These components are the laser pump, the wavelength division multiplexer (WDM), the optical isolators, and the erbium-doped fiber. With these basic components, many different amplifier topologies are possible. <sup>12</sup> To obtain gain, optical energy must be provided to the erbiumdoped fiber. The energy source is called the pump. It delivers optical power at a wavelength of 980 nm or 1480 nm. The pump power is typically in the range of ~10 mW to ~400 mW. The WDM serves to efficiently couple signal and pump light into, or away from, the rare-earth doped fiber. Isolators reduce any light reflected from the system back to the amplifier to an acceptable level. Without an isolator, optical reflections may degrade the amplifier gain performance and increase noise generation. In Figure 13.2, the pump light is traveling along the fiber in a direction opposite that of the signal. This type of pumping is referred to as counter-directionally pumped, or counter-propagating, or simply counter-pumped. Codirectionally or copropagating-pumped amplifiers have the laser pump on the input end of the amplifying fiber. Sometimes multistage amplifiers are used with an isolator separating two erbium-doped fiber (EDF) gain sections. This design allows for improved amplifier noise and output power performance. Fiber Bragg gratings<sup>13</sup> are also used for flattening the EDFA gain variation with wavelength. This improves the amplifier performance in WDM applications as well as reducing optical noise.

The erbium ions are located in the central core region of the EDF as shown in Figure  $13.3^{14}$  The central core region (diameter ~5  $\mu$ m) of the EDF is where the pump and signal wave intensities are the highest. Placement of the erbium ions in this region provides maximum overlap of pump and signal energy to the ions, resulting in better amplification. A lower index glass cladding layer surrounds the core region to complete the waveguide structure and provides for increased mechanical strength. A protective coating is added to the fiber bringing the total diameter to 250  $\mu$ m. This coating, with its increased refractive index with respect to the cladding also serves to remove any nondesired light (higher order spatial modes) propagating within the cladding. Apart from the erbium dopant, this fiber construction is the same as standard singlemode telecommunications

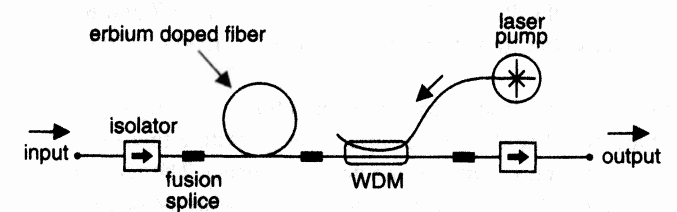


**Figure 13.2** An EDFA design showing the essential components. WDM: wavelength division multiplexier.

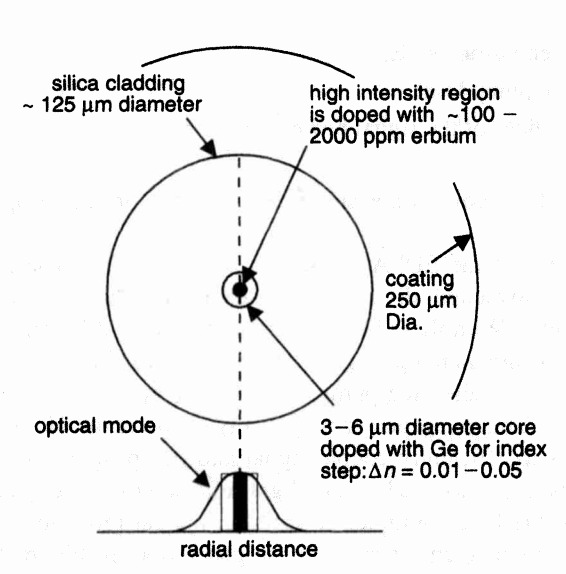


**Figure 13.3** Erbium-doped fiber core geometry.

fiber. The important characteristics for the EDF are its loss/gain per unit length at the pump and signal wavelengths. This information is often given in terms of emission and absorption cross-sections, and the confinement factors for the signal and pump light.

Energy Levels. The trivalent erbium atoms (Er<sup>3+</sup>) are the active elements in the amplifier responsible for optical gain. The relevant optical transitions are shown in Figure 13.4.15 The approximate wavelengths of the transitions are indicated with respect to the ground state. The designations on the right side are the commonly used quantum numbers assigned to each transition. These numbers are of the form  $^{2S+1}L_i$  where S is the spin quantum number, L is the orbital angular momentum, and J is the total (L + S) angular momentum. L is equal to one of: 0, 1, 2, 3, 4, 5, 6 ... which is designated by the letters S, P, D, F, G, H, I. This LSJ scheme is used in the literature to indicate the ion energy levels. 16,17 The "local crystalline" fields perturb the ion energy structure resulting in splitting of each LSJ energy level into multiple levels. This splitting is referred to as Stark splitting (Stark effect). As a result of randomness in the glass molecular structure, each ion experiences a different field strength and orientation, resulting in different Starksplitting. This splitting is responsible for the large gain bandwidth of rare-earth doped amplifiers. Within the LSJ description for the ion energy structure, the number of Stark-split lines is (2J + 1)/2 for each level. Thus the  ${}^4I_{13/2}$  and  ${}^4I_{15/2}$  levels would have 7 and 8 Stark lines respectively, resulting in 56 possible transitions between them spread out across the 1.55 µm band.

In Figure 13.4, absorption of pump laser photons excites the ion to higher energy states as shown by the upward arrows. The ion can dissipate energy with either the radiation of a photon, or by converting the energy into lattice phonons (heat). The tendency to radiate a photon when transitioning to a lower energy level increases with the energy gap.

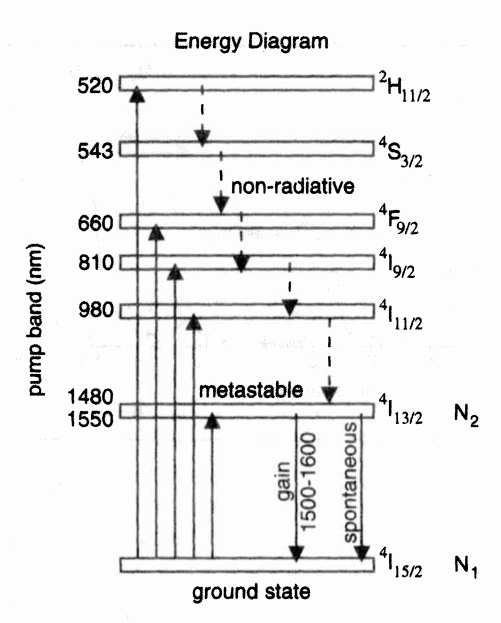


**Figure 13.4** Partial energy diagram for the trivalent erbium ion.

Fortunately the  $^4I_{13/2}$  –  $^4I_{15/2}$  transition is predominantly radiative in silica-based glasses resulting in excellent amplification characteristics in the 1.5  $\mu$ m to 1.6  $\mu$ m wavelength region.

The different transitions between the various energy levels result in detailed absorption and fluorescence spectrums from visible wavelengths to the infrared as seen in Figure 13.5. <sup>18,19</sup> The precise shape of the absorption characteristic and the magnitude of the fluorescence depends on the codopants added to the glass structure which modifies the ion energy structure. The choice of glass hosts with low phonon (vibration) energies, such as ZBLAN fluoride glass, will allow rare-earth ions to have strong fluorescence (light emission) between energy levels which normally undergo non-radiative decay in a silica glass host. In Figure 13.5a, a strong fluorescence in the 1.55  $\mu$ m region is evident for erbium ions in silica glass.

The absorption characteristic, shown in Figure 13.5b is also useful to investigate potential wavelengths for pumping the erbium ion. From the figure, the wavelengths of 1480 nm, 980 nm, 800 nm, 670 nm, and 521 nm should permit excitation of the erbium ion. All of these wavelengths have been successfully used to pump EDFAs. <sup>20,21</sup> The addition of other codopants such as ytterbium allows for pumping at other wavelengths.

The 1480 nm pump wavelength is used in EDFAs for a number of reasons including: (1) the availability of high pump power from semiconductor laser diodes operating at this wavelength; (2) good power efficiency since there is a small energy difference between 1480 nm and 1550 nm; (3) lower attenuation in optical fiber for remotely pumped EDFAs; (4) the broad absorption spectrum places less stringent demands on pump laser wavelength accuracy.

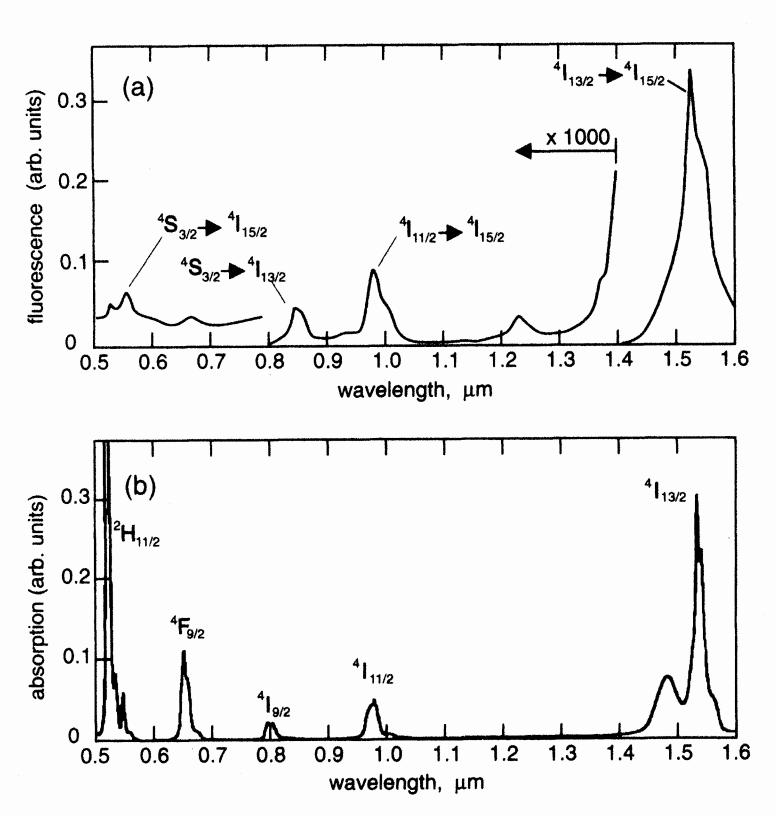


**Figure 13.5** (a) Fluorescence intensity and (b) absorption characteristic for two different erbium doped silica fibers. [With permission after ref. [18], [19] ©1988 IEEE, ©1991 IEEE.]

The 980 nm pump band offers the best EDFA noise performance but also requires tighter pump wavelength accuracy to align to the narrow absorption band about 976 nm. The advent of the fiber Bragg-grating (FBG) has alleviated this problem by providing wavelength selective feedback to the pump laser to insure operation at the proper wavelength. FBGs are constructed by radiating a Ge-doped silica fiber core laterally with UV light to create periodic refractive index perturbations along a short length (~1 cm) of fiber. This forms a wavelength-selectable narrow band (0.1 nm ~ 10 nm) reflective grating. A small reflection between approximately 1 to 10% provides feedback to lock the pump wavelength to the peak of the erbium absorption characteristic.

**Two-, Three-, and Four-Level Systems.** Optical amplifiers are classified as two-, three-, or four-level laser systems. An EDFA pumped into the  ${}^4I_{13/2}$  band as shown in Figure 13.4 ( $\lambda_p = 1480$  nm) is often approximated as a two-level system, since the pump and signal transitions are between the same energy bands. Pumping at 980 nm constitutes a

three-level system where the ion energy quickly decays ( $\sim$ 2  $\mu$ s) nonradiatively from the  $^4I_{11/2}$  level to the long-lived  $^4I_{13/2}$  metastable state. Amplifiers based on two- or three-level systems must be designed properly to limit reabsorption of the signal due to the presence of ground-state absorption at the signal wavelength. A four-level system is an extension of the three-level where there is an additional energy level below the lower level of the gain transition. Four-level systems do not have the ground-state signal reabsorption which can degrade the performance of amplifiers based on three-level systems.

Stimulated Emission, Spontaneous Emission. When the erbium ion (Er³+) is excited from the ground state through absorption of pump light, it will decay nonradiatively from the higher lying energy levels until it reaches the metastable state (⁴I₁₃/₂ state). The incident signal light (see Figure 13.2) arrives at the excited erbium atoms distributed along the optical fiber core. Stimulated emission occurs creating additional photons with the same optical phase and direction as the incident signal, thus amplification is achieved. Excited ions that don't interact with the incident light spontaneously decay to the ground state with a time constant of approximately 10 ms. The captured spontaneous emission (SE) has a random phase and direction. Typically less than 1% of the SE is captured by the optical fiber mode and becomes a source of optical noise. This noise gets amplified resulting in amplified spontaneous emission (ASE). Once in the ground state, absorption of a pump photon activates the erbium ion again and the process repeats itself. The presence of ASE causes degradation of the SNR of signals passing through the amplifier. Proper design of the amplifier will minimize the SNR degradation.

Table 13.1 gives a quick overview of the capabilities of EDFAs in terms of ranges of values for key performance characteristics.

#### 13.2 **GAIN**

Gain is the most fundamental parameter of an optical amplifier. In addition to optical gain, the amplifier produces ASE. The optical amplifier gain, G, is defined as

$$G = (P_{\text{out}} - P_{ASE})/P_s \tag{13.1}$$

**Table 13.1** EDFA Characteristics

Specification	Value	Units
gain	0 - ~ 50	dB
power output	1 -> 4000	mW
noise figure	3.5 - 12	dB
wavelength range	1520 ~ 1570	nm

Gain

where  $P_s$  and  $P_{\text{out}}$  are the amplifier input and output signal powers and  $P_{ASE}$  is the noise power generated by the amplifier which lies within the optical bandwidth of the measurement.

Predicting the gain is complicated by the distributed bidirectional nature of the amplifier, this often requires a numerical solution. An understanding of the net amplifier gain, G, can be derived from an analysis of the gain from individual "slices" along the fiber. A simplified analysis is presented here. Once the concepts are understood, the equations can be readily generalized to create a more realistic amplifier model. <sup>17,22</sup> An ASE-free two-level approximation is assumed. An EDFA is actually a concatenation of many amplifiers of incremental length  $\Delta z$  as illustrated in Figure 13.6. The net gain, G, is composed of the contributions of all the gain elements, g(z) along the amplifier fiber:

$$G = \lim_{\Delta Z \to 0} \left\{ e^{g(z_1)\Delta z} \times e^{g(z_2)\Delta z} \times \dots e^{g(z_n = L)\Delta z} \right\} = \exp\left(\int_0^L g(z) \, dz\right)$$
(13.2)

The incremental signal gain, g(z) for a photon propagating down the fiber is dependent on the metastable state population density,  $N_2$ , (see Figure 13.4), the ground-state population,  $N_1$ , the stimulated emission cross-section,  $\sigma_e$ , the absorption cross-section,  $\sigma_a$ , and the confinement (overlap) factor,  $\Gamma_s$ , between the signal field and the erbium-ion population.  $\Gamma_s$  can vary from zero to unity. A typical value is 0.3. The emission and absorption cross-sections represent the strength of the transition in other words, the ability to produce gain or absorption respectively. The gain coefficient is the difference between the upper and lower ion populations with a weighting taking into account their transition strengths:

$$g(z) = \Gamma_s[\sigma_{e,s} N_2(z) - \sigma_{a,s} N_1(z)]$$
 (13.3)

In the discussion, subscripts s and p refer to signal and pump respectively. Similarly, the pump loss in a slice of fiber is given as

$$\alpha_{p}(z) = \Gamma_{p}[\sigma_{e,p} N_{2}(z) - \sigma_{a,p} N_{1}(z)]$$
 (13.4)

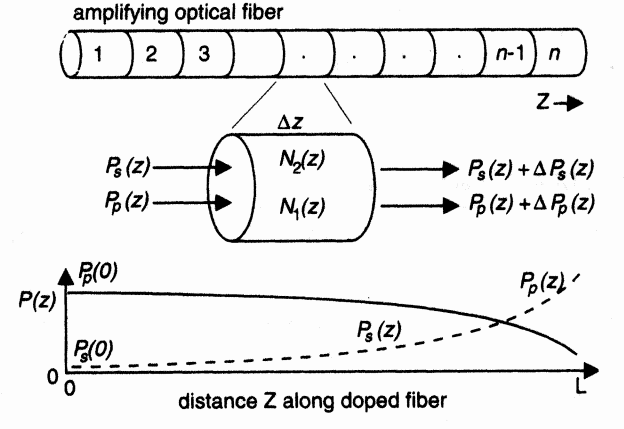


Figure 13.6 Fiber amplifier represented as a series of individual gain slices causing signal and pump power gain and absorption along the active fiber.

To achieve gain in a slice of doped fiber, the relationship  $\sigma_{e,s}N_2 > \sigma_{a,s}N_1$  must be satisfied within the slice. The cross-sections can be determined experimentally from measurements of fluorescence and absorption of a short section of fiber. Experimental data, from which the cross-sections are derived is shown in Figure 13.7 for erbium in an Al and Ge codoped silica glass. Note the peak in the absorption and emission cross-sections near 1530 nm and the shift in the absorption spectrum toward shorter wavelengths. The shift towards shorter wavelengths is typical of the rare-earths. This is due to the thermal distribution of energy within each group of Stark-split energy levels favoring the lower energy levels. The addition of the Al codopant tends to broaden the gain peak near 1533 nm and reduce the amplifier gain difference between the 1533 nm and 1550 nm bands. The glass host may also be changed to improve the amplification characteristics of EDFAs. Changing from a silica host to fluorozirconate or fluorophosphate glass has been shown to substantially flatten the overall amplifier gain spectrum. Provided the satisfication from 1530 nm to 1610 nm using a tellurite glass host has also been demonstrated.

The populations  $N_1$  and  $N_2$  are derived from the solution to the rate equation. The rate equation for the metastable state contains the contributions of pump light absorption, stimulated emission and SE.

$$\frac{dN_2}{dt} = \frac{P_p \sigma_{a,p} N_1}{Ah \nu_p} - \frac{P_s \sigma_{e,s} N_2}{Ah \nu_s} - \frac{N_2}{\tau_{sp}}$$
(13.5)

 $(N_2 \text{ change}) = (pump \text{ absorption}) - (stimulated emission) - (spontaneous emission)$ 

where  $P_p/A$  and  $P_s/A$  are the pump and signal intensities,  $hv_p$ ,  $hv_s$  are the pump and signal photon energies and  $\tau_{sp}$  is the spontaneous decay time. From Equation 13.5, any change in the upper level,  $N_2$  is due to a change in the relative values of pump absorption, stimulated emission or SE.

In the energy two-level approximation, conservation of the erbium ion population requires that

$$N_t = N_1 + N_2 (13.6)$$

where  $N_t$  is the total ion population. The incremental gain, g(z) is related to the power change across a differential slice of fiber. The simplest case occurs when the pump light

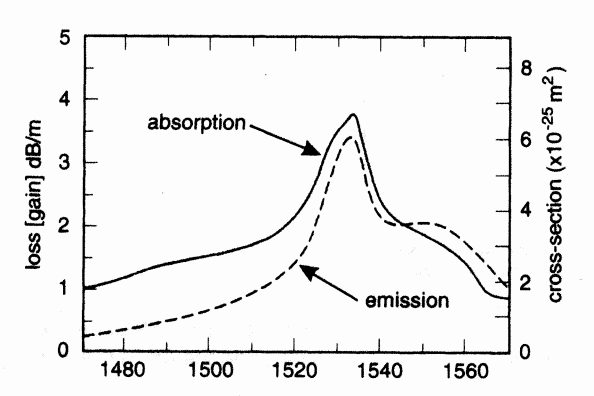


Figure 13.7 Measured absorption and gain characteristics along with calculated absorption and emission cross-sections for Al and Ge codoped EDF [With permission after ref. [22] ©1991 IEEE.]

Gain

528

and signal light propagate in the same direction along the fiber and amplified spontaneous emission is ignored (low gain approximation). The changes in pump and signal powers after passage through a slice of doped fiber are

$$\frac{dP_s}{dz} = g(z) P_s(z) \tag{13.7}$$

$$\frac{dP_p}{dz} = \alpha_p(z) P_p(z) \tag{13.8}$$

As the magnitude of the signal increases along the fiber, the upper-state population is reduced according to Equation 13.5. This results in increased pump absorption in the increment of fiber as indicated in Equation 13.4. These equations can be integrated numerically to solve for the signal and pump power as a function of length along the doped fiber.

The net amplifier gain is found from Equations 13.2 and 13.3. It depends on the average inversion level of the erbium ion population:

$$G = \exp\{\Gamma_s[\sigma_e[N_2] - \sigma_a[N_1]]L\}$$
(13.9)

The average inversion level is set by the pump and signal power levels. The gain dependency on pump power is a figure of merit for different EDFs. Figure 13.8 plots the gain versus pump power for an EDFA for two input powers. The amplifier gain coefficient in units of dB/mW is the maximum slope of the tangent to the curve that passes through the origin. Given the large emission and absorption cross-sections near 1530 nm, the highest gain coefficient is expected (from Equation 13.9) at this wavelength, provided the amplifier is highly inverted. The importance of the overlap factor is also expressed by

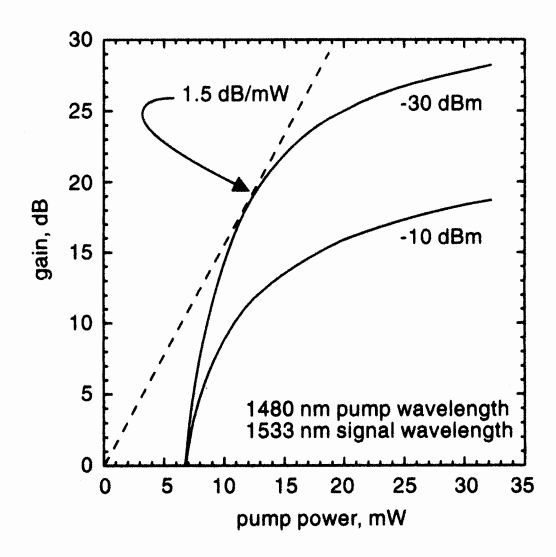


Figure 13.8 Measurement of gain dependence on EDFA pump power.

Equation 13.9. Increasing the fiber numerical aperture increases the overlap factor  $\Gamma$ , resulting in improvement to the small-signal gain. For this reason, amplifiers designed to obtain the maximum gain per milliwatt of pump power tend to have fibers with high numerical apertures. Values for EDF numerical aperture typically range between 0.2 and 0.4.

## 13.2.1 Small-Signal Gain

The small-signal region corresponds to input power levels where the signal amplification does not reduce, appreciably, the gain of the amplifier. For the purposes of defining the small-signal gain region, it is useful to estimate the effective input noise  $P_{\text{noise eff}}$  of the amplifier.

$$P_{\text{noise, eff}} \approx 2hvB_o \sim 30 \text{ nW/nm for } \lambda = 1.5 \text{ }\mu\text{m}$$
 (13.10)

where hv is the photon energy (J) and  $B_a$  is the optical bandwidth (Hz) of the amplifier. The effective input noise multiplied by the amplifier gain yields the output noise power of the amplifier. As the input signal power becomes significant relative to the input noise power, it plays a larger role in determining the inversion level,  $N_2$ . Changes in  $N_2$  result in changes in gain. As long as the input power is small compared to  $P_{\text{noise,eff}}$ , its affect on the amplifier will be insignificant and the amplifier will be in small signal operation. The amplifier gain can be plotted as a function of input power as shown in Figure 13.9. This type of curve can help identify the small signal input power region. Even at very low input power levels, a reduction in signal gain can occur.

As an example, an amplifier with 10 nm optical bandwidth about 1.55 µm has an effective input noise of  $\sim 0.3 \mu W$ . Therefore, the input signal probe should be less than 30 nW, or -45 dBm, to avoid affecting the amplifier gain. The small-signal gain is sometimes defined as the gain corresponding to a small, but practical input level, (for example, -30 dBm) with the understanding that compression effects may have already occurred to some degree.

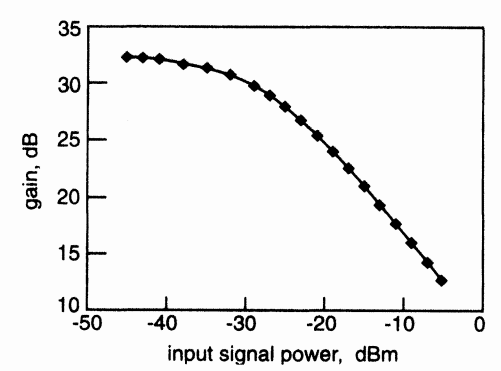


Figure 13.9 EDFA gain dependence on input signal power.

Chap. 13

#### 13.2.2 Saturated Gain

The EDFA is usually operated at input signal levels large enough to cause saturation of the amplifier gain. Gain saturation is observed in Figure 13.9 as a reduction in gain with an increase in signal power. The amplifier gain in an ASE-free model can be written implicitly as a function of the ratio of the output power,  $P_{\text{out}}$  to the saturation power,  $P_{\text{sat}}$ .

$$G = G_0 \exp\left[-\frac{G-1}{G} \frac{P_{\text{out}}}{P_{\text{sat}}}\right]$$
 (13.11)

Where  $G_0$  is the small-signal gain as discussed earlier. The saturation power,  $P_{\text{sat}}$  at a specific wavelength is the power required to invert a slice of erbium-doped fiber sufficiently to obtain optical transparency in other words zero gain.

 $P_{\rm sat}$  is written as:

$$P_{\text{sat}} = \frac{Ahv}{\sigma_a \tau_{\text{sn}}} \tag{13.12}$$

where A is the mode-field area,  $\sigma_a$  is the absorption coefficient as discussed previously, and  $\tau_{co} \sim 10$  ms, is the spontaneous lifetime of the ion in the metastable state.

The saturation power can be modified by increasing the fiber mode-field area A. The amplifier 3 dB compression point is a figure of merit describing the output power capabilities of the amplifier. This is the output power at which the amplifier gain is reduced to 50% of its small signal value. From Equation 13.11, the 3 dB compression power is proportional to the saturation power:  $P_{\text{out}}^{-3\text{dB}} = \ln(2) \ P_{\text{sat}}^{2\text{d}}$ . High-power amplifiers tend to have active fibers with larger mode-field diameters to increase the saturation power and hence the 3 dB compression point.

# 13.2.3 Polarization Hole-Burning

In an experiment where a single wavelength channel was passed through a link employing a large number of optical amplifiers, it was discovered that the small-signal optical gain in the polarization orthogonal to the large-signal polarization was greater than the large signal gain.<sup>5</sup> This polarization-dependent gain, (PDG), occurred even when the large-signal polarization was changed to various states, to differentiate it from the usual polarization-dependent loss. Subsequent studies provided confirmation to this effect whose origin is due to polarization dependence of the emission cross-section of the erbium ions in the silica host. This effect leads to polarization hole-burning with a hole depth which depends on the degree of amplifier compression  $C_n$  of :<sup>27</sup>

$$PHB \approx 0.027C_n - 0.001C_n^2 [dB]$$
 (13.13)

for  $C_p$  < 8 dB. The amplifier compression is in units of decibels. PDG induced by polarized pump light was also observed, with a magnitude of 0.07 dB for the particular amplifier studied.<sup>27</sup> Since the PHB effect within each amplifier is small (~0.2 dB), its impact is more important in large concatenations of amplifiers. Fortunately, the gain recovery for

the PHB is slow, and rapid polarization modulation of the input signal has been shown to effectively suppress the effect of PDG. <sup>28,29</sup>

## 13.2.4 Spectral Hole-Burning

A localized signal power-dependent spectral gain depression is referred to as spectral hole-burning, (SHB).<sup>30</sup> SHB occurs in EDFAs when a strong signal reduces the average ion population contributing to gain at a particular wavelength in excess of the global reduction.

SHB is relatively small in EDFAs since these amplifiers are predominantly homogeneously broadened. A homogeneously broadened amplifier has the property that an input signal at any wavelength in the amplification band can equally access the total energy stored within the amplifier. Homogeneous broadening in EDFAs is caused by the rapid transport of energy across the different Stark-broadened lines within a specific manifold (in other words,  ${}^4I_{15/2}$  or  ${}^4I_{13/2}$  in Figure 13.4). This tends to reduce the extent of the SHB. The presence of phonons (heat exchange) is responsible for the EDFA homogeneous broadening.

Research has shown that at room temperature, SHB is relatively small for EDFAs with a dependency of ~ 0.3 dB per dB increase in gain compression. The effect of SHB tends to be more significant in the 1530 nm wavelength region than the 1550 nm region. A plot of the inhomogeneous gain saturation caused by SHB is shown in Figure 13.10. This measurement was performed using an edge-emitting LED (EELED) probe in combination with a time-domain extinction technique to accurately measure gain as discussed in Section 13.5. The full-width half-maximum of SHB hole-widths are typically in the range of ~ 3 to ~ 10 nm in the EDFA gain spectrum, the narrowest hole-widths occurring near the 1530 nm region.

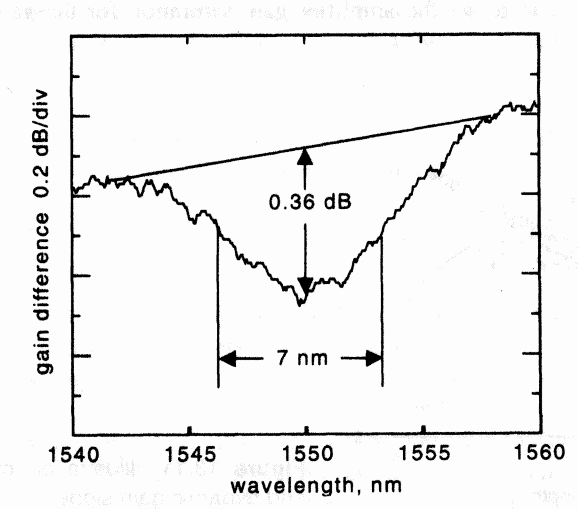


**Figure 13.10** EDFA spectral holeburning at a wavelength of 1550 nm.

The amplifier gain tilt has important implications in systems sensitive to distortion brought on by the combination of laser chirp and amplifier gain slope.<sup>33</sup> In long-haul WDM systems, the amplifier gain spectrum must remain flat to avoid dominance of the power of one channel over the rest. The change or tilt in the amplifier gain spectrum that occurs when wavelength channels are added or dropped to the WDM data stream degrades performance of long-haul telecommunications systems. Gain tilt is defined here as the ratio of the gain change at a test wavelength to the change in gain at a reference wavelength where the gain changes are caused by a change in input conditions. For a homogeneously broadened amplifier, gain tilt is invariant with input power. Once the gain tilt is characterized for one set of input conditions, it can be applied to predict the amplifier gain tilt for other input conditions.

A related concept is the amplifier gain slope. It is important to distinguish between the static gain slope (see Figure 13.11) and the dynamic gain slope. The differences between the static and dynamic gain slopes are due to the change in the amplifier inversion level that results from a change in the wavelength of the strong saturating input signal.

The static gain slope,  $m_s$  is defined by

$$m_s(\lambda_o) = \frac{G_s(\lambda_o + \Delta\lambda) - G_s(\lambda_o - \Delta\lambda)}{2\Delta\lambda}$$
(13.14)

where  $G_s(\lambda_o \pm \Delta \lambda)$  is the gain at the saturating signal wavelength as the saturation signal wavelength is tuned to  $\lambda_o \pm \Delta \lambda$ .

The dynamic gain slope,  $m_d$  is defined as

$$m_d(\lambda_o) = \frac{G_p(\lambda_o + \Delta\lambda) - G_p(\lambda_o - \Delta\lambda)}{2\Delta\lambda}$$
(13.15)

where  $G_p$  ( $\lambda_o \pm \Delta \lambda$ ) is the gain of a small signal probe at the wavelength of  $\lambda_o \pm \Delta \lambda$ . A large input signal maybe present to set the amplifier gain saturation for the gain slope

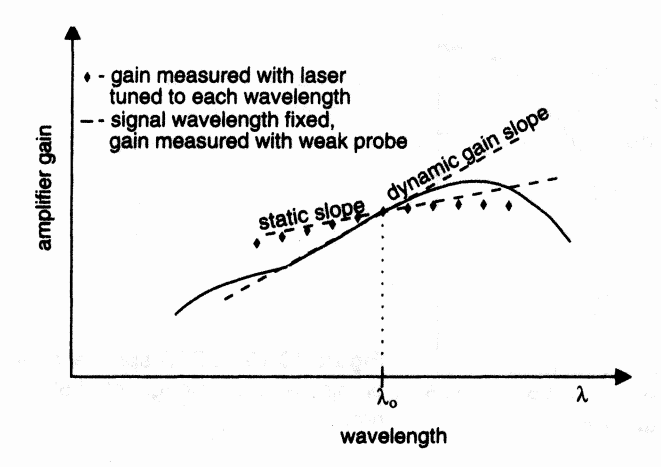


Figure 13.11 Illustration of static and dynamic gain slope.

measurement. The probe for characterizing the dynamic gain slope may be a continuously tunable laser set to low output power, or a broadband light source such as an EELED.

#### **13.3 NOISE**

Sec. 13.3

Noise

In this section, the noise associated with an amplified optical signal is discussed. Noise in two domains will be considered: optical field noise, and intensity/photocurrent noise. Optical field noise refers to the optical noise spectrum measured with the typical tuning-filter-based (for example, grating) OSA. This type of noise is usually characterized over the EDFA spectral window. ASE from an optical amplifier is the main contributor to this noise. Intensity/photocurrent noise refers to the power or current fluctuations associated with the optical beam. This noise is typically characterized up to tens of GHz in bandwidth. The intensity noise spectrum refers to the power spectrum of the optical intensity prior to detection. The intensity noise spectrum is different than the photocurrent spectrum in subtle ways when shot noise is considered. For this reason, special attention has been applied in the discussion on shot noise in view of its representation in both the intensity noise and photocurrent noise domains. The concepts of power spectral densities, relative intensity noise, and SNR will be used in this section.

## 13.3.1 Optical Noise

Within the amplifying section of optical fiber, the excited erbium ion can decay to its ground state through stimulated emission caused by a signal photon, or, spontaneously. The spontaneously emitted photon has random direction and phase. Some of the spontaneously emitted photons are captured by the propagating mode of the optical fiber. These captured photons will be amplified as they travel inside the doped fiber. This results in ASE. The total ASE power is summed over all the spatial modes that the optical fiber supports in an optical bandwidth,  $B_o$ . In the typical erbium-doped fiber there are two propagating modes of polarization with a total ASE power equal to:

$$P_{ASE} = 2n_{sp} hv (G - 1)B_o (13.16)$$

where hv is the photon energy and G is the amplifier gain.

The spontaneous emission factor,  $n_{sp}$ , is given by

$$n_{sp} = \frac{\sigma_e N_2}{\sigma_e N_2 - \sigma_a N_1} \tag{13.17}$$

with  $\sigma_{e'}$ ,  $\sigma_{a'}$ ,  $N_1$ , and  $N_2$  as defined in Section 13.2. The SE factor,  $n_{sp}$  is a measure of the quality of the inversion of the optical amplifier. An  $n_{sp}$  value near unity is possible with strong pumping in the 980 nm band. This is the lowest value of  $n_{sp}$  that can be attained. It corresponds to nearly complete inversion ( $N_1 \sim 0$ ) of the amplifier. Complete inversion, where  $N_2 = N_r$  results in the lowest optical noise figure (discussed in Section 13.4).

Depletion of pump power along the erbium-doped fiber causes the  $N_2$  population to vary as well. According to Equation 13.17, the SE factor depends on  $N_2$  and it will vary

Sec. 13.3 Noise

535

with length along the active fiber. Usually  $n_{sp}$  is defined as the effective or integrated value for the amplifier. When the 1480 nm pump wavelength is used, complete inversion is not possible since the pump and signal share the same ground and excited states. Pump photons are not only absorbed but also contribute to stimulated emission since the emission cross-section is nonzero at this wavelength. The result is an amplifier with incomplete inversion and a higher SE factor,  $n_{sp}$ . This translates to a direct increase in the noise figure of the amplifier. The effective values for  $n_{sp}$  typically range from 1 (980 pumping) to 4.

In noise figure calculations it is sometimes useful to work with the ASE spectral density (W/Hz) in a single polarization:

$$\rho_{ASE} \stackrel{\Delta}{=} n_{sp} \, hv(G-1) \tag{13.18}$$

Given a large enough amplifier gain, the ASE can become significant, resulting in saturation of the amplifier gain by the generated ASE. For this reason EDFAs can be applied as ASE sources for a variety of applications ranging from gyroscopes to "white light" interferometry (Chapter 10).

#### Example

Find the ASE power generated by an amplifier supporting two polarizations with 20 dB gain, 30 nm bandwidth, a 1.55  $\mu$ m center wavelength and an  $n_{sp}$  factor of 1.5.

#### Solution

Referring to Equation 13.16, the bandwidth in Hertz is calculated:

$$B_o \approx \frac{c\Delta\lambda}{(\lambda_o)^2} \tag{13.19}$$

This yields a bandwidth  $B_o$  of 3.75 THz. The photon energy was computed to be 1.28 × 10<sup>-19</sup> J. Using G = 100 and Equation 13.16 the total ASE power is 143  $\mu$ W. The ASE power produced in a 1 nm bandwidth is plotted as a function of optical gain in Figure 13.12 for various effective values of  $n_{sp}$ .

# 13.3.2 Intensity/Photocurrent Noise

Before embarking into the discussion on noise, the basic conversion of light intensity into electrical current by an optical receiver is discussed in terms of the receiver responsivity. The average photocurrent,  $i_{dc}$  generated in a photodetector by an optical source of average power < P > is:

$$i_{dc} = \Re \langle P \rangle \tag{13.20}$$

where the detector responsivity is defined as:

$$\Re = \frac{\eta q}{hv} \quad [A/W] \tag{13.21}$$

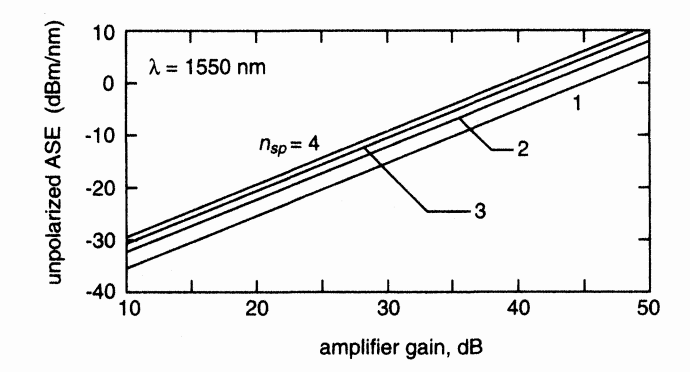


**Figure 13.12** ASE power produced in 1 nm bandwidth as a function of length for various spontaneous emission factors. Add 2.3 dB to compute power at a wavelength of 1300 nm.

The light collection quantum efficiency of the receiver is denoted by  $\eta$ . The electronic charge, q is equal to  $1.602 \times 10^{-19}$  coul. At a wavelength of  $1.55~\mu m$ , the photon energy hv, is  $1.283 \times 10^{-19}$  J. The light collection quantum efficiency  $\eta$  includes all optical losses that are part of the optical receiver. This can include optical coupling loss as well as the quantum efficiency of the receiver photodetector.

In addition to the average optical power, intensity noise is also present. Intensity noise is a significant limiting factor in optical communications systems. Photodetectors convert intensity noise directly into electrical noise. While the optical field noise can have both amplitude or phase noise, photodetectors do not directly respond to the phase noise. However, phase noise can be converted to intensity noise by interference effects. The following intensity noise types are commonly encountered in optical systems:

- · Shot noise,
- Signal-spontaneous beat noise,
- · Spontaneous-spontaneous beat noise, and
- Interference noise.

The two beat noises and the interference noise fall in the category of excess noise. It is important to differentiate between shot noise and the excess noise since the resulting photocurrent noise they generate depends differently on the responsivity of the receiver detector. Intensity noise is defined in terms of a power spectral density,  $S_p(f)$  of the light intensity fluctuations. The power spectral density of the optical intensity variations is related to the power spectral density of the electrical current  $S_i(f)$  variations according to:

$$S_{p}(f) = \frac{1}{\Re^{2}} S_{i}(f)$$
 for excess noise  
 $S_{p}(f) = \frac{1}{\Re} \frac{hv}{q} S_{i}(f)$  for shot noise (13.22)

 $S_i(f)$  is measured with an electrical spectrum analyzer. When  $S_p(f)$  is integrated over a bandwidth, it yields the mean-square optical noise power in the integration bandwidth.

It is useful to refer the noise density to the average optical power by way of the relative intensity noise  $(RIN_o)$ .  $RIN_o$  is defined with respect to the power spectral density of the optical intensity as:

$$RIN_o(f) = \frac{S_P(f)}{\langle P \rangle^2} [Hz^{-1}]$$
 (13.23)

where < P > is the average optical power. This is indicated in Figure 13.13 which illustrates the spectral density of the optical intensity variations with frequency as well as the average dc intensity. Sometimes the RIN concept is used to describe the fluctuations on the electrical current instead of the light intensity. To avoid confusing the two RINs, the electrical relative intensity noise will be referred to here as RINs. RINs is defined as:

$$RIN_{e}(f) = \frac{S_{i}(f)}{[i_{dc}]^{2}} [Hz^{-1}]$$
 (13.24)

Shot Noise. Shot noise has its origins in the uncertainty of the time of arrival of electrons or photons at a detector. When the dominant noise is due to shot noise it is referred to as shot-noise-limited or quantum-limited. Both the laser signal and ASE contribute shot noise. In this discussion, the shot noise will be examined in both the intensity and electrical domains. This will avoid confusion with respect to the impact of the quantum efficiency  $\eta$  of the optical detection. The shot-noise spectral densities are given by:

$$S_{i}(f)|_{\text{shot}} = 2q i_{dc} \quad [A^{2}/\text{Hz}]$$

$$S_{P}(f)|_{\text{shot}} = \frac{2 hvi_{dc}}{\Re} = 2hv < P > \quad [W^{2}/\text{Hz}]$$
(13.25)

where  $i_{dc}$  and < P > are the average values for the electrical current and optical power respectively.

The RIN for the intensity and electrical domains are derived using Equations 13.23, 13.24, and 13.25:

$$RIN_{e|shot} = \frac{2q}{i_{dc}} \qquad [Hz^{-1}]$$

$$RIN_{o|shot} = \frac{2\eta \, q}{i_{dc}} = \frac{2hv}{\langle P \rangle}$$
(13.26)

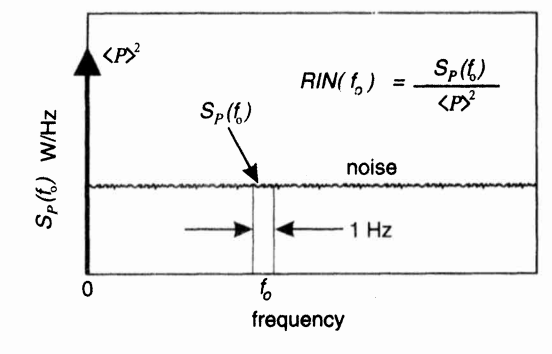


**Figure 13.13** Quantification of noise in terms of spectral density and RIN.

RIN<sub>e</sub>  $|_{\text{shot}}$  is larger than RIN<sub>o</sub>  $|_{\text{shot}}$  when the quantum efficiency of the optical detection is less than unity. RIN<sub>o</sub>  $|_{\text{shot}}$  improves (gets smaller) with an increase in optical power. Any optical signal can be made to be shot-noise limited. By attenuating the optical signal (decreasing  $\eta$ ), the excess noise sources (discussed later) reduce in magnitude faster than the shot noise, and the shot noise will eventually dominate. The RIN<sub>e</sub>  $|_{\text{shot}}$  is plotted in Figure 13.14 as a function of photodetector current. From Figure 13.14, the RIN produced by a 1 mW shot-noise-limited laser source is approximately -155 dB/Hz.

A special class of light, known as squeezed-light has an associated intensity noise content below the conventional shot noise level. The intensity noise is compressed or squeezed at the expense of an increase in phase noise. The degree of squeezing is rapidly lost when the squeezed light passes through an optical amplifier or a lossy medium.

**Signal-Spontaneous Beat Noise.** Interference between signal light and ASE causes intensity fluctuations known as signal-spontaneous beat noise. <sup>34</sup> This noise is unavoidable in EDFA-based systems and is one of the primary noise contributions in optically amplified communications systems. This beat noise is analogous to the case of two frequencies beating in a heterodyne mixer to generate a difference frequency. Recall that the mixing product is polarization dependent, so the signal will beat only with those ASE components in the same polarization as the signal. Since the ASE is typically unpolarized, only one-half will contribute to the sig-sp beat noise density. This mixing process is illustrated in Figure 13.15. The bandwidth of optical receivers is typically less than 50 GHz, ( $\sim 0.4 \text{ nm} \ @ \lambda = 1.55 \ \mu\text{m}$ ) so only those ASE spectral components within 0.4 nm of the signal wavelength contribute to the detected signal-spontaneous beat noise.

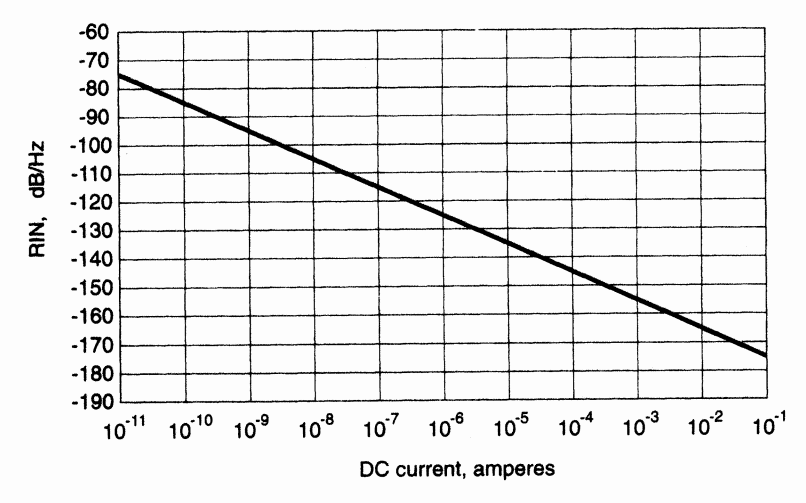
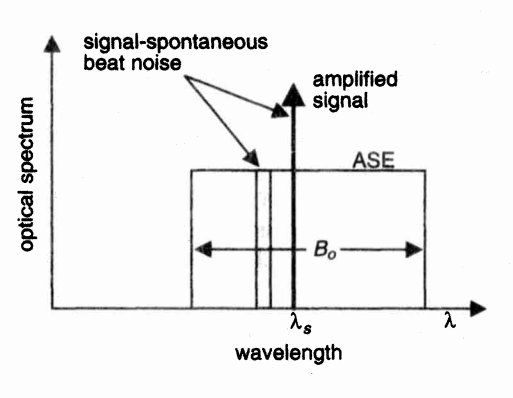


Figure 13.14 Shot-noise RIN dependency on average current.



**Figure 13.15** Signal-spontaneous beat noise between amplified signal and the spectral components of the ASE.

The detected current noise density measured with an electrical spectrum analyzer has a low-frequency  $(f < B_o/2)$  value of:

$$S_{i_{\text{them}}}(f) = 4\Re^2 GP_s \,\rho_{\text{ASE}} \, [A^2/\text{Hz}]$$
 (13.27)

According to Equations 13.18 and 13.27, the signal-spontaneous beat noise varies as the square of the optical gain and linearly with input signal power. The use of the RIN concept with signal-spontaneous beat noise has the complication due to the average power contribution of the ASE. Taking the average unpolarized ASE power as  $P_{\rm ASE}$ , the signal-spontaneous beat noise RIN is given by:

$$RIN_{sig-sp} = \frac{4GP_s\rho_{ASE}}{(GP_s + P_{ASE})^2} [Hz^{-1}]$$
 (13.28)

The following observations can be made about sig-sp beat noise:

- $S_{i_{sign},p}(f)$  increases linearly with the input signal.
- $S_{i_{sig-sp}}(f)$  does not depend on the ASE spectral width,  $B_o(f_o << B_o)$ .
- $S_{i_{sig-sp}}^{i_{sig-sp}}(f)$  can not be reduced by placing a polarizer at the amplifier output.
- RIN  $_{sig-sp}$  is approximately independent of gain when G > 10.

Spontaneous Spontaneous Beat Noise. The beating between the different spectral components of the SE results in intensity noise known as spontaneous-spontaneous, (sp-sp) beat noise.<sup>34</sup> This is illustrated in Figure 13.16. Each pair of ASE spectral components generates an intensity beat tone at their difference frequency. Thus, the entire ASE spectrum contributes to the sp-sp intensity beat noise. If the ASE is unpolarized, the ASE in each of two orthogonal polarizations will contribute to the total sp-sp beat noise. From Figure 13.16, the maximum frequency extent of the beat noise is equal to the maximum width of the ASE spectrum. Thus the beat noise could well have an intensity spectrum beyond 1000 GHz, and certainly beyond the bandwidth of electronic receivers. The frequency content of the photocurrent noise generated by sp-sp beating can be significantly reduced by placing an optical filter before the photodetector. This is easily understood from Figure 13.16 where the total number of possible beating pairs decreases as the opti-

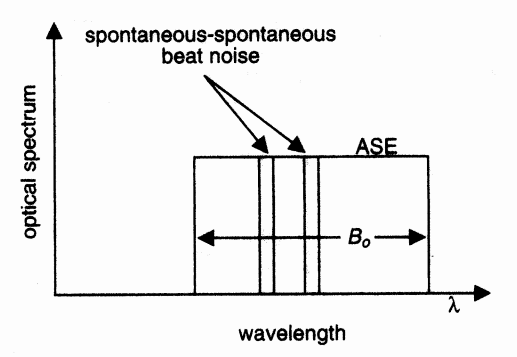


**Figure 13.16** Spontaneousspontaneous beat noise between ASE spectral components.

cal bandwidth decreases. The photocurrent spectrum for the case of an unpolarized ASE spectrum with a rectangular shape is:

$$S_i(f) = 4\Re^2 \rho_{ASE}^2 B_o \Lambda(f/B_o) [A^2/Hz]$$
 (13.29)

where  $\Lambda(f/B_o)$  is the triangle function which has a value of unity at 0 Hz and linearly decreases to 0 at  $f = B_o$ .

In general, the peak magnitude of the RIN is dependent on the actual shape of ASE spectrum. This is discussed also in Section 13.5.2. When the signal power is small or absent, the RIN caused by sp-sp beat noise varies inversely with the spectral width of the ASE source. A rectangle-shaped ASE spectrum delivers the most RIN of any optical shape 35 with a value equal to:

$$RIN_{rect} = \frac{1}{B_o} \quad \text{(for unpolarized light)} \tag{13.30}$$

Reducing the optical bandwidth increases the RIN. This simple relation can also be remembered as follows: RIN is related to the inverse of the number of degrees of freedom the system supports. In the case of ordinary telecom-grade optical fiber, and intensity detection, there are two spatial orientations for polarization, and  $B_o/(1 \text{ Hz})$  possibilities for bandwidth. For polarized light, the RIN increases by a factor of two since one degree of freedom is absent.

Table 13.2 gives the analytical relations for the frequency dependent sp-sp RIN for several different ASE spectral shapes. The optical field shape refers to the ASE spectral shape as measured with an OSA.

To provide a comparison of the way the different noise types discussed vary with signal power, the shot, sig-sp and sp-sp beat noises are plotted in Figure 13.17. The noise levels are plotted versus amplified signal power for an amplifier having a 5 nm passband and 37 dB gain. Thermal noise is also shown for an electrical system noise figure of 8 dB and a 50 ohm impedance. At low signal levels, the noise is dominated by sp-sp beat noise. Eventually, sig-sp beat noise dominates, increasing linearly with signal power. At low

Noise

Optical field shape	Normalized $S_{\mathcal{E}}(v)$	RIN(f)	RIN(f=0)
Rectangle	$\Pi\left(\frac{\nu-\nu_o}{B_o}\right)$	$\frac{1}{B_o}\Lambda\left(\frac{f}{B_o}\right)$	$\frac{1}{B_o}$
Gaussian	$\exp\left\{-\left(4\ln 2\right)\left(\frac{\nu-\nu_o}{B_o}\right)^2\right\}$	$\frac{1}{B_o} \frac{\sqrt{2 \ln 2}}{\sqrt{\pi}} \exp \left\{ -(2 \ln 2) \left( \frac{f}{B_o} \right) \right\}$	$\left(\frac{1}{a_o}\right)^2$ $\frac{0.66}{B_o}$
Lorentzian	$\frac{B_o^2}{B_o^2 + (2(\nu - \nu_o))^2}$	$\frac{B_o/\pi}{B_o^2+f^2}$	$\frac{0.32}{B_o}$

signal powers the shot noise is actually dominated by the ASE average power contribution.

**Reflection Noise/Multipath Interference.** The presence of optical reflections within the optical amplifier, such as those shown in Figure 13.18 will cause an interferometric conversion of laser phase noise into intensity noise. This intensity noise degrades the SNR at the optical receiver.<sup>6,7</sup> The converted noise is known as multipath interference noise or MPI. Important parameters determining the magnitude of MPI are the reflection levels, the optical gain, the signal linewidth and the time delay between the reflectors. The presence of optical gain can greatly increase the impact of small reflections. The worst-case RIN occurs when the polarizations of the delayed and non-delayed beams are aligned and the average interference phase is near quadrature. The interferometer is said to be in quadrature when the output power is halfway between its minimum and maximum values.

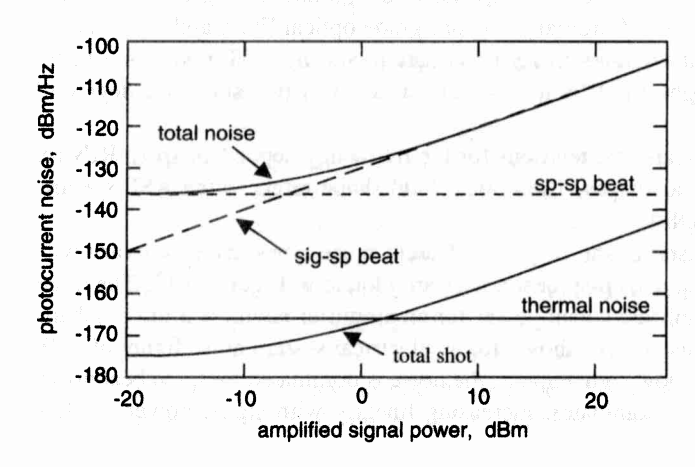


**Figure 13.17** Total and individual noise contributions from an EDFA as a function of the amplified signal power.

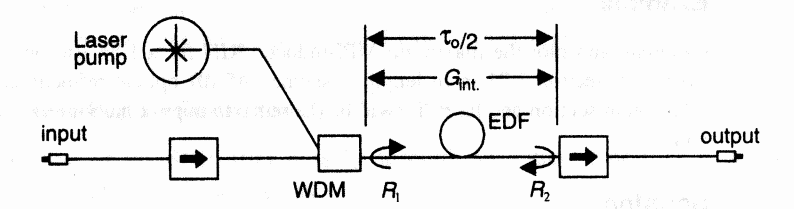


**Figure 13.18** Fiber optic amplifier showing optical reflections contributing to multi-path interference noise.

The following relations can be used to estimate the RIN generated by a pair of small optical reflections when illuminated by a laser with a Lorentzian-shaped optical spectrum. The two reflections, denoted by  $R_1$  and  $R_2$  are assumed to satisfy:  $R_1$ ,  $R_2 << 1$ . The expected RIN for three regimes of coherence (see Chapter 5) and with the interferometer in quadrature is: any coherence

$$RIN_{\Delta\phi_{\text{max}}}(f) = \frac{4G_{\text{int}}^2 R_1 R_2}{\pi} \frac{\Delta \nu}{\Delta \nu^2 + f^2} \left[ 1 + e^{-4\pi\Delta\nu\tau_o} - 2\cos(2\pi f\tau_o)e^{-2\pi\Delta\nu\tau_o} \right]$$
(13.31)

coherent case

$$\Delta \nu \tau_o < 0.1$$
,  $f < 1/2 \pi \tau_o$ , maximum RIN

$$RIN_{\Delta\phi_{max}}(f=0) = 16\pi\Delta\nu \tau_o^2 G_{int} R_1 R_2$$
 (13.32)

incoherent case

$$\Delta v \tau_o > 1$$

$$RIN_{\Delta\phi_{max}} = \frac{4G_{int}^2 R_1 R_2}{\pi} \frac{\Delta\nu}{\Delta\nu^2 + f^2}$$
 (13.33)

where  $\Delta \nu$  is the laser FWHM linewidth, f is the baseband frequency,  $\tau_{\rm o}$  is the delay time of the reflected light and  $G_{\rm int}$  is the optical gain of the medium separating the reflections. The gain-reflection product is assumed to be small (in other words,  $G_{\rm int}R_1R_2 <<1$ ) for the above equations to hold.

In the coherent case, the conversion of phase noise into intensity noise increases as the square of the distance separation between the reflections. Therefore, when using highly coherent lasers in test systems, the lead lengths should be kept as short as possible to reduce the phase noise to intensity noise conversion. As the product of the laser linewidth and the delay  $\tau_o$  increases, the noise spectrum tends toward a Lorentzian function as defined by Equation 13.33. The gain,  $G_{\rm int}$  causes a significant increase in the MPI-induced RIN. Thus reflections must be kept small when optical gain is present. An understanding of the parameters affecting the MPI process can be applied to improve the optical amplifier design or the amplifier test system to limit the effects of this unwanted noise.

## Example

Calculate and plot the maximum MPI-induced RIN for a 1.55  $\mu$ m optical amplifier with a fiber gain section 1.71 m in length. Assume -45 dB optical reflections at each end of the 30 dB gain section and laser linewidths (Lorentzian approximation) varying from 10 MHz to 1 GHz.

#### Solution

The linewidth-delay time product is calculated first. A fiber refractive index of n = 1.46 is assumed. The delay time is calculated  $(\tau_o = 2nL/c)$  to be 16.6 ns. Thus the smallest and largest  $\Delta\nu\tau_o$  products are 0.166 and 166 for linewidths of 1 MHz and 1 GHz respectively. Equation 13.31 is valid for this wide range of the  $\Delta\nu\tau$  product. The estimated MPI RIN is shown in Figure 13.19.

From the above discussion, it is interesting to note that the RIN generated by the reflections internal to the amplifier depends on the linewidth of the source. Therefore, the noise generated by the amplifier is a function not only of the laser wavelength and power, but the signal linewidth as well.

#### 13.4 NOISE FIGURE

The amplifier noise figure is a figure of merit quantifying the SNR (related also to the carrier-to-noise ratio, CNR) degradation after passage through the amplifier. Large-noise figures are detrimental to system performance, it causes poor received SNRs, increased jitter in soliton-based systems and ASE accumulation in long-haul amplified links. The main contributors to the noise figure are the effects of amplified spontaneous emission generated within the amplifier and importantly for analog communications, the phase-noise to intensity noise conversion due to internal optical reflections. The ASE manifests

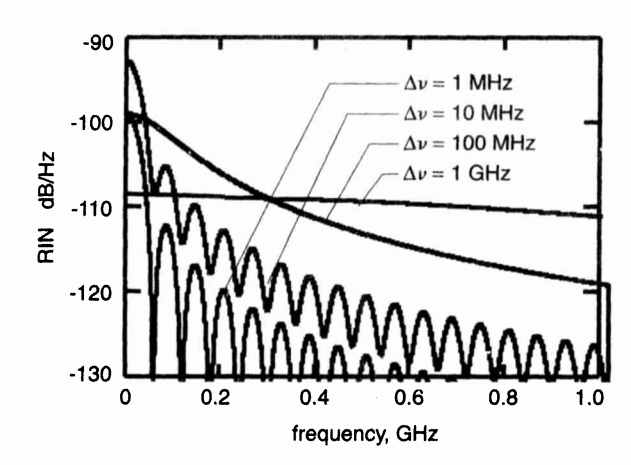


Figure 13.19 Optical amplifier MPI-induced relative intensity noise versus frequency for various signal laser linewidths.

itself through the generation of beat noise. In this section, the noise figure is defined, and later cast in a form that can be readily applied from a measurement standpoint.

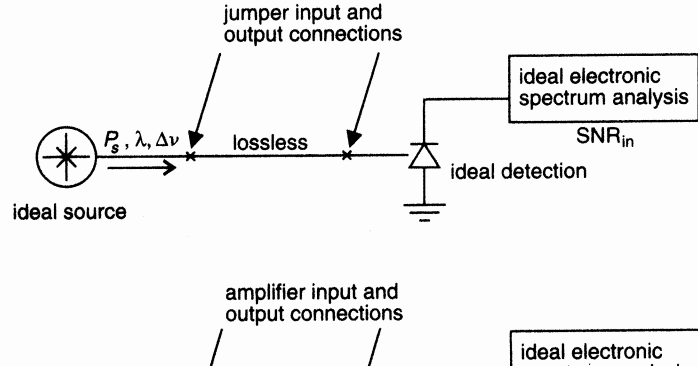
# 13.4.1 Noise-Figure Definition

The degradation of the SNR after passage through an optical amplifier is quantified in terms of the noise figure, F, defined as

$$F = \frac{\text{SNR}_{\text{in}}}{\text{SNR}_{\text{out}}} \tag{13.34}$$

In the discussions that follow, the noise figure in decibels is determined according to:  $F = 10 \log(F)$ . The SNRs are referred to the output of an ideal photodetector which is capable of converting each photon of incident light into electrical current (in other words, 100% quantum efficiency). The input SNR is defined to be that from a shot-noise-limited source. The shot-noise-limited input reference is critical to the definition. If an optical source with a large amount of intensity noise were used to measure the noise figure of an amplifier, the amplified source noise would dominate over the amplifiers own noise contribution and lead to an erroneous noise figure of 0 dB, in other words, no observed SNR degradation caused by the amplifier.

The noise figure concept is illustrated in Figure 13.20. The input SNR is determined with the amplifier bypassed using an idealized source and receiver. The amplifier is inserted and the output SNR is determined. Equation 13.34 is next used to calculate the amplifier noise figure. The idealized source is shot-noise-limited and set to the appropriate



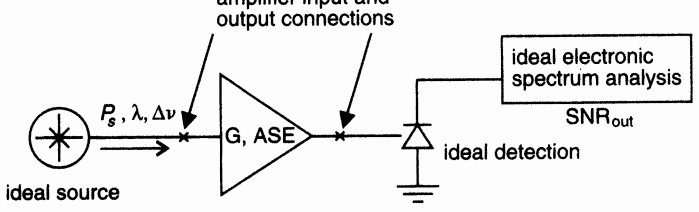


**Figure 13.20** Noise figure concept in terms of idealized source and receiver.

Chap, 13

power, wavelength, and linewidth. The idealized receiver has a calibrated frequency response and contributes no excess noise of its own. Obviously the real world is not yet ideal and much of the work involving noise figure measurements is in dealing with the source and the receiver non-idealities.

**Signal-Spontaneous Beat-Noise-Limited Noise Figure.** A commonly used definition of noise figure is the quantum-beat-noise-limited noise figure, sometimes referred to as the sig-sp beat-noise-limited noise figure. This noise figure is more restricted than the general definition defined by Equation 13.34. It doesn't include, for example, the output SNR degradation due to sp-sp beat noise, or MPI. The quantum-beat-noise-limited noise figure is advantageous in simplifying measurement procedures. It is measured with both optical and electrical techniques which are discussed later.

The quantum-beat-noise-limited noise figure is derived using Equations 13.18, 13.25, and 13.27 in Equation 13.34:

$$NF = \frac{2\rho_{ASE}}{G hV} + \frac{1}{G}$$

$$sig-sp \quad shot$$
(13.35)

where  $\rho_{ASE}$  is the amplifier ASE output density in the same polarization and wavelength as the signal as defined in Equation 13.18. This noise-figure definition is useful because of the ease with which it can be implemented. The ability to correlate noise figure measurement results between different laboratories is improved when this definition is used. The shot noise effect on the noise figure is sometimes excluded for noise calculations involving concatenated amplifiers.

#### Example

Calculate the quantum beat-noise-limited noise figure for an amplifier with 30 dB of gain, producing 12  $\mu$ W of ASE in a 0.5 nm optical bandwidth at the signal wavelength of 1.55  $\mu$ m.

#### Solution

Using Equation 13.19, the gain, ASE density, and photon energy are 1000, 0.19 f W/Hz, and  $1.28 \times 10^{-19}$  J respectively. Substituting into Equation 13.35 yields a noise figure of 3.0 or 4.8 dB. Notice that the shot noise contributed little to the noise figure because of the high gain of the amplifier.

The 3 dB Noise-Figure Myth. A minimum 3 dB (actually,  $\log_{10}(2) = 3.01$  dB) amplifier noise figure is sometimes attributed to the EDFA. If taken out of context this can result in a considerable misunderstanding of the EDFA noise performance. To better understand where the 3 dB limit originates, let us examine the noise figure under moderate signal conditions as the amplifier gain varies. Moderate signal conditions imply that the signal power is much greater than the ASE power in the optical bandwidth of interest. This ensures that the sig-sp beat noise dominates over that of the sp-sp beat noise as indi-

cated by Figure 13.17. Consider the case of a fiber amplifier where initially there are no erbium ions in the "active" optical fiber. Discounting any loss in the optical fiber, the noise figure is unity, in other words, no SNR degradation since the signal passes from amplifier input to output unchanged. As the erbium-ion-doping increases, so does the optical gain, the ASE level, and the signal level. The noise figure increases from 0 dB to 3 dB, or beyond, if other noise sources or optical losses are present. This can be seen from the equation for sig-sp beat noise and shot-noise-limited noise figure derived by substituting Equation 13.18 into Equation 13.35:

$$F = 2n_{sp}\frac{(G-1)}{G} + \frac{1}{G} \tag{13.36}$$

which for large gains yields:  $F \approx 2n_{sp}$  where the SE factor,  $n_{sp} \ge 1$ . A fully inverted amplifier can be achieved with 980 nm pumping resulting in an effective SE factor of unity which leads to a noise figure of 3 dB. Equation 13.36 is plotted versus gain in Figure 13.21. From the figure, a fully inverted amplifier (in other words,  $n_{sp} = 1$ ) with 4 dB of gain and zero input coupling loss has a noise figure near 2 dB. The 3 dB value is the limit for a high-gain amplifier with zero input coupling loss and a fully inverted amplifying fiber. Any loss near the amplifier input, or departure from complete inversion will cause the noise figure to exceed 3 dB.

A special class of amplifiers, referred to as phase-sensitive amplifiers, can achieve a noise figure less than 3 dB. Most optical amplifiers in use, such as EDFAs are phase insensitive, which means that the amplifier gain does not depend on the optical phase of the input signal. Thus the noise generated by the amplifier is amplified in both the in-phase and quadrature phase components. This is the physical origin of the 3 dB limit in high

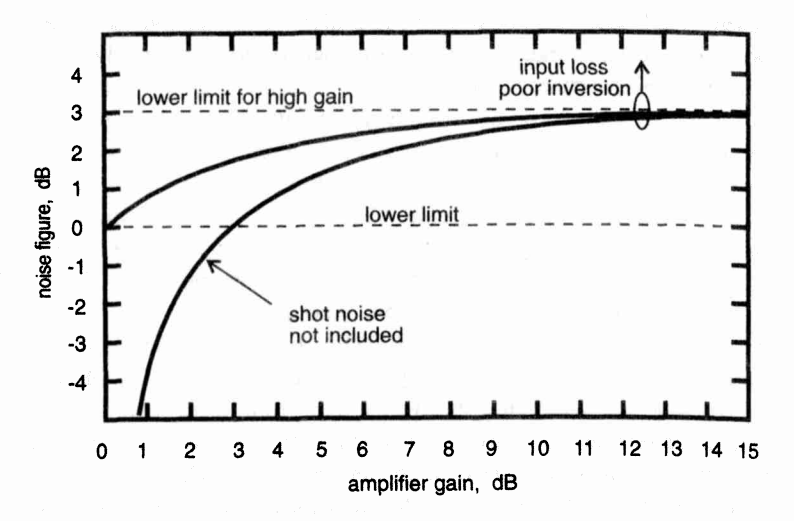


Figure 13.21 Noise figure dependence on optical amplifier gain with and without the shot-noise contribution.

gain amplifiers such as the EDFA. In calculations with concatenations of amplifiers, it is convenient to suppress the shot noise until the signals are analyzed at the detector. In the calculation of noise figure for a single amplifier, failure to include the shot noise will result in significant error in the gain regime below 15 dB.

#### 13.5 CHARACTERIZATION OF GAIN AND NOISE FIGURE

The amplifier gain and noise figure are the fundamental parameters concerning their application to an optical communications link. By measuring these parameters over wavelength, power, input signal polarization, and temperature, the characterization of the amplifier is nearly complete. The measurement of noise figure requires the measurement of gain according to Equations 13.34 and 13.35. The noise-figure measurement techniques are classified into two groups:

- · Optical method: optical spectrum analyzer-based,
- Electrical method: electrical spectrum analyzer-based.

Both methods have their merits. The selection of which to use depends on the application of the measurement result and the available instrumentation. Sometimes both electrical and optical methods are used.

The electrical method is often used in optical-amplifier characterization for analogoptical communications. It can be argued that this method provides a more complete noise figure since it directly measures the complete photocurrent noise at the receiver. Hence it provides characterization of amplifier nonidealities such as multipath interference (MPI) caused by reflections internal to the amplifier. This method, however, requires stringent control over measurement system effects that would otherwise be difficult to separate out from the amplifier characteristics.

Optical methods, on the other hand, are often used for amplifier characterization for long-haul digital communications systems. Accurate measurements of amplifier ASE spectra and gain are performed with OSAs. Based on these measurements, Equation 13.35 is used to compute the noise figure. This method is more tolerant of test system reflections and is capable of rejecting the effects of optical source nonidealities.

The optical and electrical methods have demonstrated their ability to perform single-channel EDFA characterization. Another area of EDFA characterization is for multichannel or WDM amplifiers. WDM is an obvious method to more fully utilize the available transport bandwidth that optical fiber provides. In WDM systems, multiple optical carriers are used to transport information. Multiplexers and demultiplexers are used to combine or separate the various wavelength channels to and from the fiber. WDM systems present similar measurement challenges for the EDFA but at multiple optical carrier frequencies. The suitability of the different measurement techniques for the WDM environment are considered separately in this chapter. At the risk of overgeneralization, Table 13.3 is provided to help compare the level of measurement difficulty, as well as the ap-

Table 13.3 Test Method Comparisons

Characterization of Gain and Noise Figure

Sec. 13.5

Method	Measure MPI	Applicability for WDM	Difficulty: scale 1 to 5
optical: source subtraction	no	moderate	2
optical: polarization extinction	no	poor poor	3
optical: time-domain extinction	no	excellent	3 4
electrical	yes	moderate	4

plicability of the various techniques to WDM measurements. The relative merits of the different methods may change as the measurement art advances.

## 13.5.1 Amplifier Gain

Several methods of measuring the gain of an optical amplifier are discussed here. While not necessarily a complete list of all possible methods, it covers the most commonly used methods. In the discussions on noise figure measurement that follow, the issue of gain measurement with respect to the specific noise figure measurement techniques is also addressed.

Optical Power Meter: Optical Gain. Measurement of optical gain can be performed using the simple approach shown in Figure 13.22. In this approach, the incident source power is measured along with the filtered amplifier output using an optical power meter. The system is calibrated by replacing the amplifier with a lossless connection. An important source of measurement error is the presence of ASE incident on the optical power meter. This is reduced significantly by filtering. Filtering the source reduces the effect of source spontaneous emission (SSE) on the amplifier saturation. The combined effects of ASE and amplified SSE contribute to a net gain measurement error. The gain measurement error, defined here as the ratio of the measured gain to the actual gain is given by:

$$\frac{G_m}{G} = 1 + B_o \frac{Fhv}{P_s} \tag{13.37}$$

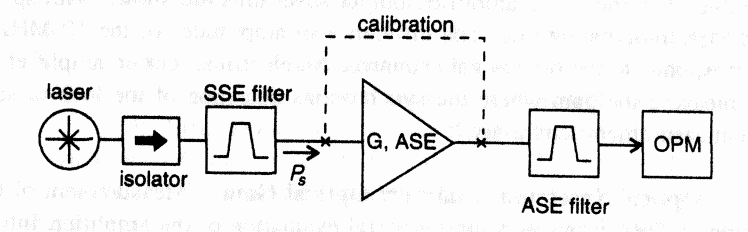


**Figure 13.22** Optical amplifier gain measurement with an optical power meter and bandpass filters. OPM: optical power meter.

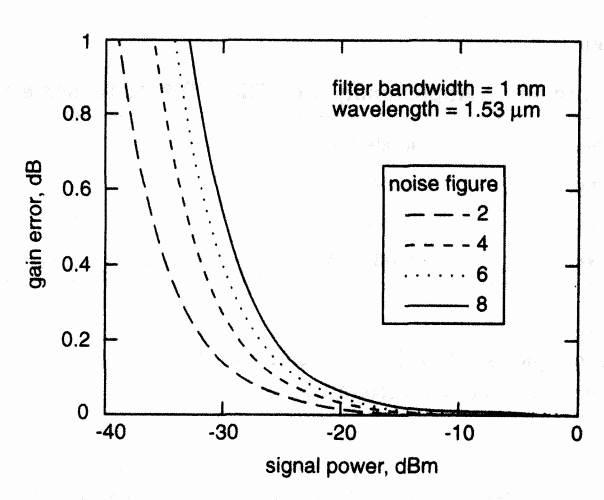
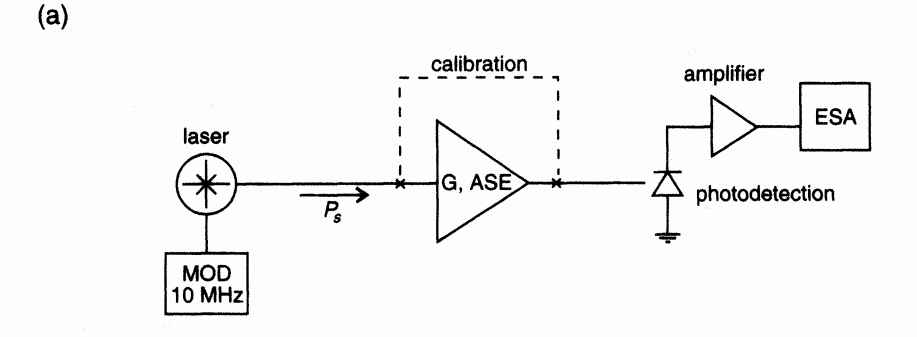


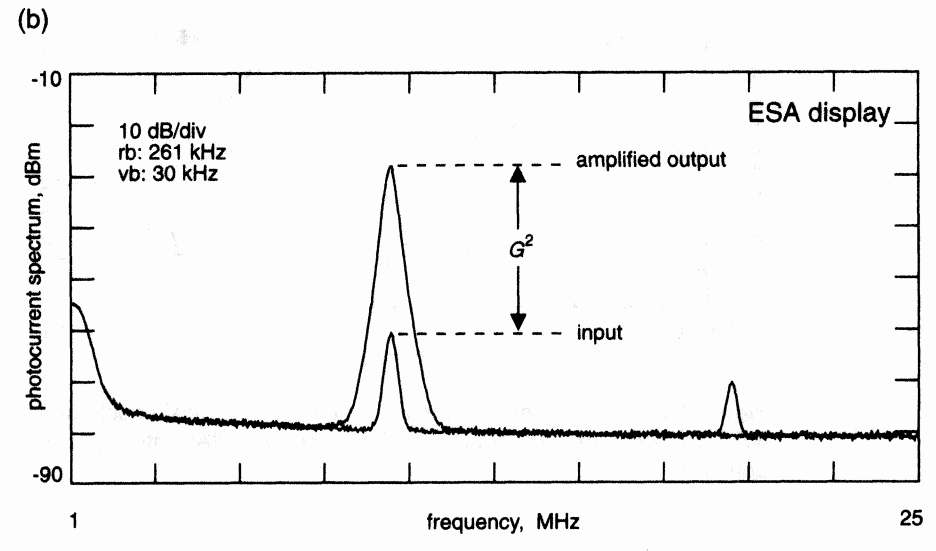
**Figure 13.23** Gain measurement error due to additive effect of ASE.

where F is the noise figure,  $B_o$  the filter bandwidth, and  $P_s$  is the input power. This is plotted in Figure 13.23 for different noise figures assuming a 1 nm filter bandwidth. Input powers below approximately -20 dBm result in appreciable errors for the 1 nm filter bandwidth.

Electrical Spectrum Analyzer: Optical Gain. One method to measure gain at lower input powers is to use source modulation in conjunction with a frequency selective receiver. An electrical spectrum analyzer can be used to measure a small intensity modulation index imparted onto the optical source. By performing measurements of the photocurrent spectrum at the modulation frequency with and without the optical amplifier, the gain can be determined. The advantage of this approach is that the signal is separated from the ASE by the modulation. The modulation frequency is set to be significantly faster than the inverse of the EDFA gain recovery time (~ 300 µs) so as not to modulate the ASE. The measurement set-up, using an electrical spectrum analyzer, is shown in Figure 13.24a. A measurement using this setup is shown in Figure 13.24b. The laser source (a DFB with an electroabsorption modulator) was sinusoidally modulated at a 10 MHz frequency and passed on to the receiver directly for gain calibration. Next the amplifier was inserted for the gain measurement. The measurement results are shown Figure 13.24b. The input and amplified output spectrums are shown with spectral peaks at the 10 MHz modulation rate. The difference in amplitudes of the 10 MHz modulation tone corresponds to the optical gain squared. An electrical lock-in amplifier may also be used to measure the gain where the synchronous detection of the lock-in amplifier improves the measurement sensitivity.<sup>36</sup>

Optical Spectrum Analyzer: Optical Gain. Measurement of the amplifier gain using an OSA provides a more general evaluation of the amplifier. Information concerning the ASE spectral shape, source characteristics, and the presence of spurious signals such as pump laser feedthrough is obtained as well. The basic measurement setup is

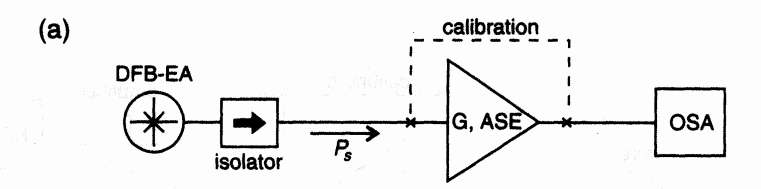




**Figure 13.24** Optical amplifier gain measurement. (a) Measurement setup using modulated source. (b) Displayed ESA data. ESA:-electrical spectrum analyzer.

shown in Figure 13.25a. A gain measurement of an EDFA under the same input signal conditions as in Figure 13.24b is shown in Figure 13.25b.

The amplifier dynamic gain spectrum can be readily measured by combining a small-probe signal with the laser that sets the EDFA saturation level. This is illustrated in Figure 13.26. The probe signal could be a broadband noise source such as an EELED or a tunable laser. <sup>30,36,37</sup> The EELED approach is more rapid if the tunable laser is not capable of sweeping synchronously in wavelength with the OSA. The tunable laser probe power has less of an impact on the amplifier saturation level for a given measurement SNR as compared with the EELED approach. The effect of the probe on the saturation level of the amplifier should be monitored closely. Preferably the probe power is set to a value less than the effective input noise of the amplifier as given by Equation 13.10, but this is not



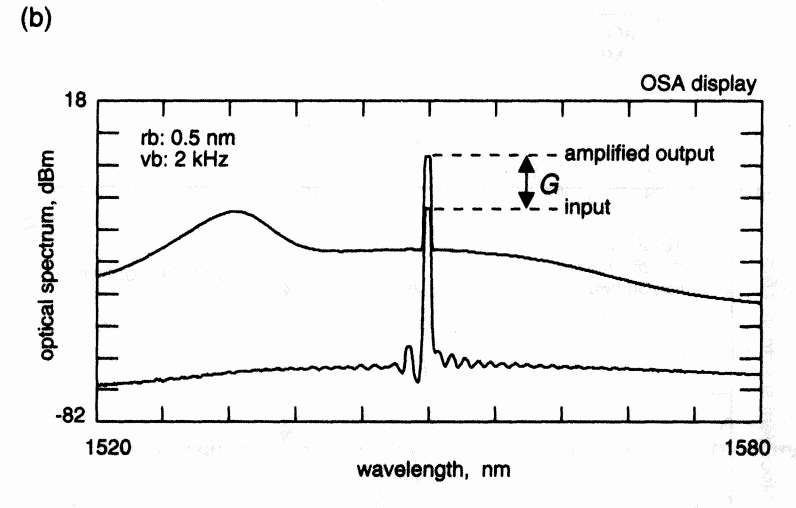


**Figure 13.25** Amplifier gain measurement using optical spectrum analyzer. (a) Measurement setup. (b) OSA display. OSA: optical spectrum analyzer.

always practical in view of measurement speed and sensitivity considerations. Actual measurements using the EELED probe technique are presented in the discussion on the time-domain extinction method for noise figure measurement.

# 13.5.2 Measurement of Noise Figure

Generally, noise figure measurements involve two activities: (1) making noise and gain measurements, (2) removing the test-system noise contribution. Before discussing some of the various techniques available to measure amplifier noise figure, it is worth discussing one of the villains that manifests its presence in electrical and optical methods: laser noise.

Source Spontaneous Emission. One of the challenges that the various noise figure characterization techniques have had to address in their evolution was how to deal with the excess noise present with optical sources. The excellent noise performance of the EDFA allows laser noise to mask the observed amplifier noise. Recall that the noise fig-

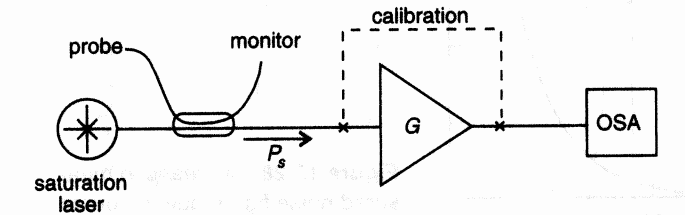


Figure 13.26 Optical amplifier gain measurement with small-signal probe combined with strong signal laser.

ure was defined in terms of a shot-noise limited source. A typical laser source, such as a DFB-LD, consists of an optical amplifier made from semiconductor material with distributed mirrors providing feedback for the lasing process. The DFB-LD internal optical gain generates ASE in the same way as the EDFA. This source noise is referred to as SSE. The SSE is broad in bandwidth, as shown in the measured DFB-LD optical spectrum shown in Figure 13.27. In addition to SSE, laser side-modes are also observed adjacent to the coherent signal. A telltale sign of imminent SSE problems is the observation of source spectral structure in the amplifier output.

Impact on Optical Methods. The optical methods of noise figure measurement rely on a measurement of the ASE density at the EDFA output. Therefore, steps must be taken to insure that SSE doesn't cause an overestimate of the amplifier noise figure. The effect of SSE on the noise figure is shown in Figure 13.28. The measured noise figure (in linear units) will be the numerical error shown in Figure 13.28 added to the actual noise

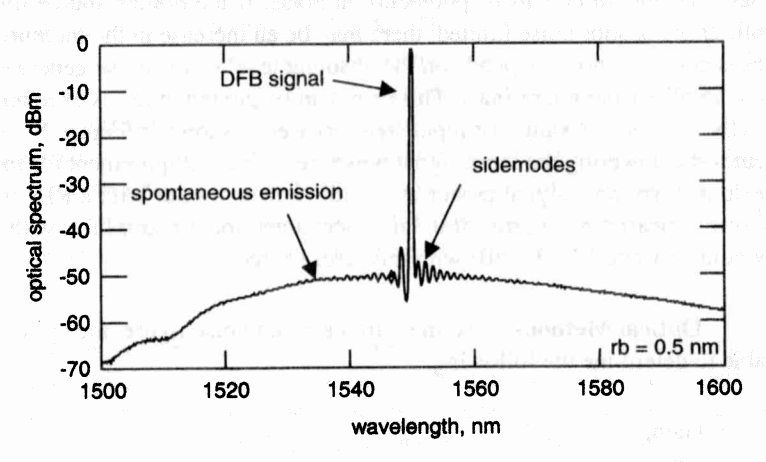
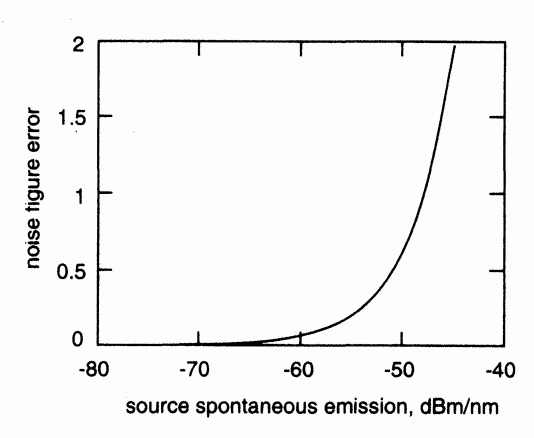


Figure 13.27 Optical spectrum of a DFB laser showing sidemodes and spontaneous emission.

Chap. 13



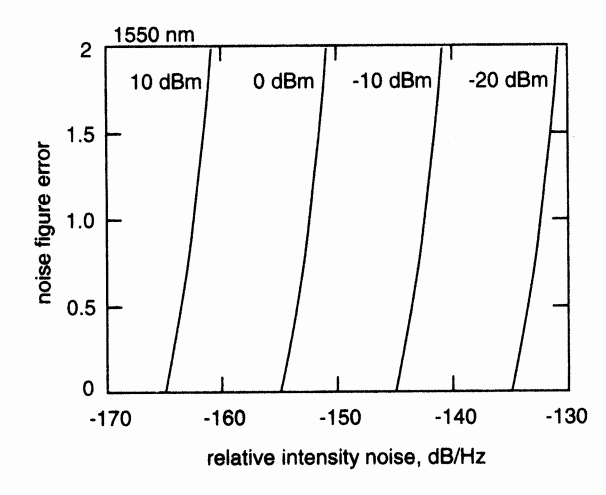
**Figure 13.28** Increase in measured noise figure due to source spontaneous emission at amplifier input.

figure. An SSE density of -50 dBm/nm will add approximately 0.6 to the actual noise figure in linear units. It is apparent that to make accurate measurements, the absolute SSE level at the input to a low-noise amplifier should be below approximately -65 dBm/nm. The -50 dBm/nm SSE level of the DFB laser shown in Figure 13.27 would create a large measurement error, if unaccounted for. The simplest method to reduce the SSE is to attenuate the source to achieve the specified measurement accuracy. The short-coming of this approach is the need to measure the amplifier response at relatively high input levels. Reducing the bias current through a semiconductor laser to lower its output power does not alter significantly the SSE generation. An optical attenuator is preferred for setting power levels because it reduces both signal and noise power.

**Impact on Electrical Methods.** The electrical methods calculate noise figure based on measurements of photocurrent noise. If the optical source illuminating the amplifier is not shot-noise limited, there may be an increase in the measured noise. The error caused by this noise depends on the absolute level of the noise generated by the source at the amplifier input terminals. This error can be plotted in terms of relative intensity noise, (RIN) for various values of input signal power as shown in Figure 13.29. The figure indicates that lowering the input signal power relaxes the requirement for the laser RIN. As an example, an input signal power of -10 dBm from a laser with a RIN of -144 dB/Hz will cause a measurement error of 0.3 if unaccounted for. An amplifier with a noise figure of 2 would measure 2.3 (3.6 dB) with this laser source.

**Optical Methods.** To measure gain and noise figure, the optical methods must be able to determine the following:

- · Gain,
- ASE spectral density,
- Wavelength.



**Figure 13.29** Noise figure error due to excess source noise in terms of RIN for different input signal power levels.

Three basic optical methods are used for noise figure measurement:<sup>38</sup> (1) source subtraction technique; (2) polarization nulling; (3) time-domain extinction or pulse method. The differences in these methods are in the ways the source SSE is accounted for and how the noise and gain are measured. The source subtraction method has the simplest setup and allows for rapid measurement of amplifier noise figure. It is best suited for single-channel environments but can be applied in WDM environments. Limitations on the spectral selectivity of OSAs make it difficult to measure close to the channel wavelength with this technique. The polarization extinction method has a more complicated setup with polarization synthesis requirements and longer measurement time. It is useful for single-channel amplifier characterization and allows for noise figure measurements close-in to the actual signal wavelength. The time-domain extinction method is useful for both single or multichannel testing of EDFAs. This method allows for noise figure measurement close-in to the actual signal wavelength and offers very rapid measurement through-put. In all the optical techniques, the amplifier ASE and gain are measured. From these measurements the noise figure is calculated according to Equation 13.35.

In the following discussions on noise figure measurement, the OSA bandwidth,  $B_o$  refers to the effective noise bandwidth of the OSA in units of Hertz. It may vary, by up to  $\sim 20\%$ , from the nominal displayed resolution bandwidth. The reader is referred to Chapter 3 for more detail on this. In the next three sections, the three optical techniques are described in detail.

Optical Source-Subtraction Method. The optical source subtraction method provides for straightforward characterization of the gain and noise figure performance of optical amplifiers. In its simplest form, the measurement setup consists of a laser to provide the input signal, and an amplitude calibrated OSA as shown in Figure 13.30. As discussed above, the SSE causes an error in the noise figure measurement. With the optical source subtraction approach, the SSE is carefully measured during calibration and later

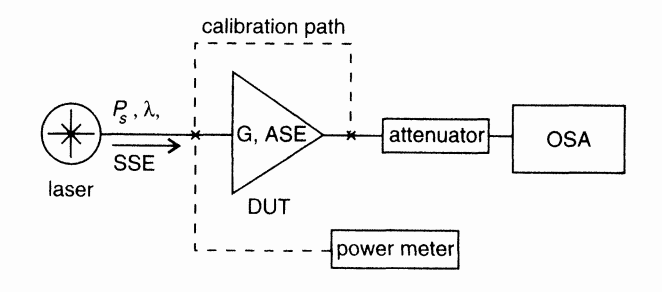


**Figure 13.30** Gain and noise figure measurement setup using the optical source subtraction method.

subtracted from the total noise emitted by the amplifier to obtain the true amplifier ASE. In the calibration sequence, the power delivered to the amplifier input connector must be determined as well as the loss from the amplifier output to the OSA.

To measure amplifier noise figure, the following quantities must be obtained:

- ν optical signal frequency
- P<sub>s</sub> signal power incident at the amplifier input
- $P_{\text{out}}$  total amplifier output power within the OSA resolution bandwidth measured at the signal wavelength including ASE and amplified SSE.
- $P_{\rm ASE}$ —total noise spectral density from the EDFA, including SSE, at the signal wavelength due to both polarizations
- $P_{\text{SSE}}$ —SSE spectral density at the signal wavelength caused by both polarizations

From these quantities, the gain and quantum-limited noise figure are calculated according to Equation 13.1 and:

$$NF = \frac{P_{\text{ASE}}}{G \, h \nu \, B_o} + \frac{1}{G} - \frac{P_{\text{SSE}}}{h \nu \, B_o} \tag{13.38}$$

noise figure - SSE correction

The last term performs the subtraction of the amplified SSE. The presence of the amplified signal prohibits the measurement of  $P_{\rm ASE}$  and  $P_{\rm SSE}$  at the signal wavelength. Interpolation is required to estimate these noise powers at the signal wavelength.

**Experiment: Interpolation-Source Subtraction.** The noise figure and gain of an EDFA was measured at a wavelength of 1.55  $\mu$ m using an interpolation technique with source subtraction to remove the effects of SSE. The setup is shown in Figure 13.30. The input signal,  $P_{in}$ , was provided by a tunable external cavity laser (HP 8168). An optical attenuator (HP 8157) reduced the high powers from the EDFA to an acceptable level for the OSA (HP 71450). The input signal, was first measured with an optical power meter (HP 8153/HP 81532A). Next the OSA and attenuator were calibrated as an ensemble by comparison with the power meter reading. The correction was +1.4 dB. The SSE was measured at the  $\pm 1$  nm offset interpolation wavelengths using the built-in noise marker func-

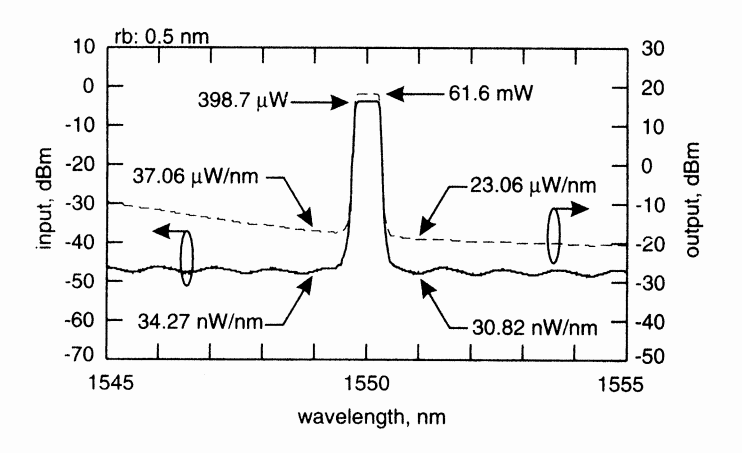


**Figure 13.31** Noise figure and gain measurement of an EDFA using the optical source subtraction method combined with ASE interpolation.

tion which refers the measured noise to a 1 nm equivalent noise bandwidth. The corrected signal input and EDFA output spectrums are shown in Figure 13.31. The attenuator was set to 20 dB when the amplifier was inserted into the measurement setup. The EDFA output ASE measurements were made at the interpolation wavelengths and the amplified signal power was measured. The resulting data is tabulated in Table 13.4 along with the noise figure computed according to Equation 13.38.

**Polarization Extinction.** The polarization extinction method offers an alternative way to reduce the error in the noise figure measurement due to SSE. An additional benefit offered by this method is that for a given OSA wavelength resolution, measurement of ASE can be performed closer to the optical carrier than with the source subtraction tech-

**Table 13.4** Noise Figure Measurement Data

Parameter	Value	Units
$P_s$ : power meter	398.7	μW
$P_s$ : OSA	306.2	$\mu \mathbf{W}$
$P_{\rm SSE}^*$	32.5	nW/nm
$P_{\mathrm{out}}^{}$ *	61.6	mW
Gain	21.9	dB
$P_{ASE}$	30.1	μW/nm
ASE density	25.1	μW/nm
Noise Figure	10.1	dB

<sup>\*</sup>With power meter correction.

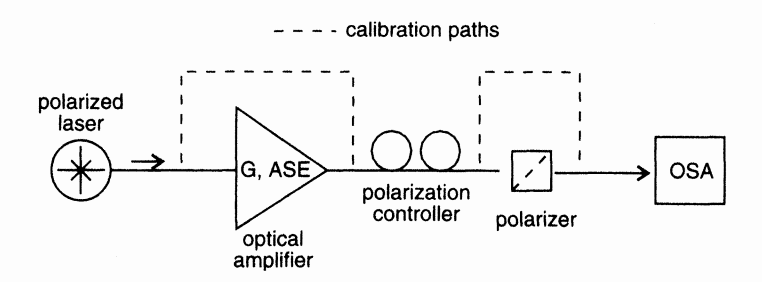


**Figure 13.32** ASE measurement setup using polarization nulling technique.

nique. A simple measurement setup to implement this technique is shown in Figure 13.32. For this technique to work, the EDFA ASE should be unpolarized and the SSE must be polarized in the same polarization state as the laser signal. The polarizer in Figure 13.32 allows separation of signal and SE according to polarization states. When the polarization controller is set to suppress the laser signal at the OSA, the SSE will also be suppressed, or extinguished over a certain optical bandwidth. Under these conditions, the OSA measures half the EDFA-produced ASE with reduced measurement corruption by SSE. To obtain the total ASE, the amplitude of the measured spectrum is multiplied by two.

The measurement is calibrated by measuring the loss from the laser to the OSA display as well as characterizing the loss of the polarizer to a signal aligned to the transmitted polarization state. With the system calibrated, the following quantities are determined:

- ν optical signal frequency
- P<sub>s</sub> signal power incident at the amplifier input
- $\bullet$   $P_{\text{out}}$  output power measured at the signal wavelength (polarizer bypassed)
- $P_{ASE}$ —total noise at the signal wavelength (polarizer bypassed)
- $P_N$  ASE power at the signal wavelength (signal nulled)

The OSA amplitude response is calibrated with an average optical power meter. OSAs with noise marker capability simplify the measurement of noise densities by automatically referring the measured noise to a 1 nm effective noise bandwidth. Often it is not practical to completely suppress the amplified signal and so some residual signal may be observed with the OSA. Thus interpolation may be required to estimate  $P_N$ , at the signal wavelength.

Once the signal and ASE powers at the signal wavelength are determined, the optical gain and noise figure is calculated according to Equations 13.1 and 13.35 where  $\rho_{ASE} = P_N/B_o$ .

**Impact of Polarization Hole-Burning.** Polarization hole-burning as discussed in Section 13.2.3 results in a lower amplifier gain in the same polarization as the saturating signal.<sup>5</sup> The gain and ASE will be larger in the polarization orthogonal to the saturating

signal polarization. Therefore a measurement of the ASE when the signal is nulled will actually be larger than the ASE in the same polarization as the signal laser. Recall that the noise figure depends strictly on the ASE in the same polarization as the signal. If polarization hole-burning is significant, noise figure measurement by polarization extinction will yield an overestimate of the actual noise figure of the amplifier.

Characterization of Gain and Noise Figure

Impact of Polarization Mode Dispersion. Polarization mode dispersion (see Chapter 12) will affect the ability of the measurement systems to reject the SSE over a broad spectral bandwidth. This is caused by the wavelength-dependent birefringence in the measurement system and test amplifier. While the polarization controller in Figure 13.32 can be set to null the signal at one wavelength, the SSE, with its large spectral extent will not be nulled across all wavelengths. A measurement of the null width of the measurement setup of Figure 13.32 is shown in Figure 13.33. In Figure 13.33a the amplifier of Figure 13.32 was bypassed and the laser was set to 1555 nm while the polarization controller was adjusted to obtain a null of approximately 60 dB at the laser wavelength. Next the laser wavelength was tuned from a wavelength of 1520 nm to 1570 nm while the OSA was set to record the maximum observed signal level (bottom trace of Figure 13.33a. Next the polarization controller was adjusted for maximum signal transmission and the laser wavelength was tuned across the band (top trace of Figure 13.33a). It is apparent that PMD in the test system limited the null-width resulting in a null depth in excess of 35 dB across most of the band.

Next the EDFA was inserted and the measurement procedure was repeated. The measured null width was considerably reduced as shown by the bottom trace in Figure 13.33b. The null width for 30 dB extinction was reduced to about 1 nm for this EDFA.

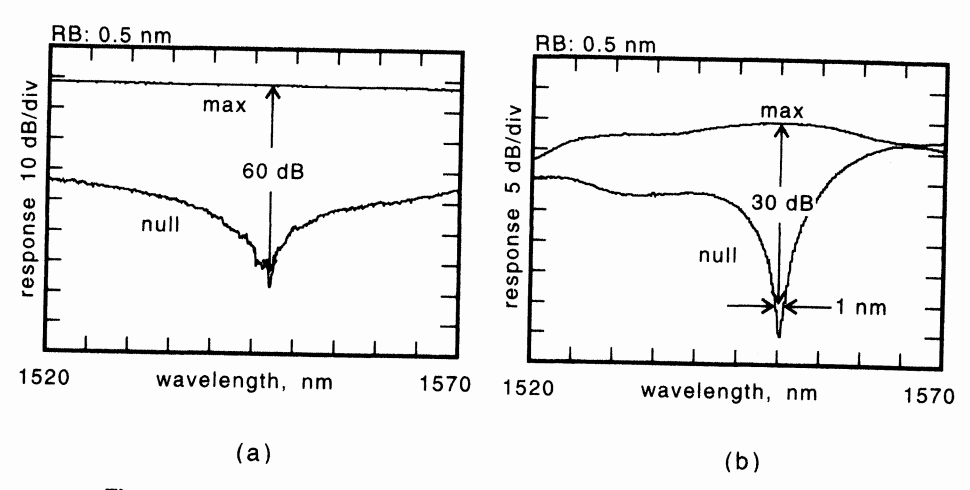


**Figure 13.33** Measurement of signal rejection using polarization extinction at a wavelength of 1550 nm (a) EDFA bypassed; (b) EDFA inserted.

The top trace corresponds to the case where the polarization controller was set for maximum signal transmission at a wavelength of 1555 nm. From the figure, it is apparent that the degree of suppression of the SSE in the noise figure measurement depends heavily on the PMD in the test system and importantly, on the EDFA. Therefore the null width and depth should be characterized to insure adequate extinction of SSE is obtained prior to the measurement of ASE.

#### **Example: Noise Figure and Gain Measurement**

The noise figure and gain of an EDFA was measured using the setup shown in Figure 13.32. The loss through the polarizer was calibrated using the unpolarized ASE from the EDFA as a signal source. The polarizer loss was measured to be 1.1 dB. Next the input signal to the amplifier was characterized by connecting it directly to the OSA, the measurement result is shown in the lower trace of Figure 13.34a. Comparison with a calibrated power meter indicated a correction of 0.47 dB to the OSA readings was required.

The SSE was found to be approximately -53 dBm in a 1 nm noise bandwidth. From Figure 13.28, at an SSE density of -50 dBm/nm (add 3 dB to the SSE since the measured ASE is multiplied by 2) the SSE will add approximately 0.6 to the measured noise figure if not rejected. The gain was measured by connecting the amplifier output directly to the OSA (polarizer was bypassed) as shown by the top trace in Figure 13.34a.

With the polarizer and EDFA in place, the polarization controller was set to maximize the signal displayed on the OSA (Figure 13.34b). This measurement provides a reference to determine the degree of polarization extinguishing achieved by the measurement setup. Next the polarization controller was set to null the signal as indicated by the lower trace in Figure 13.34b. Here the signal could not be completely nulled, thereby requiring the ASE to be estimated by interpolation. With the signal nulled, the ASE was measured at a 0.3 nm spacing from the signal wavelength as shown. While the signal null obtained was approximately

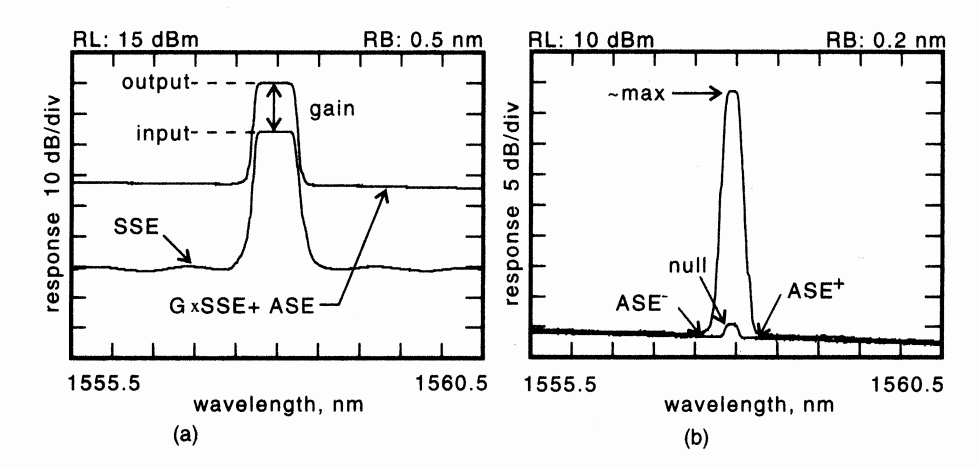


**Figure 13.34** Measurement of EDFA gain and noise performance at a wavelength of 1558 nm using polarization extinction. (a) gain (b) ASE generation.

38 dB, the finite null width limited the extinction of SSE to approximately 26 dB at the ASE measurement frequencies. According to Figure 13.28, the 26 dB rejection will make the error due to the presence of SSE negligible. Some of the measurement data and results are shown in Table 13.5.

The noise figure is calculated using the data in Table 13.6 after conversion to MKS units. The ASE density is converted to watts/Hz using Equation 13.19. The noise figure is calculated according to Equation 13.35 yielding 6.1 dB for this amplifier.

**Time-Domain Extinction/Pulse Techniques.** The slow gain dynamics of the EDFA may be used advantageously for the measurement of amplifier gain and noise figure using the time-domain extinction (TDE) technique.<sup>39</sup> In this section, the basic TDE concept will be discussed. A discussion of the transient response of the EDFA and its impact on the measurement is also given. Next the TDE method is extended to cover the measurement of dynamic gain (see Section 13.2.5) using an incoherent probe. This extended method has also been referred to as noise gain profiling.<sup>37</sup> TDE with dynamic gain-spectrum measurement enables the user to rapidly characterize the wavelength-dependent gain profile for a particular amplifier saturation condition.

**Time-Domain Extinction.** In the TDE method, the input signals, that would otherwise interfere with the measurement, are momentarily gated off.<sup>39,40</sup> The gated light is usually the signal or signals that affect the saturation level of the amplifier. By temporarily blocking the signals, several measurements can be performed: (1) measure the amplifier-generated ASE, (2) probe the amplifier with a small signal to measure the dynamic gain (noise-gain profiling).<sup>37</sup>

The basic measurement setup is shown in Figure 13.35. The cw optical saturating source leading to the amplifier is gated at frequency,  $f_{\rm TDE}$ . When the input switch (SW1 in the figure) is opened, the output switch (SW2) is closed allowing the OSA to sample the amplifier ASE output. The switching may be performed either electronically (within the laser source and the OSA) or optically (for example, using acousto-optic modulators). Since the signal is extinguished during the measurement, it does not corrupt the measure-

Table 13.5 Noise Figure Measurement Data

Symbol	Parameter	Value	Units
$\lambda_s$	wavelength	1558	nm
$P_s$	input power	70.4	$\mu W$
G	gain	38.2	linear
Δλ	interpolation offset	0.3	nm
$\rho^{+}_{ASE}$	ASE density at $\lambda_s + \Delta \lambda$	1.18	μW/nm
$\rho^{+}_{ASE}$	ASE density at $\lambda_s - \Delta \lambda$	1.25	μW/nm
$\rho^{+}_{ASE} = P_{N}/B_{o}$	interpolated ASE density	1.22	μW/nm

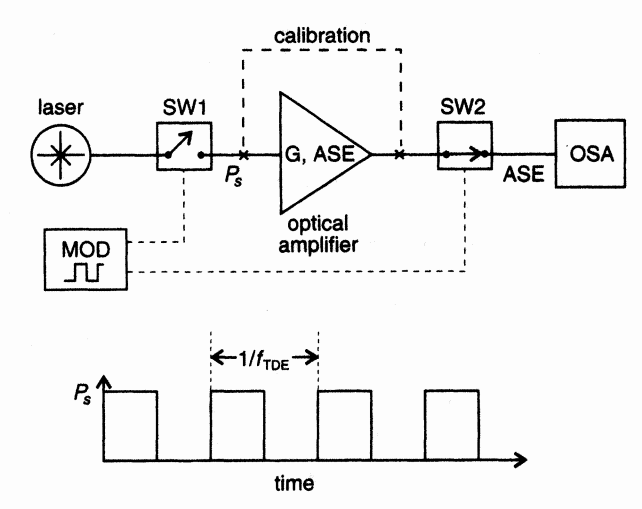
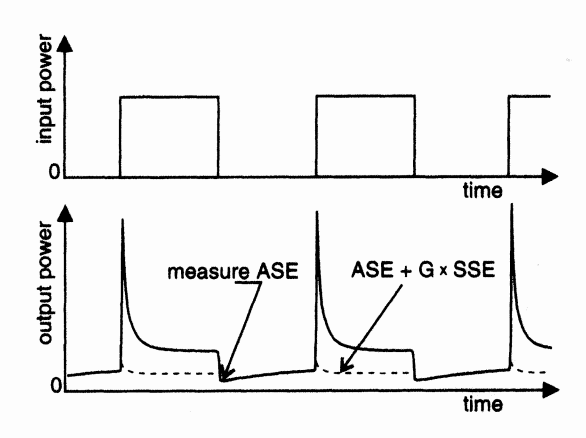


Figure 13.35 Optical amplifier ASE measurement setup for the time-domain extinction technique. OSA measures when signal is gated off. Gain measurement is performed with switches operating in unison.

ment of ASE required for noise figure calculations. This is illustrated for slow gating in Figure 13.36. Spiking in the amplifier output is observed because of the increased energy storage in the amplifier when the signal was gated off. Stimulated emission of the input signal quickly reduces the energy stored (causing spiking) to achieve a steady-state value towards the end of the gated-on period. At low repetition rates (below ~ 1 kHz) and high input powers, spiking may actually cause self-destruction of the EDFA.

When the source is gated at higher frequencies, the spiking is no longer present and the ASE follows a triangle-shaped waveform as shown in Figure 13.37. Increasing the gate frequency reduces the ASE peak-to-peak variation. In the limit of an infinite gate frequency, the triangle waveform converges to its average value. For gate frequencies above



**Figure 13.36** Input and output waveforms for low frequency timedomain extinction measurement.

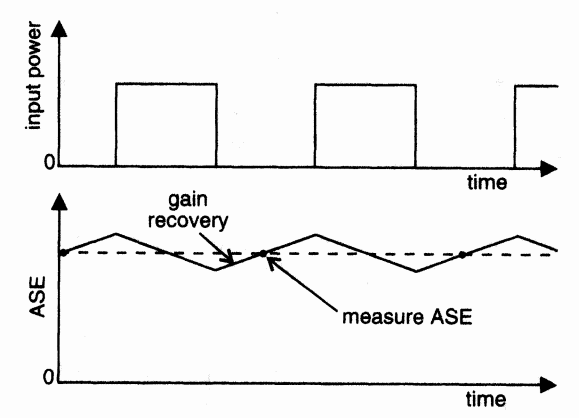


**Figure 13.37** Input and output waveforms for high frequency timedomain extinction technique.

approximately ~ 20 kHz the ASE sampled at the midpoint through the gain recovery time corresponds to the average ASE. The actual low frequency limit depends on factors such as the applied pump power to the EDFA and the presence of active control circuits for output power leveling. The effective input signal power to the amplifier is the average power of the gated signal as measured with an optical power meter. Once the ASE is determined, the amplifier noise figure is calculated according to Equation 13.35. The amplifier gain can be characterized by a variety of techniques. A broadband EELED probe technique (discussed further on) may be included in the measurement setup to provide a rapid gain measurement across many wavelengths.

**EDFA Transient Response.** The mechanisms of pump absorption, energy storage, stimulated emission, and fluorescent decay all contribute to determine the response of the EDFA to changes in signal level.<sup>4</sup> When the signal level is abruptly changed, the EDFA will slowly stabilize to a new level of gain. The recovery time after the signal is gated-off is of the order of  $100~\mu s$  but depends strongly on the EDFA pump power. In general, the recovery characteristic, measured in terms of the transient response of a small probe signal, varies approximately exponentially with time. Using the approximation:  $e^{at} \approx 1 + at$ , for small time t, the recovery will follow a linear recovery immediately after the signal is gated off. In the method discussed here, the data sampling must be made in the regime where the gain recovery varies linearly with time to obtain accurate measurements.

Characterizing the EDFA gain recovery is straightforward. The measurement setup used in the following experiment is shown in Figure 13.38. In the measurement, the counter-propagating-pumped EDFA delivered 32 mW of 1480 nm pump light to the erbium-doped amplifying fiber. Isolators at the amplifier ports shielded the unit from reflections. The saturating signal wavelength was set to 1533 nm and the input signal power was square-wave modulated. This caused gain modulation at all wavelengths in the erbium band. The gain modulation was measured with a small signal laser probe tuned to a wavelength of 1552 nm. The magnitude of the gain variation depended strongly on modulation rate as shown in Figure 13.39 where the amplified saturating signal, and the small signal probe are plotted. Where the gain perturbation is small, an expanded scale with off-

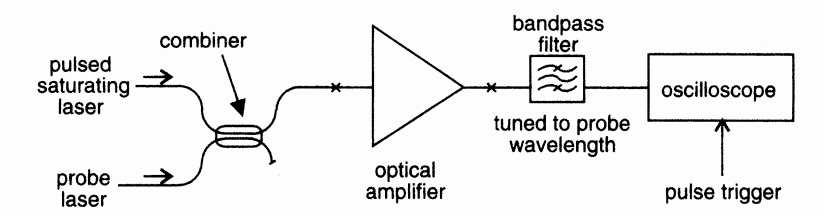


**Figure 13.38** Measurement of EDFA transient gain recovery using a pulsed saturating source and a small signal probe.

set is used to show the probe variations. As discussed above, the initial peak in the saturating signal output power at signal turn-on was caused by the higher level of inversion realized after gain recovery. The signal transient can be quite rapid, with amplifier dependent decay-time constants on the order of  $\sim 10~\mu s$ . The reduction of the probe signal gain is evident as the saturating signal depletes the erbium inversion level. As the rate of modulation is increased, the amplifier recovery is truncated, the maximum instantaneous amplifier inversion level decreases, and the gain modulation at the probe wavelength of 1552 nm decreases. With further increases in modulation rate, the gain modulation takes on a triangle waveform profile with a peak-to-peak variation decreasing with modulation rate.

Gain Recovery Errors. Proper use of the TDE method requires setting the signal gate frequency to the appropriate value. The gate frequency should be set such that the gain recovery has a linear response. If the gate frequency is set too low, the recovery is not linear as indicated by the probe gain recovery in Figure 13.39a. Deviation from a linear response leads to measurement error since the measurement at the midpoint of the gain recovery characteristic is no longer representative of the average high-frequency value.

The error caused by nonlinear gain recovery was measured for an EDFA. The results are shown in Figure 13.40 The error is defined as the ratio of the measured probe gain at the test frequency divided by the probe gain measured at 300 kHz. Below a gaterate of 10 kHz, the error significantly increases. This was performed for several different values of 1480 nm pump power incident on the erbium-doped fiber. From the data, it can be shown that the error due to nonlinear gain recovery increases linearly with pump power.

**Transient Gain Saturation.** Transient gain saturation is responsible for the spiking observed in Figures 13.36 and 13.39. This spiking does not affect the probe gain measurement, but it can impact the measured output signal power, which in turn affects the accuracy of the gain calculation. The error in the determination of output power occurs when the power is measured midway through the non-linear transient gain saturation recovery. This problem is solved by increasing the gate frequency and making an average power measurement. In practice, the gate frequency may be set appropriately by increasing it from ~ 20 kHz, until the transient gain saturation recovery becomes approximately

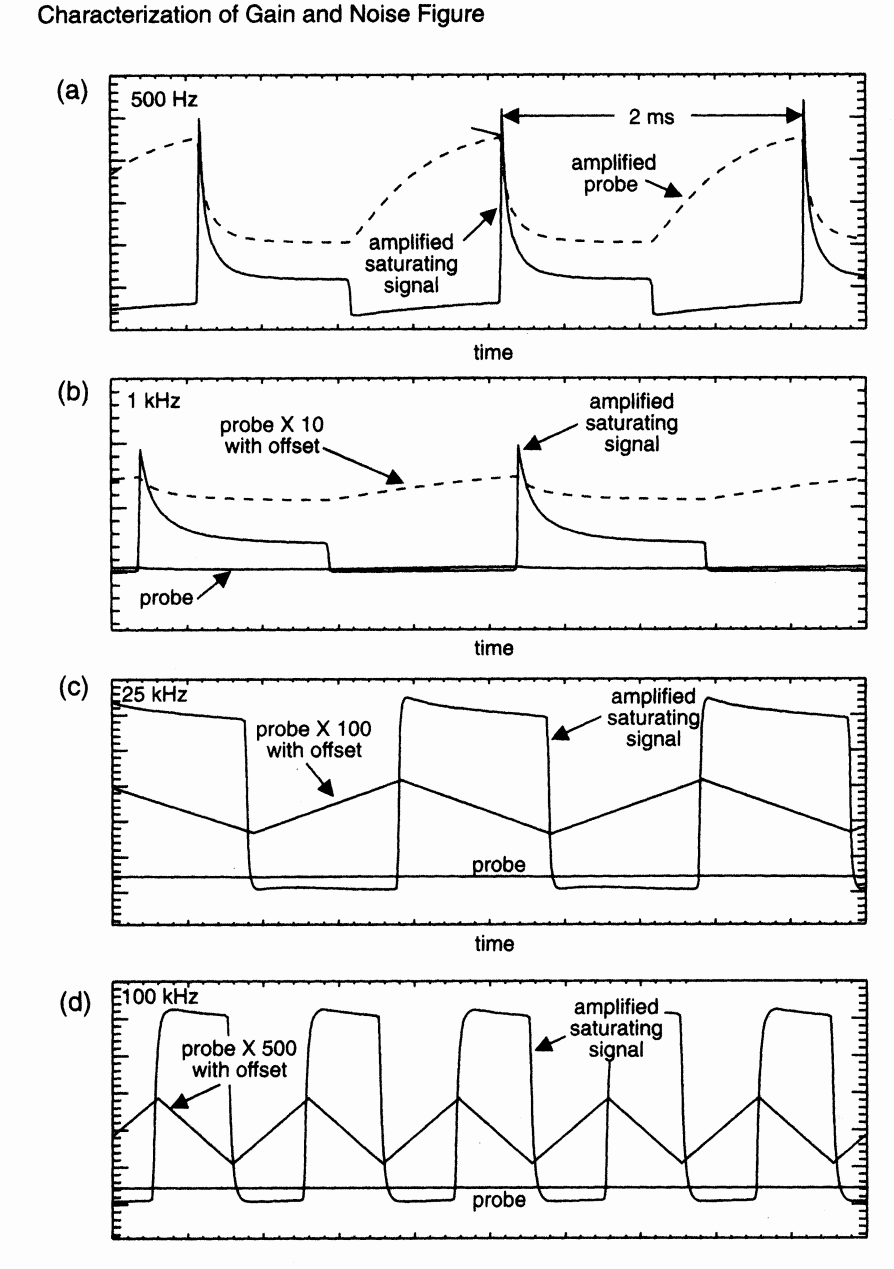


**Figure 13.39** Measurement of EDFA transient response for different gate rates. (a) 500 Hz. (b) 1 kHz. (c) 25 kHz. (d) 100 kHz.

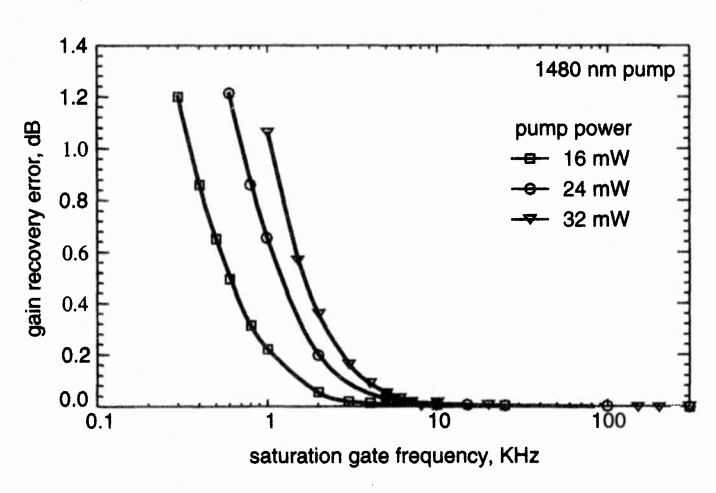
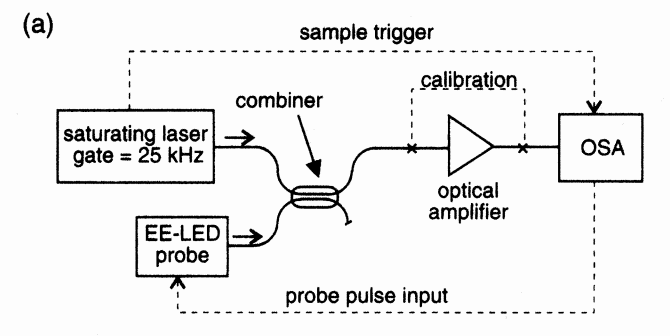


**Figure 13.40** Measured error in gain as a function of gate frequency for various EDFA pump powers.

linear. This may require an optical receiver and an oscilloscope as part of the measurement setup.

Experiment: Time-Domain Extinction with Dynamic Gain Measurement. The noise figure and the dynamic gain spectrum of an EDFA were measured for various lengths of erbium-doped fiber. The dynamic gain spectrum refers to the gain of a small signal probe, measured versus wavelength, with the EDFA saturation set by a saturating signal. The slope of the dynamic gain spectrum is the dynamic gain slope as discussed in Section 13.2.5. The measurement setup is shown in Figure 13.41a. The saturating signal wavelength and power were 1554.4 nm and 40 µW respectively. The saturating signal laser had internal pulse capability allowing its output power to be pulsed at a 25 KHz rate. The laser source (HP 8168) trigger output (synchronized with the pulse modulation) was passed to the OSA (HP 71450) to trigger the OSA's internal time-domain detection capability. This allowed the OSA to sample the optical power 10 µs after the saturating signal was extinguished. The time-domain capability of the OSA was used in place of the second switch shown in Figure 13.35. The control input to the EELED (HP 83437) allowed it to be pulsed on when the falling edge of the gated signal was detected by the OSA. By operating the EELED output in pulsed mode, the EELED average output power is reduced. This reduces the effect of the EELED power on the amplifier saturation. The timing diagram for the measurement is shown in Figure 13.41b. Initially, the measurement was calibrated by bypassing the EDFA as shown in the figure. The EELED was pulsed on by a command from the OSA and its power was measured by the OSA 10 µs after the falling edge of the saturating signal laser. This yielded the wavelength-dependent calibration  $P_{\rm cal}(\lambda)$ :

$$P_{\text{cal}}(\lambda) = P_{\text{LED}}(\lambda) \tag{13.39}$$



Characterization of Gain and Noise Figure

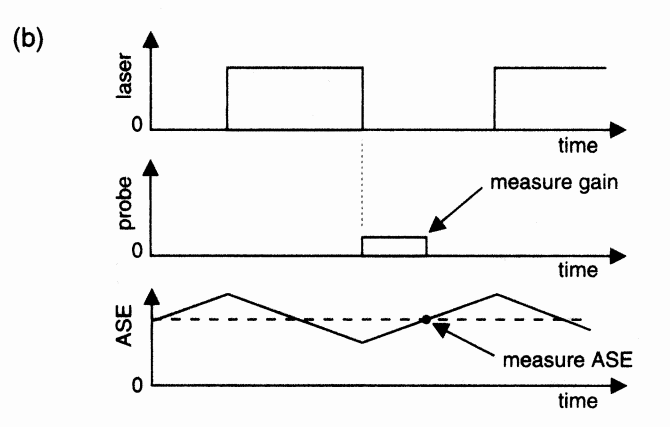


Figure 13.41 Time-domain extinction measurement with dynamic gain spectrum measurement.

(a) Measurement setup; (b) optical waveforms for saturating laser, EE-LED probe and EDFA ASE.

Next the EDFA was inserted into the test setup and the OSA measured the output spectrum ( $P_1(\lambda)$ ) 10  $\mu$ s after the saturating laser was gated off, with the EELED pulsed on. This measurement yielded:

$$P_1(\lambda) = G(\lambda) \times P_{\text{LED}}(\lambda) + P_{\text{ASE}}(\lambda)$$
 (13.40)

To solve for gain  $G(\lambda)$ , the ASE spectrum  $(P_2(\lambda))$  is measured with the EELED output off, 10  $\mu$ s after the saturating signal was gated off, yielding:

$$P_2(\lambda) = P_{ASE}(\lambda) \tag{13.41}$$

The dynamic gain spectrum is calculated according to:

$$G(\lambda) = \frac{P_1(\lambda) - P_2(\lambda)}{P_{\text{cal}}(\lambda)}$$
(13.42)

The noise figure is computed according to Equation 13.35 using Equation 13.19 and  $\rho_{ASE}(\lambda) = P_2(\lambda)/2B_o$ .

After each gain and noise figure measurement, the erbium-doped fiber in the amplifier was reduced in length. The results of the noise figure and dynamic gain spectrum for

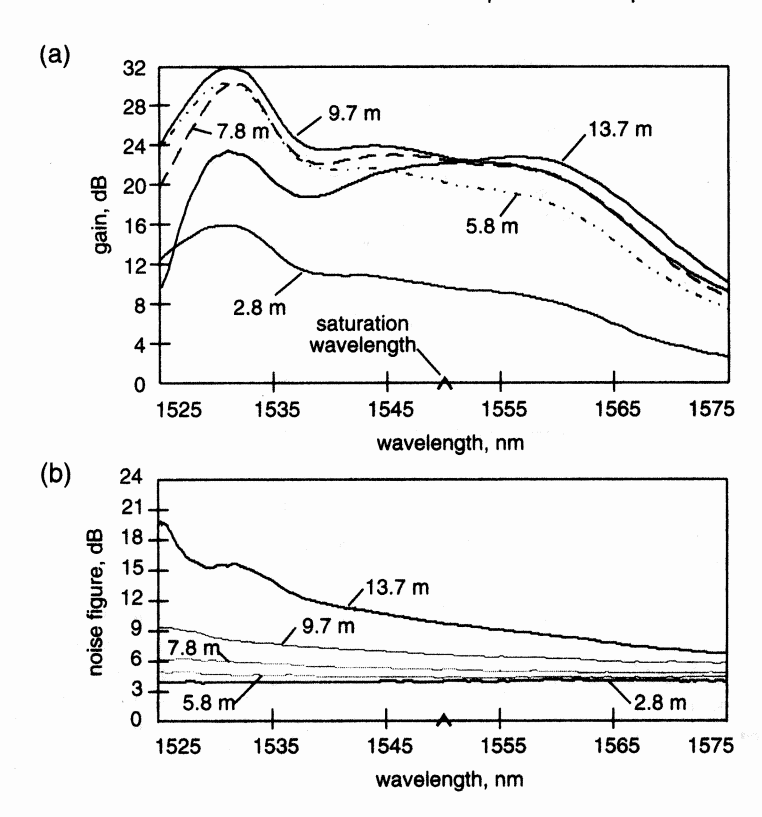
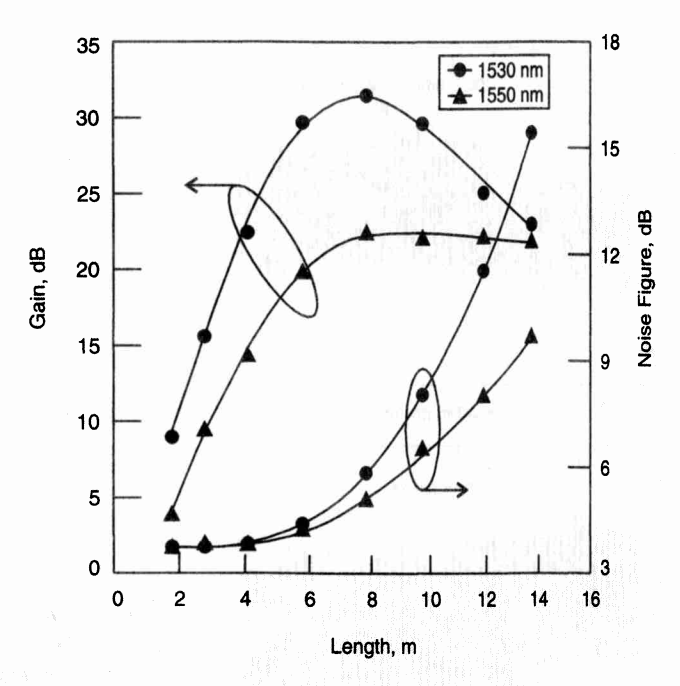


Figure 13.42 EDFA dynamic gain and noise figure measurement for various lengths of erbium-doped fiber. (a) Gain. (b) Noise figure.

the various lengths are shown in Figure 13.42. From the curves, it is apparent that the amplifier can be optimized separately in terms of maximum gain, lowest noise figure, and gain flatness. The gain and noise figure results are plotted, in Figure 13.43, versus length for the two wavelengths of 1530 nm and 1550 nm. From the figure, it is clear that the optimum gain length does not correspond to the lowest noise figure. The erbium-doped fiber length is particularly critical for low noise operation in counter-pumped amplifiers, such as the one measured here, since the noise figure depends heavily on the inversion level near the input. The sensitivity of the amplifier performance at 1530 nm to fiber length (and inversion level near the input) is a reflection of the fact that the absorption crosssection of the erbium-doped fiber peaks near this wavelength (see Figure 13.7).

WDM Characterization. Wavelength division multiplexed (WDM) transmission is a versatile method to increase the transmission capacity of singlemode optical fiber. Laboratory experiments using WDM have demonstrated over 2.6 Tb/s transmission capacity along a single fiber. In Figure 13.44, the input and output spectrums are shown for a very dense 1.1 Tb/s WDM transmission experiment using a transmitter composed of



Characterization of Gain and Noise Figure

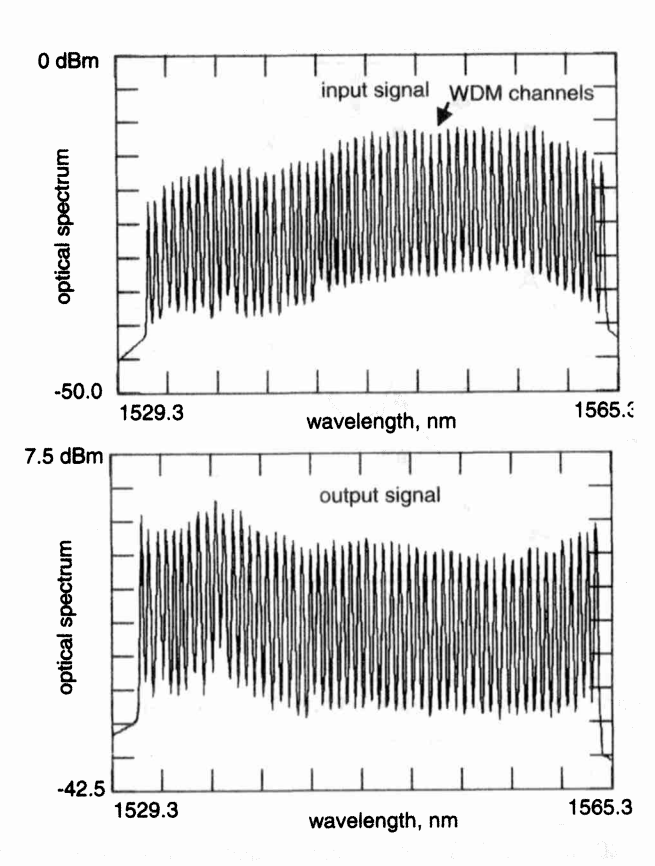
Figure 13.43 Gain and noise figure versus erbium-doped fiber length at the wavelengths of 1530 nm and 1550 nm.

55 lasers, each modulated at a 20 Gb/s rate. 41 The wavelength range of the lasers spanned most of the EDFA gain range from 1529 nm to 1565 nm as shown in the figure. Qualification of EDFAs for WDM applications will require measurement of gain and noise figure over a broad range of wavelengths. In principle, characterization of EDFAs for the WDM environment is an extension of the techniques used for single wavelength test. In WDM gain characterization, the optical gain is measured at each channel wavelength for a set of input conditions. The input conditions include the channel powers and wavelengths or "events" such as an added or dropped channel.

One of the principle challenges for making WDM noise figure and gain measurements is the required assembly of the large numbers of lasers. This process can be complex and costly to maintain. Measurement of the ASE generation at a specific wavelength also becomes more difficult as channel spacings become narrow.

In this section, the TDE method combined with dynamic gain-spectrum measurement is discussed for characterization of WDM gain and noise figure. The polarization extinction method is not covered since polarization nulling of a large number of wavelength channels is time-consuming and not practical due to the polarization-mode dispersion (PMD) effects discussed in Section 13.5.2.

The source-subtraction technique may be used for WDM characterization of EDFAs. Careful attention to the stability of the WDM lasers, and the effects of overlap-



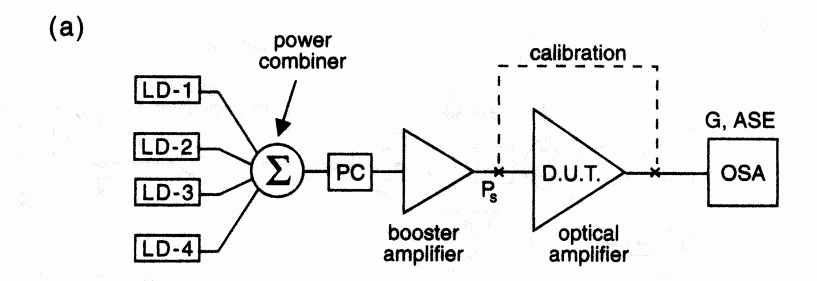
568

Figure 13.44 Optical spectrums for a 1.1 Tb/s 55 channel WDM transmission experiment: (a) input signal (b) output signal after passage through 150 km optical fiber containing two EDFAs. (With permission, after ref [41] ©1996, Optical Society of America.)

ping SSE from the WDM lasers at the measurement wavelength are required. Because of the similarities with the single-channel method, the reader is referred to the discussion on source-subtraction in Section 13.5.2.

A method allowing the same EDFA saturation effects due to multiple WDM channels while using fewer saturating signal lasers will be presented. This allows a significant simplification of the test system while maintaining amplifier conditions similar to those encountered with the actual number of channels.

Multichannel Method. The EDFA gain is measured by comparing the input and output powers at each channel wavelength. This is similar to the methods used for the single channel case discussed earlier. Instead of gating a single laser, for multichannel TDE test, all the lasers in the WDM transmitter are synchronously gated. The addition of the small signal probe, as discussed in Section 13.5.2 permits measurement of the dynamic gain spectrum allowing gain shape measurement between the WDM channels. The multichannel TDE method with the small-signal gain probe will be compared to the multichannel spot gain measurement method in an experiment with a four channel WDM source.



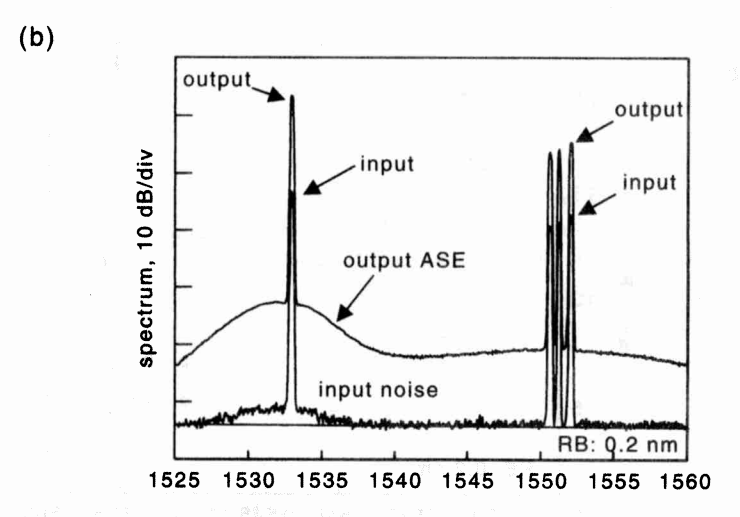
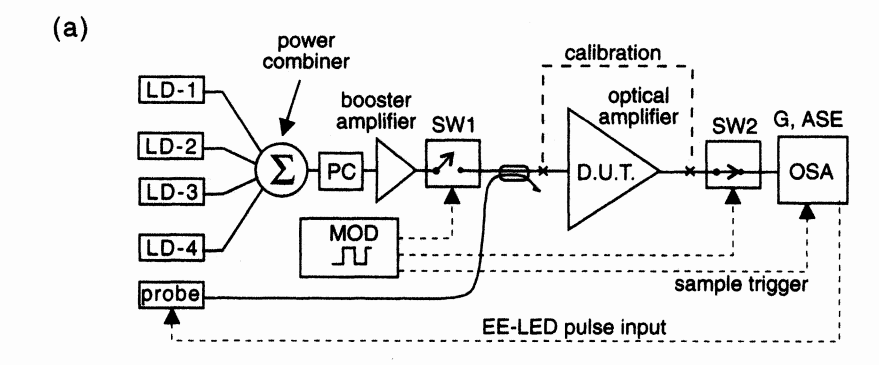
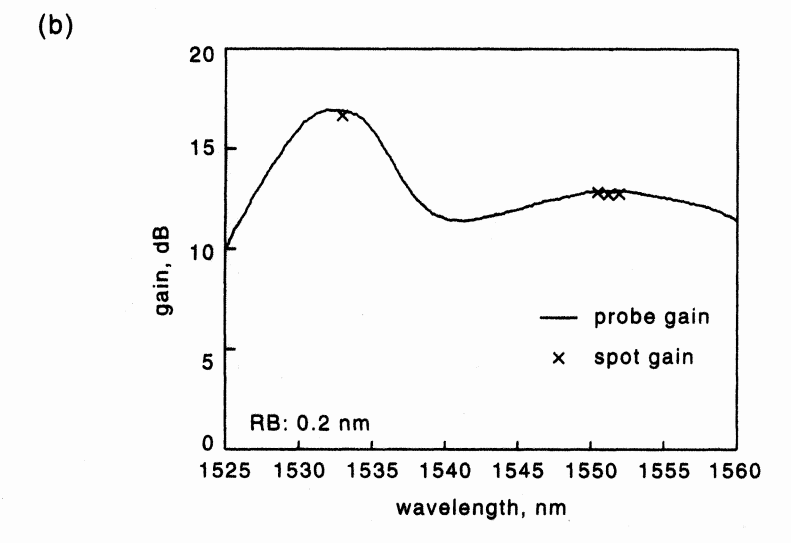


Figure 13.45 Multichannel gain measurement of an EDFA: (a) measurement setup, (b) optical spectrums of input and output signals.

**Experiment: WDM Multichannel Gain.** The gain of an EDFA was measured two ways. The setup shown in Figure 13.45a was used in the first experiment to measure the EDFA spot gains at each channel wavelength. Four lasers were combined using fused-fiber directional couplers. The polarization controller (HP 11896A) was set to randomly vary the light-combined lasers. The EDFA booster amplifier compensated for the optical loss (~8 dB) incurred in the power combiner. An OSA measured the optical power spectrums of the input signal to the EDFA and the amplified output spectrum. The input and output spectrums are shown in Figure 13.45b. The EDFA gains at the signal laser wavelengths of 1533.0 nm, 1550.5 nm, 1551.1 nm, and 1552.0 nm were measured to be 16.65 dB, 12.79 dB, 12.70 dB, and 12.65 dB respectively.

In the next experiment, the EDFA gain is measured with a multichannel TDE method using a small-signal probe. The experiment setup is shown in Figure 13.46a. FC/PC connectors were used to connect to the EDFA. The input signal powers and wavelengths were the same as with the previous measurement. An EELED was used as a small





**Figure 13.46** Four-channel WDM gain using time-domain extinction with a multichannel stimulus and small signal probe: (a) measurement setup, (b) dynamic gain measurement.

signal probe to measure the wavelength-dependent dynamic gain. The optical switches (acoustooptic modulators) were driven by two pulse generators. One pulse generator provided the trigger for the second pulse generator and the sampling trigger of the OSA (HP 71450). The OSA provided a signal to pulse the EELED output power as discussed in Section (13.5.2). The combination of the optical switch at the EDFA output and the time-domain capability of the OSA resulted in complete extinction of the amplified four-channel WDM source. This permitted a continuous measurement of the EDFA gain across the measurement range as shown in Figure 13.46b. The spot gains measured in the first experiment are plotted in Figure 13.46b for comparison. The two measurement tech-

niques agreed to  $\sim 0.2$  dB. This agreement is within the uncertainty of the connector insertion loss.

Multisource Approximations. For multichannel measurements, such as those required for WDM applications, the cost and complexity increases with the number of channels. In situations where the test cost/complexity are excessive, an approximate method may be considered. The reduced-source approximation can be considered for testing EDFAs in WDM applications. The assumption behind this method is that the amplifier gain spectrum, or at least some portion of it, is homogeneously broadened. In EDFAs, homogeneous broadening has been shown to be predominant. This is another way of saying that the gain saturation caused by a signal at any wavelength in the EDFA gain band reduces the amplifier inversion (common energy reservoir) responsible for gain at all other wavelengths.

It has been shown that spectral hole-burning (SHB) exists in EDFAs to a small degree. To the extent that within a given bandwidth, SHB is insignificant, a single source can represent the ensemble of signals found in the spectral interval. This concept is shown in Figure 13.47. Recall from Equation 13.9 that the gain depends on the metastable state population,  $N_2$ . The  $N_2$  population level defines the operating state of the amplifier. To mimic the effects of several channels, the representative source method must place the amplifier in the same state that would exist if the channels were actually present. This yields a requirement on the amplifier inversion level for the two cases

$$N_{2, rs} = N_{2, wdm} ag{13.43}$$

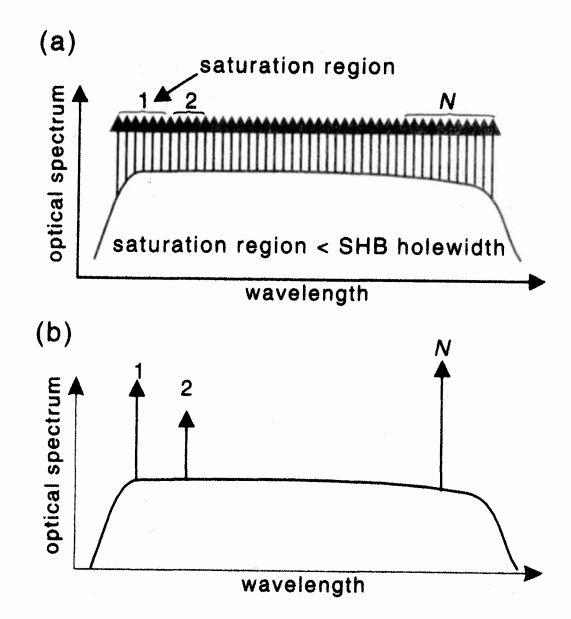


Figure 13.47 Reduced source concept for multichannel gain characterization. Homogeneous broadening across an interval permits representation of multiple signals with a single source.

Chap. 13

where  $N_{2,rs}$  is the inversion level established with the reduced set of saturating signal sources and  $N_{2,wdm}$  is the inversion level established in the presence of all the WDM channels. The steady-state population  $N_{2,wdm}$  is derived from a generalization of Equation 13.5 to include multiple signal beams. Equating the excited state populations in the two experiments places conditions on the reduced-source power and wavelength to achieve the best simulation of WDM amplifier performance. This leads to the following requirements for the optical power from a single source to simulate the effects of a cluster of WDM sources about the single source wavelength.<sup>42</sup>

$$P_s = \frac{1}{\lambda_s G_s} \sum_n P_n \lambda_n G_n \tag{13.44}$$

where  $P_s$  and  $P_n$  are the input single-source and WDM-input channel powers, respectively. The single-source wavelength can be set on the basis of the weighted wavelength

$$\lambda_s = \frac{1}{G_c P_s} \sum_n P_n \lambda_n G_n \tag{13.45}$$

In Equations 13.44 and 13.45, the channel gains are not known initially. Therefore  $G_n$  may be set equal to  $G_s$  as a starting guess to set the initial values for  $P_s$  and  $\lambda_s$ . After the dynamic gain spectrum is measured, better estimates of  $G_s$  and  $G_n$  are obtained. The measurement procedure converges in about two iterations.

**Experiment: Single-Source WDM Gain.** The single-source and multichannel WDM gain methods are compared for a four-channel WDM system. <sup>42</sup> The WDM gain measurement was performed with four independent channels combined through a power combiner as shown in Figure 13.46. The channel powers and wavelengths were: 41.1  $\mu$ W, 1549.6 nm; 39.9  $\mu$ W, 1553.0 nm; 35.1  $\mu$ W, 1555.9 nm; and 33.9  $\mu$ W, 1558.2 nm. Calibration was performed by bypassing the EDFA. In the reduced-source method, a single saturating source was combined with an EELED-ASE source as shown in Figure 13.48. Both the saturating laser (HP 8168) and the OSA (HP 71450) detection circuitry had gating capability which eliminated the need for external optical switches. The EELED (HP 83437) and saturating laser were pulsed using the noise-gain probe

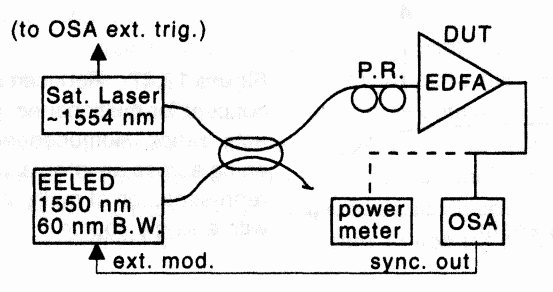


**Figure 13.48** Measurement setup using a single laser to represent four channels. P. R.: polarization randomizer.

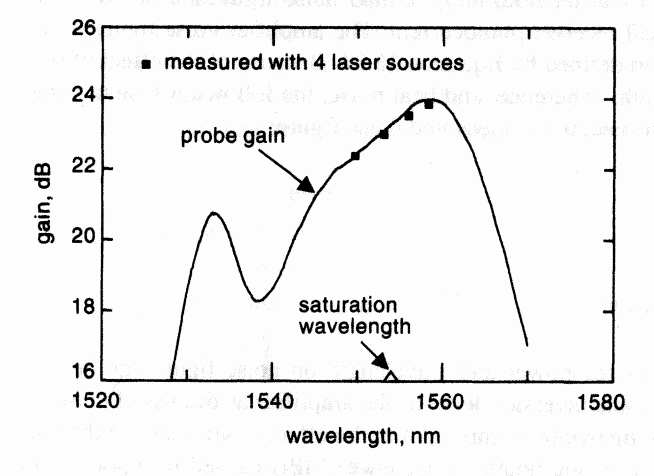


Figure 13.49 Comparison of fourchannel WDM gain measurement using four lasers and a single laser with an EE-LED probe.

method described for the TDE technique (Section 13.5.2). The measurement results comparing the four-channel stimulus to the reduced source method with a noise-gain probe are shown in Figure 13.49. The two measurements agree well. There was a maximum of 0.2 dB difference at the third-channel wavelength.

In choosing the number of channels for the reduced source method, the following factors will come to bear:

- · Degree of inhomogeneity in the amplifier saturation,
- · Total power represented by each reduced-source channel,
- WDM channel spacings.

If the amplifier gain is determined to be completely homogeneously broadened, then a single channel will be sufficient to set the saturation. If inhomogeneous broadening (SHB) is significant and the reduced-source stimulus power becomes large to accommodate the ensemble of WDM channels, a spectral hole will reduce the probe gain in the vicinity of the saturation wavelength. In the wavelength band near 1.55  $\mu$ m, the FWHM SHB hole-widths in EDFAs are  $\sim 8$  nm which allows the use of fewer saturating signals than at a wavelength of 1.53  $\mu$ m where the hole-width is  $\sim 4$  nm. Finally, the combination of amplifier inhomogeneity and wide WDM-channel spacings may necessitate multiple sources for the reduced source set to best replicate the amplifier saturation. Ultimately, prior to the application of this technique, a comparison must be made with a complete WDM source to authenticate the measurement. Any significant difference between the measurements could serve as a correction factor for the reduced source method.

Electrical Methods. Noise figure measured by the electrical method is generally perceived to be a more complete measure of the intensity noise generated by the optical amplifier. It includes effects such as sig-sp beat noise, sp-sp beat noise, and multipath in-

terference noise. In the electrical method, the gain and noise figure are derived from a spectral analysis of the optical receiver photocurrent. The amplifier noise figure is calculated with the general relation defined by Equation 13.34. Because of the effect of source noise, laser power, wavelength, coherence, and beat noise, the following system parameters must be specified with respect to the measured noise figure:

- Source power,
- · Source wavelength,
- · Source linewidth, and
- · Receiver optical bandwidth.

The influence of the source power and wavelength on noise figure can be understood from their influence on the inversion level of the amplifier as discussed in Sections 13.2, and 13.3.1. The source linewidth is important in the effect it will have on the phase-to-intensity noise conversion, or multipath interference (MPI) caused by optical reflections within the EDFA as discussed in Section 13.3.2. Equations 13.31 through 13.33 indicate that the MPI-induced noise varies with the source linewidth, the reflection magnitudes as well as the time delay between the optical reflections. The source linewidth is specified as a stimulus parameter. The receiver optical bandwidth determines the spectral width of the ASE incident on the photodetector. This affects the contribution that the sp-sp beat noise will make to the measured noise. Additionally, the optical filter bandwidth determines the ASE shot noise and the spectral extent of the sig-sp beat noise in the photocurrent power spectrum. Normally this is not observed unless wide bandwidth optoelectronic detection (> 50 GHz) is used along with narrow optical filtering (< 1 nm).

Accurate noise figure measurements require that careful attention is placed on the effect of excess source laser noise, test system MPI noise, and receiver thermal noise. The amplifier noise figure should not depend on these noise contributions. Effects such as the source optical linewidth and the receiver optical bandwidth can result in measurement ambiguities which must be fully specified in the actual measurement. The power levels measured on the electrical spectrum analyzer must be calibrated to an absolute standard to obtain meaningful results. Two methods for this purpose are discussed: the RIN transfer technique and the IM index transfer technique.

To measure the amplifier noise figure the following must be determined:

- · Gain,
- Input power,
- Intensity noise density produced by the amplifier:  $S_P(f)$ , and
- Photon energy.

The gain, input power and photon energy (or wavelength) are assumed to be known according to the methods discussed in Section 13.5.1 and Chapter 3. The principal task is to determine the spectral density of the amplifier intensity noise,  $S_p(f)$ . Low-noise optical amplifiers are designed to minimize  $S_p(f)$ .

Measurement of Optical Amplifier Noise. In this section, a method is discussed to separate the optical amplifier excess noise,  $S_P(f)$ , from the total noise spectrum given by an electrical spectrum analyzer. The corrupted noise spectrum refers to the optical-amplifier-generated noise, plus the other noise sources or effects that originate from the test system. The basic steps in the noise measurement procedure are<sup>43</sup>:

- · Calibrate receiver,
- Measure the corrupted amplifier noise spectrum,
- · Remove thermal noise,
- Remove measured shot noise, and
- Calculate  $S_{P}(f)$ .

A test system for measuring optical amplifier noise is shown in Figure 13.50. There are a number of factors affecting the measured data as shown in the figure. The receiver thermal noise, detected shot noise, and frequency response of the system will contribute to measurement error. The amplifier noise must be separated from the total measured noise.

The electrical spectrum analyzer display is proportional, by way of  $|k(f)|^2$  to the power spectrum of the photocurrent. The bandwidth limitations of the photodetector and electronics are included in  $|k(f)|^2$ .

With the amplifier under test illuminated by the an optical source with the required wavelength, power and linewidth, the measured photocurrent power spectrum  $S_{\rm ESA}(f)|_{\rm mea}$  is described by:

$$S_{\text{ESA}}(f)|_{\text{mea.}} = |k(f)|^2 [\Re^2 S_P(f) + S_i(f)|_{\text{shot}}] + S_{\text{ESA}}(f)|_{th} [\text{W/Hz}]$$
 (13.46)  
(measured noise = excess noise + shot noise + thermal noise)

The terms on the right-hand-side correspond to the excess noise contributions of the optical amplifier, the photocurrent shot noise, and the thermal noise. In an ideal measure-

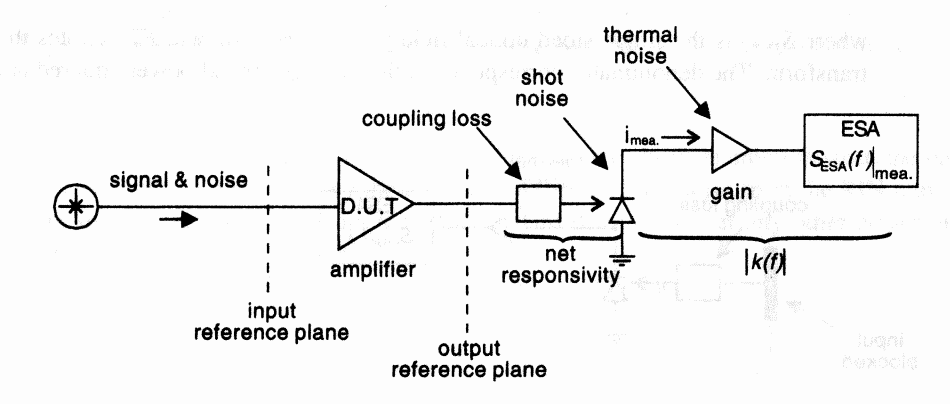


**Figure 13.50** Basic measurement setup for measuring optical amplifier noise using the electrical method. ESA: electrical spectrum analyzer.

ment, the thermal noise would be negligeable and  $|k(f)|^2$  would be the reference resistance,  $R_{\rm ESA}$ , of the electrical spectrum analyzer, which is typically 50  $\Omega$ .

**Thermal Noise Correction.** The thermal noise density,  $S_{\rm ESA}(f)|_{th}$  is measured with the input light blocked as shown in Figure 13.51. Under the assumption that the thermal noise density is independent of the magnitude of the optical signal, it is measured by completely blocking the light from the photodetector. The measured thermal noise spectrum is denoted by  $S_{\rm ESA}(f)|_{th}$ . Subtracting the density  $S_{\rm ESA}(f)|_{th}$  from  $S_{\rm ESA}(f)|_{\rm mea}$  performs the thermal noise correction.

RIN Transfer: System Transfer Function Correction. The frequency dependent system transfer function,  $|\Re k(f)|^2$  is measured next. A calibrated source of excess optical noise replaces our source (for example, amplifier) under test. The setup with the calibration source is shown in Figure 13.52. This step is referred to as a RIN transfer calibration since the optical noise source is characterized by a RIN which is very stable over time. A practical way to implement the noise source is to optically filter the ASE from an EDFA. A typical filter bandwidth is of the order of 1 nm. This will yield a flat intensity noise spectrum up to  $\sim 2$  GHz. The RIN associated with the filtered ASE source is not required to be flat for the calibration to be valid. The only requirements are that the RIN caused by the standard is large compared to the receiver thermal and shot noise, and that the frequency dependence of the RIN is known.

The RIN associated with the filtered source can be derived from an analysis of the optical intensity associated with the filtered optical field spectrum. For an arbitrarily shaped, bandwidth-limited unpolarized ASE source, the frequency-dependent RIN is given by:

 $RIN_{cal}(f) = \frac{FT \Big[ |FT^{-1} \{ S_E(\nu) \}|^2 \Big]}{\Big[ \int S_E(\nu) \, d\nu \Big]^2} \quad [Hz^{-1}]$  (13.47)

where  $S_E(\nu)$  is the single-sided optical field power spectrum, and FT denotes the Fourier transform. The denominator corresponds to the average optical power-squared and the nu-

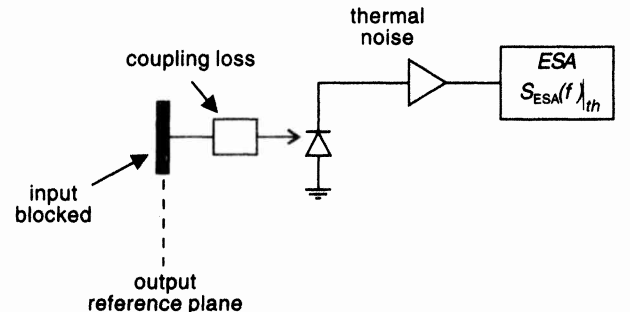


Figure 13.51 Measurement of receiver system thermal noise.

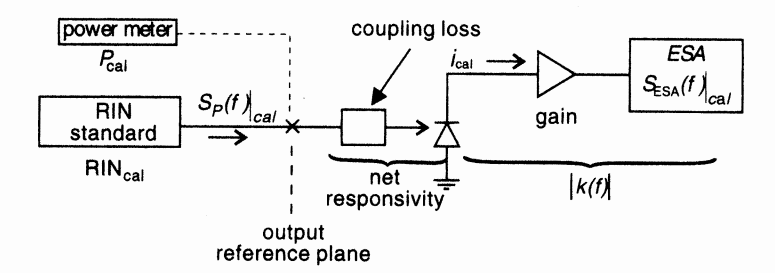


Figure 13.52 RIN transfer technique for receiver calibration.

merator corresponds to the expected spontaneous-spontaneous intensity beat noise. The absolute RIN is determined from a simple measurement of the optical field spectrum using an OSA. The RIN must be calculated numerically, except when the filtered ASE shape follows simple functional forms such as those given in Table 13.2. The RIN depends only on the shape of the ASE spectrum and not on the absolute amplitude. This results in a very stable RIN transfer standard since the bandwidth of the optical filter is fixed.

When the RIN transfer standard is combined with a calibrated optical power meter, the filtered ASE source provides an absolute spectral noise power reference according to Equation 13.23. The two fundamental quantities for the reference are the RIN of the filtered ASE source and the average power. The average power measurement is performed accurately with an optical power meter. Thus, according to Equation 13.23, the absolute optical noise reference density is:

$$S_p(f)|_{\text{cal}} = \text{RIN}_{\text{cal}}(f) \times P_{\text{cal}}^2 \quad [W^2/\text{Hz}]$$
 (13.48)

Where  $P_{\rm cal}$  is the RIN standard average output power measured with an optical power meter.

The electrical spectrum analyzer measures the photocurrent noise spectrum  $S_{ESA}(f)|_{cal}$  due to the RIN transfer standard. Using Equation 13.46, the spectral density is:

$$S_{\text{ESA}}(f)|_{\text{cal}} = |\Re k(f)|^2 S_P(f)|_{\text{cal}}$$
 (13.49)

The thermal and shot noise are not included in the above expression since the photocurrent noise is dominated by the detection of the intensity noise from the RIN transfer standard. The excess noise from the RIN standard dominates over any other noises present.

The unknown calibration constant is found according to:

$$|\Re k(f)|^2 = \frac{S_{\text{ESA}}(f)|_{\text{cal}}}{S_P(f)|_{\text{cal}}}$$
(13.50)

With this second calibration step, the system transfer function is now known across the frequency range of interest.

Introduction

Correcting the Shot Noise. The actual receiver shot noise must be corrected to obtain the shot noise that would be produced by an ideal receiver according to the noise figure definition given in Equation 13.34. The differences between the actual receiver shot noise and the shot noise obtained with an ideal receiver are caused by the optical coupling loss to the receiver and the limited quantum efficiency of the actual receiver photodetector. The correction procedure subtracts out the measurement system shot noise from the measured noise and adds the shot noise generated by an ideal receiver to the amplifier noise measurement.

The photocurrent spectrum of the shot noise in the measurement receiver is given by Equation 13.25. The DC responsivity R must be found to complete the shot noise subtraction. Two measurements are required to determine R. The setup for the system transfer function measurement shown in Figure 13.52 is used. The average photodetector current,  $i_{cal}$ , is measured. The other required measurement,  $P_{cal}$ , was already performed (see Equation 13.48). This data permits determination of the net DC responsivity according to:

$$\Re = \frac{i_{\text{cal}}}{P_{\text{cal}}} \tag{13.51}$$

At this point, the calibration process is complete. The next step is to use the calibration data to determine the optical amplifier noise.

Corrected Amplifier Noise. Equation 13.46 can be solved for the unknown intensity noise  $S_{P}(f)$ :

$$S_{P}(f) = \frac{S_{ESA}(f)|_{mea} - S_{ESA}(f)|_{th}}{|\Re k(f)|^{2}} - \frac{2qi_{mea}}{\Re^{2}}$$
(13.52)

Equation 13.52 indicates the need for the three operations discussed: thermal noise correction, amplitude frequency response correction, and shot-noise subtraction.

Inserting the calibration coefficients given by Equations 13.50 and 13.51 into 13.52, the excess amplifier noise is found in terms of measured parameters:

$$S_{P}(f) = \frac{S_{ESA}(f)|_{mea} - S_{ESA}(f)|_{th}}{\frac{S_{ESA}(f)|_{cal}}{RIN_{cal}(f) P_{cal}^{2}}} - \frac{2qi_{mea}}{\left(\frac{i_{cal}}{P_{cal}}\right)^{2}} [W^{2}/Hz]$$
(13.53)

This equation is one of the principle results of this section. It shows how the intensity noise  $S_p(f)$  (excluding shot noise) from the optical amplifier under test is found by making measurements of: (1) the uncalibrated measurement of the amplifier noise  $S_{\rm ESA}(f)|_{\rm mea.}$  and photocurrent  $i_{\rm mea.}$ ; (2) the thermal noise; and (3) the average optical power  $P_{\rm cal}$  and DC photodetector current  $i_{\rm cal}$  when the receiver is connected to the calibrated noise standard. The measurement data and calibration coefficients are summarized in Table 13.6

In the preceding analysis, the effective system quantum efficienty  $\Re$  was frequency independent. All frequency-dependent system effects have been confined to the electronics which includes transit time effects in the photodetector and bandwidth limitations in **Table 13.6** Variable Definitions for Equation 13.53.

Symbol	Description	Units
$S_{P}(f)$	Spectral density of optical intensity noise	W <sup>2</sup> /Hz
$S_{ESA}(f) _{mea}$	Uncorrected amplifier noise spectrum	W/Hz
$S_{ESA}(f) _{th}$	Electrical spectrum analyzer noise with input light to photodetector blocked	W/Hz
$S_{ESA}(f) _{cal}$	Electrical spectrum analyzer noise data with RIN-transfer source applied to measurement system input	W/Hz
$RIN_{cal}(f)$	RIN-transfer standard	$Hz^{-1}$
Pcal	Average power of RIN-transfer standard	W
$P_{dc}$	Average amplifier output power	W
$i_{ m cal}$	Average photocurrent produced by RIN-calibration standard	Α
q	Elementary electronic charge: $1.602 \times 10^{-19}$	coul.

the electronics. Therefore, the test system must be free from optical reflections which could create significant amplitude ripple, otherwise the measurement technique should be modified to account for the system interference effects. The effect of the reflections between the amplifier and receiver will be to impart a frequency ripple onto the intensitynoise spectrum and to convert source laser phase noise to amplitude noise. Therefore, it is wise to use low-reflection connections and an optical receiver with a low optical backreflection.

Calculation of Noise Figure. The amplifier noise figure defined in Equation 13.34 requires the determination of the amplifier input and output SNRs. The input SNR is calculated on a shot-noise basis. The output SNR is computed based on the photocurrent signal and noise created in an ideal receiver illuminated by the amplified signal GP. and the amplifier excess noise  $S_P(f)$  obtained from Equation 13.53. The ideal receiver has a flat frequency response, no thermal noise, and unity quantum detection efficiency  $(\mathcal{R}_{ideal} = q/hv).$ 

**Input SNR.** The shot-noise density given by Equation 13.25 is multiplied by the detection bandwidth B<sub>e</sub> to obtain the mean-squared shot noise. The input SNR is calculated by taking the ratio of the signal-to-noise powers at the ideal receiver electrical output:

$$SNR_{in} = \frac{\Re_{ideal}^2 P_s^2}{2qi_{dc}B_e} = \frac{P_s}{2hv B_e}$$
 (13.54)

Output SNR. The output noise density of the ideal receiver is the sum of the contributions from the amplifier generated noise  $S_{P}(f)$ , and the shot noise:

$$S_i(f) = S_i(f)|_{\text{excess}} + S_i(f)|_{\text{shot}}$$
(13.55)

The amplifier contribution to the ideal photocurrent noise is determined by computing the photocurrent spectral density (see Equation 13.22) corresponding to the excess noise in Equation 13.53:

$$S_i(f)|_{\text{excess}} = S_P(f) \times \Re^2_{\text{ideal}}$$
 (13.56)

Integrating the excess and shot noises given by Equations 13.56 and 13.25 over the detection bandwidth  $B_e$  yields the output SNR:

$$SNR_{out} = \frac{\langle GP_s \rangle^2}{S_P(f)B_e + 2 \langle GP_s \rangle hv B_e}$$
 (13.57)

The noise figure is calculated by taking the ratios of Equations 13.54 and 13.57 with  $B_a$  set to 1 Hz:

$$F = \frac{P_s S_P(f) B_e + 2 < GP_s > hv B_e}{2hv < GP_s > 2}$$
(13.58)

Equation 13.58 reduces to:

$$F = \frac{S_P(f)}{2hv G^2 P_s} + \frac{1}{G}$$
 (13.59)

noise figure = excess noise factor + shot-noise factor

This equation is the main result of the electrical noise figure section. This general relation is composed of two parts. One part contains all the excess-noise contributions to the net-noise figure. The second part is the shot-noise contribution. This result is very general since it does not specify or constrain the type of noises that contributes to the amplifier excess noise. It is valid with sig-sp, sp-sp beat noises as well as MPI-induced phase-to-intensity converted noise. The amplifier excess noise,  $S_P(f)$ , is measured according to Equation 13.53,  $P_s$  is determined using a calibrated optical power meter, and the amplifier gain G is measured using the techniques described in Section 13.5.

As a check for Equation 13.59, the limiting form of this expression is found where sig-sp beat and shot noise are the dominant noise processes. Substituting into Equation 13.59 the sig-sp beat noise from Equation 13.27 and applying the conversion indicated in Equation 13.22, the noise figure obtained is:

$$F = \frac{2\rho_{ASE}}{G hv} + \frac{1}{G} \tag{13.60}$$

which is the same relation as defined in Equation 13.35 for the optical method for noise-figure measurement.

Laser Sources with Excess Noise. Any excess noise (in excess of the usual shot noise) from the source illuminating the amplifier under test must be taken into account in order to make an accurate noise characterization of the amplifier. The effect of the source

noise on the accuracy of the electrical method is shown in Figure 13.29. One difficulty with the electrical method is there are not many options available to correct for the excess source noise. If the excess noise from the laser is stable over time, it can be measured and later subtracted from the result obtained when the amplifier is in place.<sup>44</sup> This method will be the focus of the following discussion.

Let the excess source noise be designated by:  $S_p(f)|_{\text{source}}$ . Measurement of the source excess noise is accomplished using the same procedures outlined earlier for characterizing the amplifier excess noise. Any optical attenuation between the source and the receiver should be minimized to obtain the best measurement of the source excess noise. Let T denote the variable optical transmission factor (0 < T < 1) between the source and the amplifier under test. T does not include any losses present when the excess source noise  $S_p(f)|_{\text{source}}$  was measured. T originates from unavoidable optical-coupling losses as well as deliberate optical attenuation provided to control the input signal level  $P_s$  to the amplifier. Taking the transmission factor T into account, effective noise power at the amplifier input terminals is:

$$S_P(f)|_s = T^2 S_P(f)|_{\text{source}}$$
 (13.61)

The noise at the amplifier output is a combination of internally generated noise and the amplified excess noise from the source:

$$S_P(f) = S_P(f)|_{\text{amp}} + G^2 T^2 S_P(f)|_{\text{source}}$$
 (13.62)

The amplifier noise figure is corrected for the excess source noise according to:

$$F = \frac{S_P(f) - G^2 T^2 S_P(f)|_{\text{source}}}{2hv G^2 P_s} + \frac{1}{G}$$
 (13.63)

Alternate Receiver Calibration Method: IM Index Transfer. An alternative method to the RIN transfer technique for calibrating the optical receiver is the IM indextransfer technique. This technique offers calibration at a single frequency or point by point through multiple calibrations. In this method, the modulation index  $m_I$  of a fixed-frequency sinusoidally intensity modulated light is first accurately measured. Let P(t) designate the output intensity versus time of the modulated optical source

$$P(t) = P_{\text{cal}} \left( 1 + \frac{\Delta P}{P_{\text{cal}}} \cos 2\pi f_m t \right)$$
 (13.64)

where  $P_{\rm cal}$  is the average power detected by the optical receiver. By measuring the DC and modulation strength, the intensity modulation index  $m_l$  is obtained at the frequency  $f_m$ .

$$\Delta P(f_m) = \langle P_{\text{cal}} \rangle m_I(f_m) \tag{13.65}$$

The corresponding power spectral density at the frequency  $f_m$  is:

$$S_P(f_m)|_{cal} = m_I^2(f_m) \times P_{cal}^2 \quad [W^2/Hz]$$
 (13.66)

When this source of intensity modulation is applied to the optical receiver, the electrical spectrum analyzer will measure:

$$S_{\text{ESA}}(f_m)|_{\text{cal}} = (\Re k(f_m))^2 S_P(f_m)|_{\text{cal}}$$
 (13.67)

The unknown multiplicative constants are next calculated:

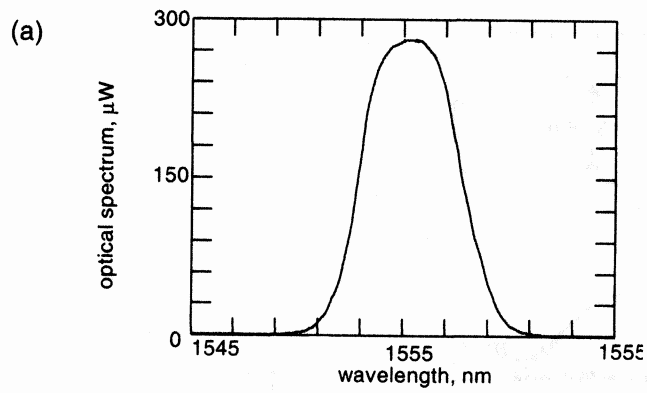
$$[\Re k(f_m)]^2 = \frac{S_{\text{ESA}}(f_m)|_{\text{cal}}}{S_{\Delta P}(f_m)|_{\text{cal}}}$$
(13.68)

With the IM index-transfer method, the optoelectronic detection chain as well as the electrical spectrum analyzer is calibrated for a deterministic modulation. Note that with this method, the electrical noise bandwidth of the receiver is not calibrated. The electrical spectrum analyzer IF filter noise bandwidth must be calibrated separately.

Noise Figure Experiment. Using the RIN-transfer calibration technique, the noise figure of an EDFA was measured at a wavelength of 1550 nm with an amplifier input power of -20 dBm. The experiment setup is similar to that shown in Figure 13.50. With the source attenuator set to 0 dB, the source RIN was approximately -149.2 dB/Hz at a power level of -3.6 dBm. The addition of 16.4 dB of attenuation to bring the input signal level to -20 dBm results in an input RIN of -135 dB/Hz. This RIN level according to Figure 13.29 will have no significant impact on the noise figure measurement, the attenuated source is essentially shot-noise-limited.

In the first step, the transfer function from the optical amplifier to the electrical spectrum analyzer display was calibrated. An optically filtered ASE source with an FWHM spectrum of approximately 2.5 nm served as the RIN transfer standard. The optical spectrum of the transfer standard is shown in Figure 13.53a. The RIN for this source was calculated according to Equation 13.47 yielding a low frequency RIN of -116.18 dB/Hz. The calculated RIN spectrum is shown Figure 13.53b. Across the frequency range of interest, the frequency roll-off of the RIN transfer standard is small, and the noise power it generates dominates over all other noise sources.

The gain of the EDFA was measured with an OSA. The optical spectrums of the input and amplified output signals are shown in Figure 13.54a. The EDFA was equipped with an optical filter with an FWHM of approximately 1.6 nm. This filter served to reduce the sp-sp beat noise contribution to the amplifier noise figure. The EDFA produced 15.05 dB of gain as seen from the figure. The three lower traces in Figure 13.54b correspond to the RIN standard, the EDFA, and the thermal noise powers. The thermal noise,  $S_{\rm ESA}(f)|_{\rm th}$  was subtracted from the EDFA noise  $S_{\rm ESA}(f)|_{\rm mea}$  as indicated by Equation 13.53. A measurement of the average power generated by the RIN-transfer standard along with the calibration noise data,  $S_{\rm ESA}(f)|_{\rm cal}$ , shown in Figure 13.54b, permitted absolute amplitude calibration of the display according to Equation 13.53. The shot-noise correction required measurement of the electrical currents produced by the transfer standard and the amplified signal which resulted in an effective responsivity,  $\Re$ , of 0.428. The shot-noise correction for the coupling loss to the detector was small in this experiment, contributing less than 0.1 dB to the noise figure. Using the values for the gain and excess noise, the noise figure was approximately 7.8 dB as shown in Figure 13.54b.



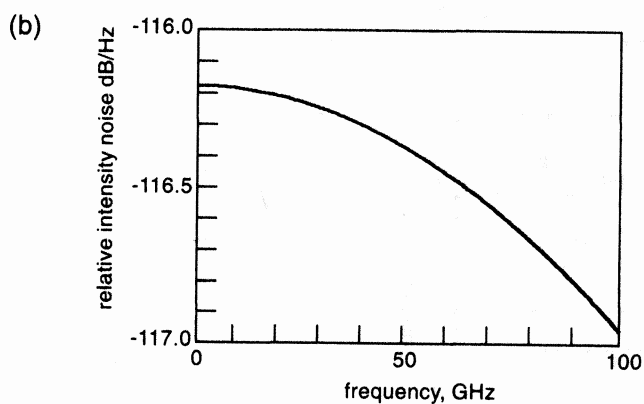


**Figure 13.53** RIN transfer standard spectrums. (a) Measured optical power spectrum. (b) Calculated RIN spectrum.

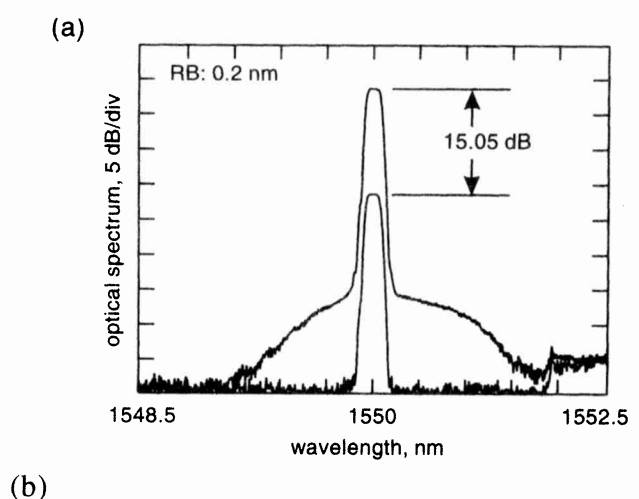
# 13.6 OTHER TYPES OF OPTICAL AMPLIFIERS

# 13.6.1 Rare-Earth Doped Fiber Amplifiers

Amplification at a variety of wavelengths has been demonstrated in rare-earth doped optical fibers. The mechanism for gain is similar to that of the EDFA: excitation of the rare-earth ion with pump light causes population inversion between a pair of energy levels. This produces gain at a wavelength corresponding to the energy difference between the inverted levels. A partial energy diagram for the rare-earths in a LaCl<sub>3</sub> host is shown in Figure 13.55. This diagram is also useful for other glass hosts since the electronic structure of the trivalent ions provides some shielding of the transitions from the host crystalline fields.

1.3  $\mu$ m Amplifiers. When praseodymium ions are doped in a low-phonon energy glass host such as a fluorozirconate fiber, optical gain can be achieved at a number of different wavelengths. Indeed, with this ion, practical demonstrations of amplification or lasing has been achieved from the visible to the infrared. The transition responsible for gain near the important 1.3  $\mu$ m telecom window is designated by 'a' in Figure 13.55. This

Chap. 13



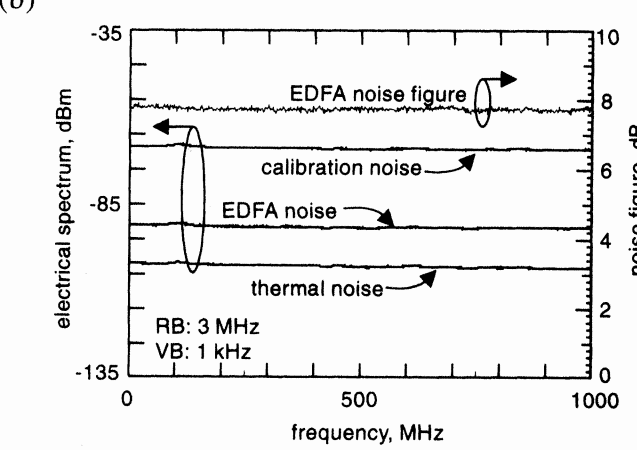
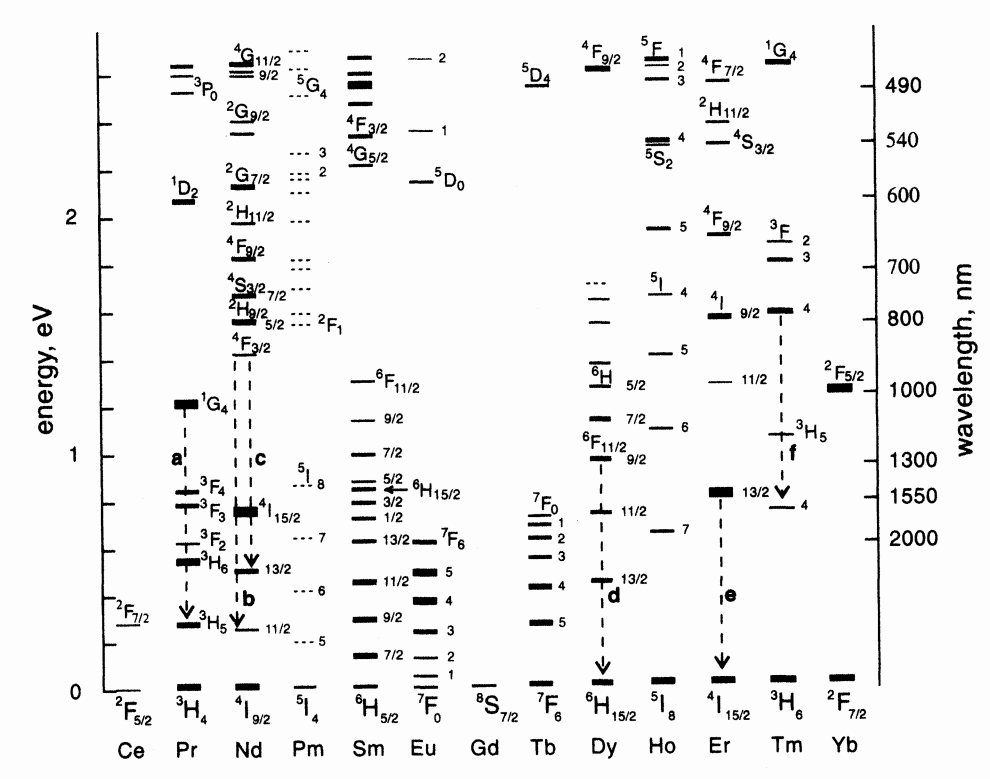


Figure 13.54 Noise figure measurement: (a) optical amplifier gain, (b) electrical spectrum analyzer display and noise figure result.

transition is activated by pumping into the  $^{1}G_{4}$  band near 1  $\mu$ m. The praseodymium-doped fluoride fiber amplifier (PDFFA) has demonstrated optical gains in excess of 40 dB, saturated output powers of 20.1 dBm and a sig-sp beat-noise-limited noise figure as low as 3.2 dB.  $^{50-55}$  The PDFFA has a useful gain spectrum in excess of 30 nm as indicated in Figure 13.56. For communications applications, the problem of making a robust connection between the fluoride fiber and the silica fiber used for transmission has been solved, making commercialization of the PDFFA possible.  $^{55}$  Alternate decay routes from the  $^{1}G_{4}$  level reduces the fluorescent lifetime to  $\sim 110~\mu$ s. This is the reason the PFFDA operates most efficiently with stronger input signals. Weak signals must compete with the short fluorescent lifetime for the stored ion energy. For this reason, the PDFFA is usually used as a booster amplifier.

The trivalent neodymium ion  ${}^4F_{3/2} - {}^4I_{13/2}$  transition provides gain about the 1.32  $\mu$ m wavelength in fluorozirconate fiber. Pumping near the 0.8  $\mu$ m wavelength provides a

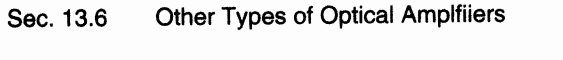


**Figure 13.55** Partial energy level diagram for the trivalent rare earth ions. Some notable transitions: a: 1.31  $\mu$ m, b: 1.06  $\mu$ m, c: 1.34  $\mu$ m, d: 1.32  $\mu$ m, e: 1.53  $\mu$ m, f: 1.47  $\mu$ m. [after ref [15]].

ground-state  ${}^4I_{9/2}$  to  ${}^4F_{5/2}$  absorption which then populates the  ${}^4F_{3/2}$ -level. This transition is designated by 'c' in Figure 13.55. The efficiency of this amplifier is compromised by the strong 1.05  $\mu$ m transition, designated by 'b' in the figure, which depopulates the metastable state population. Also upconversion of signal light to the  ${}^4G_{7/2}$  level further competes with the desired transition.  ${}^{56}$  Practical use of this transition will require suppression of the ASE generated by the large optical gain of the 1.05  $\mu$ m transition.

Research is also being directed at the 1.32  $\mu$ m ( $^6H_{9/2}$   $^{-6}F_{11/2}$ ) doublet to ground state  $^6H_{15/2}$  transition of the dysprosium ion in low-phonon energy glasses. <sup>57,58</sup> This transition is designated by 'd' in Figure 13.55. This transition and the glass host is less mature than either the neodymium or praseodymium investigations in fluoride fiber, more work needs to be performed to fully evaluate its potential.

1.47  $\mu$ m Amplifier. Gain near 1.47  $\mu$ m from the trivalent thulium  ${}^3F_4 - {}^3H_4$  transition (designated by 'f' in Figure 13.55) has a number of applications ranging from transmission line monitoring to the possibility of opening up a new telecommunications band



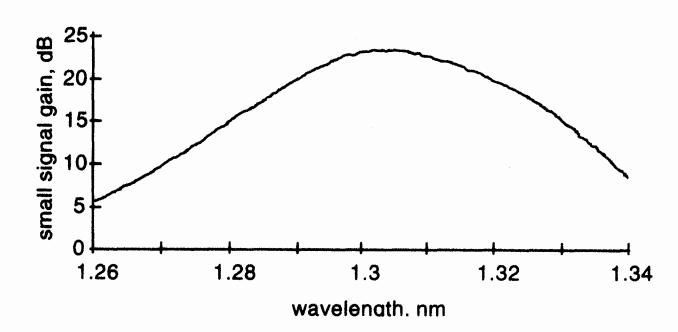


**Figure 13.56** Small-signal gain spectrum for praseodymium-doped fluoride fiber amplifier. [with permission after ref [53] ©1993 BT Technol. J.].

in optical fiber. This transition can be pumped at a wavelength of  $0.78~\mu m$  or  $1.064~\mu m$  using an upconversion pumping scheme. The fluorozirconate glass host with its low-phonon energy has yielded the best performance. In one experiment, shown in Figure 13.57, an amplification bandwidth from 1440 nm to 1505 nm has been demonstrated with a maximum small-signal gain of 25 dB when 450 mW of pump power was applied.<sup>59</sup>

**0.8**  $\mu$ m Amplifier. Thulium-doped fluoride fiber also provides transitions that can be used for 0.8  $\mu$ m amplifiers. Low phonon energy fluoride fiber was used in an experiment that demonstrated 20 dB of gain with a saturated output power in excess of 10 dBm. The optical gain was due to the  ${}^3F_4$  to ground state  ${}^3H_6$  transition shown in Figure 13.55. The  ${}^3F_4$  energy level was populated by pumping at a wavelength of 790 nm. An amplification wavelength range from 795 nm to 820 nm appears to be feasible using this system.

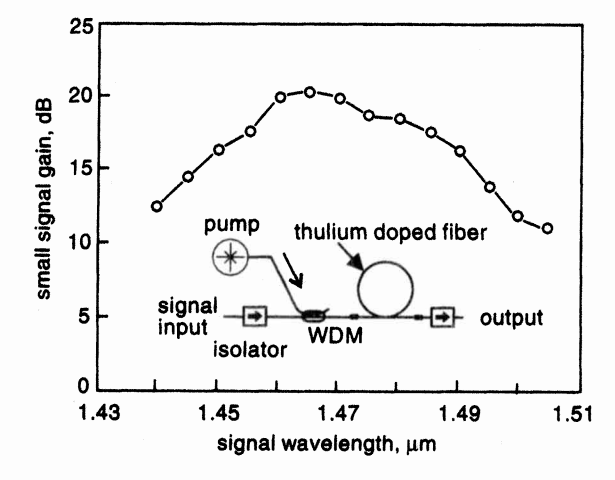


Figure 13.57 Small signal gain spectrum of thulium fluoride fiber amplifier as a function of wavelength [with permission after ref [59] ©1993 IEE].

# 13.6.2 Gain from Fiber Nonlinearities

Raman Amplifier. When pump-light intensity within an optical fiber becomes large, the glass molecules become excited into different vibrational states. In stimulated Raman scattering (SRS), the difference in energy between two vibrational states can be used to amplify an optical signal. This forms the basis for the Raman fiber amplifier (RFA). Unlike the rare-earth doped fiber amplifiers, the RFA doesn't require the addition of special dopants, the optical fiber in the transmission link acts as the gain medium. The RFA is made by coupling pump light into the transmission fiber. At a signal wavelength of 1.55  $\mu$ m, pump powers and fiber lengths are of the order of 1 W and tens of kilometers respectively (see Appendix B). The pump laser and signal frequency separation is equal to the Raman shift frequency which depends on the characteristics of the glass fiber. This shift is approximately -12 THz, or +100 nm at a wavelength of 1.55  $\mu$ m in telecommunications fiber. Therefore to obtain gain in the 1.55  $\mu$ m wavelength band, the wavelength of the pump laser is set to  $\sim 1.45 \mu$ m. An example of an RFA gain spectrum is shown in Figure 13.58. The useable gain bandwidth is approximately 50 nm (6 THz).

Some simple approximate relations are useful for providing insight into the RFA.  $^{62,63}$  Assuming that the stimulated Brillouin scattering and/or pump depletion is small, the amplifier gain for a fiber of length L is given by:

$$G \approx e^{\frac{g_r P_o L_{\text{eff}}}{A_{\text{eff}}} - \alpha_r L} \tag{13.69}$$

where  $P_o$  is the input pump power (watts) and  $L_{\rm eff}$  is the effective length (meters). The Raman efficiency coefficient  $C_r$  is defined by  $C_r = g/KA_{\rm eff}$  where  $g_r$  is the peak Raman gain, K=2 corresponds to nonpolarization maintaining optical fiber and  $A_{\rm eff}$  is the effective core area. 62-64 The Raman gain coefficient,  $C_r$ , depends on wavelength and the type of optical fiber. Increasing the germanium concentration tends to increase  $C_r$ . Measure-

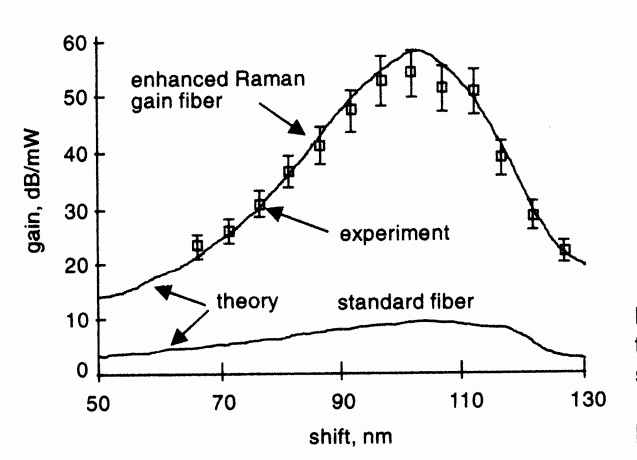


Figure 13.58 Raman gain spectrum for highly doped fiber and standard fiber. Pump wavelength is 1485 nm [with permission after ref [61] ©1990 IEE].

ments of the Raman gain coefficient on different optical fibers in the wavelength range of 1540 nm to 1565 nm yielded a range of values of  $C_r$  from  $1.8 \times 10^{-4}$  to  $6 \times 10^{-4}$  W<sup>-1</sup> m<sup>-1</sup>.<sup>64</sup> The effective length is reduced compared to the physical length due to fiber losses.  $L_{\rm eff}$  is related to the fiber loss at the pump wavelength,  $\alpha_p \, (m^{-1})$  as:<sup>62</sup>

$$L_{\text{eff}} = \frac{1}{\alpha_p} \left[ 1 - e^{-\alpha_p L} \right] \tag{13.70}$$

## Example

Equations 13.69 and 13.70 are illustrated by way of example. The gain and effective length dependence on fiber length are calculated under the following conditions:  $C_r = 5 \times 10^{-4}$  W<sup>-1</sup> m<sup>-1</sup> (nonpolarization maintaining fiber), pump power is 500 mW, and the losses at the pump and signal wavelengths are assumed to be 0.25 dB/km. The exponential loss factor is first calculated using  $\alpha = 0.001 \times \ln(10^{0.25/10})$  m<sup>-1</sup>. The effective length is next calculated using Equation 13.70 which is used in Equation 13.69. The results are plotted as a function of fiber length in Figure 13.59. Figure 13.59a shows the gain/loss for the case of no pumping and also with 500 mW of pump power applied. Figure 13.59b shows the effective length, as

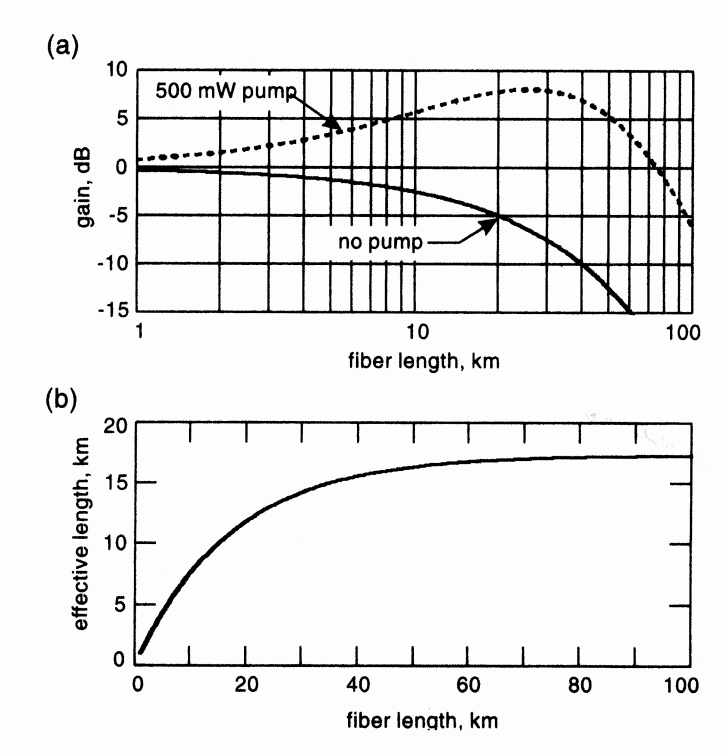


**Figure 13.59** (a) Raman gain dependence on fiber length. (b) Effective fiber length as a function of actual length.

limited by propagation loss, as a function of actual fiber length. For a given pump power there is an optimum fiber length. Beyond the optimum length, the RFA gain decreases.

Stimulated Brillouin Scattering: Brillouin Amplifier. The Brillouin amplifier is based on the acoustic waves (phonons) created when high-intensity light passes through an optical fiber. The optical field causes electrostriction in the fiber which then creates acoustic waves. These acoustic waves scatter light in the backward direction creating optical gain for signals, at the proper frequency, traveling in the opposite direction as the original high intensity light. The gain spectrum is shifted approximately 11 GHz from the pump frequency in silica fiber at 1.55 µm. This is compared to a shift of approximately 6 THz for the Raman effect. The exact shift depends on factors such as the fiber geometry and the residual stress in the glass. The SBS gain spectrum is also quite narrow, on the order of 10 ~ 20 MHz as indicated by the SBS ASE spectrum shown in Figure 13.60. Stimulated Brillouin scattering (SBS) is detrimental in optical links employing narrow linewidth lasers. Even at low power levels, on the order of 1 mW, SBS can create significant backscatter of the forward propagating signal. As a result of the narrow gain bandwidth of the SBS amplifier, it hasn't yet attracted much attention for amplification of telecommunications signals. SBS has received significant attention due to the unwanted optical backscatter it creates.

## 13.6.3 Semiconductor Amplifiers

The semiconductor optical amplifier (SOA) provides a wavelength flexible solution to optical amplification. It offers efficient economical amplification at every telecommunications wavelength and is a contender for 1.3 and 1.55 µm amplification. There are a number of technical obstacles that have limited their deployment in communications applications. This includes: gain-saturation-induced-crosstalk, gain-ripple, polarization-dependent gain, and poor mode-match to optical fiber resulting in excess optical loss and an increase in noise figure. Device structure improvements to improve the SOA along with the utilization of gain clamping techniques to reduce crosstalk are improving their applicability to communications systems. 65,66,67

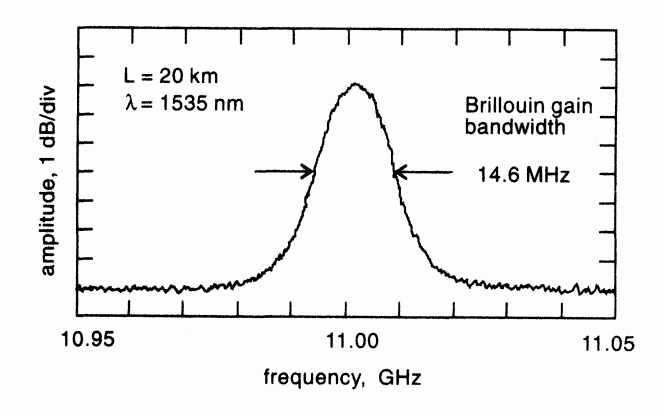


**Figure 13.60** Brillouin gain spectrum for 1.3  $\mu m$  zero dispersion optical fiber.

# 13.6.4 Measurement of Other Types of Optical Amplifiers

In this chapter, optical and electrical methods for noise figure and gain measurement were discussed with an emphasis on their application to the EDFA. Many of these techniques can be applied to the various non EDFA amplifiers discussed. A brief discussion is given here concerning the applicability of the measurement methods to other types of optical amplifiers.

With the optical method, the optical source subtraction technique can be applied, in principle, to any of the amplifiers discussed above. The polarization nulling and time domain extinction methods require certain assumptions on the amplifier polarization dependence and gain recovery time constants which must be considered. The polarization-nulling method works best for amplifiers with polarization-independent gain and low polarization mode dispersion. The TDE method requires instrumentation capable of gating optical signals rapidly compared to the recovery time of the optical amplifier under test. This may prove very challenging in amplifiers with short gain recovery times (< 1 ns) such as the Raman fiber amplifier (RFA).

The electrical noise figure methods, while more complicated, are quite versatile if performed properly. They can be applied to all optical amplifiers. It is beyond the scope of this text to provide an analysis of each technique for each type of optical amplifier. However, as a suggestive guide, Table 13.7 indicates which technique(s) may be most applicable for the most commonly used amplifiers.

# 13.7 SOURCES OF MEASUREMENT ERRORS

The characterization of optical amplifiers can involve a variety of instrumentation with many possible configurations and measurement procedures. This tends to make the analysis of measurement error specific to the particular experimental arrangement at hand. There are, however, common sources of measurement error that contribute to the measurement uncertainty. <sup>68</sup> The major sources of measurement uncertainty with some typical values are listed here:

- Connector uncertainty: ± .25 dB;
- OSA effective optical noise bandwidth: ± 0.1 dB;

**Table 13.7** Guide to Measurement Methods

Amplifier	Source subtraction	Time-domain extinction	Polarization extinction	Electrical method
EDFA	yes	yes	yes	yes
PDFA	yes	yes (need rapid gate)	yes	yes
Raman	yes	no	depends on PMD	yes
Semiconductor	yes	no (unless gain-clamped)	yes	yes

## Sec. 13.6 Other Types of Optical Amplfiliers

- OSA scale fidelity: ± 0.05 dB;
- OSA polarization dependence: ± 0.1 dB;
- Power meter amplitude accuracy: ± 0.1 dB; and
- Amplitude instability due to interferometric effects.

From this list, it is clear that eliminating optical connectors at the amplifier and using fusion splices instead will significantly improve the measurement uncertainty. Most of the other uncertainties are addressed by the instrument specifications. The use of polarization randomizers and measurement averaging can reduce the uncertainty due to polarization dependencies in the test equipment.

# 13.8 USEFUL CONSTANTS FOR EDFA MEASUREMENTS

Table 13.8 includes a list of physical constants that may be useful for optical amplifier noise and gain calculations.

#### 13.9 SUMMARY

In this chapter a variety of measurement techniques were discussed related to amplifier gain and noise figure characterization. The various measurement techniques covered represent a subset, though significant, of the diverse set of methods available for characterization of optical amplifiers.

Some discussion was given to the inner workings of the EDFA to familiarize the reader who is new to this kind of optical amplifier. The discussions on gain and noise in Sections 13.3 and 13.4 provide background information helpful for the discussion on noise figure and measurement techniques. In Section 13.5, the measurement methods for noise figure and gain were grouped into two broad categories: OSA-based, and electrical spectrum analyzer-based. The optical methods included the source subtraction method, the polarization-extinction technique, and the TDE technique. The TDE was extended with the addition of a broadband EELED to permit measurement of the amplifier dynamic gain.

Table 13.8 Useful Physical Constants

Description	Symbol	Value	Units
Electron charge	The state of the s	$1.602 \times 10^{-19}$	coul.
Velocity of light		$2.99793 \times 10^{8}$	ms <sup>-1</sup>
Planck's constant	<b>h</b> :	$6.625 \times 10^{-34}$	J-s <sup>-1</sup>
Boltzmann constant	k k	$1.3806 \times 10^{-23}$	J-K <sup>-1</sup>
1 electron volt	1 eV	$1.602 \times 10^{-19}$	J

Chap, 13

WDM characterization EDFAs was discussed in terms of relevancy of the single-channel techniques previously discussed. An approach was presented to measure the WDM-gain spectrum that uses a reduced set of saturating sources. This technique reduces test costs when large numbers of WDM channels are required.

The electrical technique for noise figure measurement was discussed. This method provides the most complete characterization of the noise performance of an optical amplifier. The electrical method tends to be less tolerant to errors in the measurement technique.

A brief survey of other types of optical amplifiers was given in Section 13.6. This provides a quick appreciation of other existing amplifier technologies. A discussion was also given concerning the relevancy of the measurement methods to these amplifier types. The dominant causes of measurement uncertainty in terms of instrument limitations was outlined in Section 13.7. Finally, the most often used physical constants for noise figure calculations is tabulated in Section 13.8 to save the reader the time required to search this information in texts on physics.

#### REFERENCES

- 1. Nilsson, J., Lee, Y.W., Kim, S.J., Lee, S.H., and Choe, W.H., 1996. Analysis of AC gain tilt in erbium-doped fiber amplifiers. *IEEE Photon. Technol. Lett.* 8 (4):515-517.
- Desurvire, E., Giles, C.R., and Simpson, J.R. 1989. Gain saturation effects in high-speed, multichannel erbium-doped fiber amplifiers at λ=1.53 μm. J. Lightwave Technol. 7 (12):2095-2104.
- 3. Freeman, J. and Conradi, J. 1993. Gain modulation response of erbium-doped fiber amplifiers. *IEEE Photon. Technol. Lett.* 5(2): 224–226.
- 4. Giles, C.R. and Desurvire, E. 1989. Transient gain and crosstalk in erbium-doped fiber amplifiers. Optics Lett. 14:880-882.
- 5. Taylor, M.G. 1993. Observation of new polarization dependence effect in long haul optically amplified system. *IEEE Photon. Technol. Lett.* 5 (10):1244–1246.
- 6. Gimlett, J.L., Iqbal, M.Z., Curtis, L., Cheung, N.K., Righetti, A., Fontana, F., Grasso, G. 1989. Impact of multiple reflection noise in Gbit/s lightwave systems with optical fiber amplifiers. *Electron. Lett.* 25 (20):1393-1394.
- 7. Kobayashi, M., Ishihara, T., and Gotoh, M. 1993. Power penalty due to optical reflections in erbium-doped fiber preamplifier. *IEEE Photon. Technol. Lett.* 5 (8):925-928.
- 8. Snitzer, E. 1961. Optical maser action of Nd3+ in a barium crown glass. *Phys Rev. Lett.* 7: 444-449.
- 9. Koester, C.J., Snitzer, E.A. 1964. Amplification in a fiber laser. Applied Optics 3 (10):1182.
- Mears, R.J. et al. 1986. Low threshold, tunable cw and Q-switched fibre laser operating at 1.55 μm. Electron. Lett. 22 (3):159.
- 11. Mears, R. J., Reekie, L. Jauncey, I.M., and Payne, D.N. 1987. High gain rare-earth doped fiber amplifier at 1.54 μm. in Conference on Optical Fiber Communication/International Conference on Integrated Optics and Optical Fiber Communication Technical Digest Series 1987, Vol. 3, (Optical Society of America, Washington, DC 1987):167.
- 12. Delavaux, J-M, P., and Nagel, J.A. 1995. Multi-stage erbium-doped fiber amplifier designs. J. Lightwave Technol. 13 (5):703-720.

- 13. Hill, K.O., Malo, B., Bilodeau, F., Johnson, D.C., and Albert, J. 1993. Bragg gratings fabricated in monomode photosensitive optical fiber by UV exposure through a phase mask. *Appl. Phys. Lett.* 62 (10):1035–1037.
- 14. Ainslie, B.J. 1991. A review of the fabrication and properties of erbium-doped fibers for optical amplifiers. J. Lightwave Technol. 9 (2):220-227.
- 15. Dieke, G.H., and Crosswhite, H.M. 1963. The spectra of the doubly and triply ionized rare-earths. *Applied Optics*, 2 (7):675–686.
- 16. Optical fibre lasers and amplifiers, 1996. Edited by P.W. France. Blackie & CRC Press Inc.
- 17. Desurvire, E. Erbium Doped Fiber Amplifiers, Principles and Applications, John Wiley & Sons, Inc. 1994.
- 18. Ainslie, B.J., Craig, S.P., and Davey, S.T. 1988. The absorption and fluorescence spectra of rare-earth ions in silica-based monomode fiber. *J. Lightwave Technol.* 6 (2):287–293.
- 19. Miniscalco, W.J. 1991. Erbium-doped glasses for fiber amplifiers at 1500 nm. J. Lightwave Technol. 9 (2):234-250.
- 20. Horiguichi, M., Shimizu, M., Yamada, M., Yoshino, K., Hanafusa, H. 1990. Highly efficient optical fibre amplifier pumped by a 0.8 μm band laser diode. *Electron. Lett.* 26 (21):1758–1759.
- 21. Horiguichi, M., Yoshino, M., Shimizu, M., and Yamada, M. 1993. 670 nm semiconductor laser diode pumped erbium-doped fiber amplifers. *Electron. Lett.* 29 (7):593–595.
- 22. Giles, C.R. and Desurvire, E. 1991. Modeling erbium-doped fiber amplifers. J. Lightwave Technol. 9 (2):271-283.
- 23. Clesca, B., Bayart, D., and Beylat, J.L. 1995. 1.5 µm fluoride-based fiber amplifiers for wide-band multichannel transport networks. *Optical Fiber Techn.* 1:135–157.
- 24. Ono, H., Nakagawa, K., Yamada, M., and Sudo, S. 1996. Er3+-doped fluorophosphate glass fibre amplifier for WDM systems. *Electron. Lett.* 32 (17):1586-1587.
- Mori, A., Ohishi, Y., Yamada, M., Ono, H., Nishida, Y., Oikawa, K., and Sudo, S. 1997. 1.5
  μm broadband amplification by tellurite-based EDFAs. In Optical Fiber Communication Conference, Vol. 6, 1997 OSA Technical Digest Series vol. 6 (Optical Society of America, Washington, D.C.), PD1.
- 26. Agrawal, G.P. 1995. Non linear fiber optics. 2nd ed. San Diego, CA: Academic Press.
- 27. Mazurczyk, V.J., and Zyskind, J.L. 1994. Polarization dependent gain in erbium doped-fiber amplifiers. *IEEE Photon. Technol. Lett.* 6 (5):616-618.
- 28. Taylor, M.G. and Penticost, S.J., 1994. Improvement in performance of long haul EDFA link using high frequency polarization scrambling modulation. *Electron. Lett.* 30 (10): 805–806.
- 29. Bergano, N.S., Davidson, C.R., and Heismann, F. 1996. Bit-synchronous polarization and phase modulation scheme for improving the performance of optical amplifier transmission systems. *Electron. Lett.* 32 (1):52-54.
- 30. Desurvire, E., Zyskind, J.L., and Simpson, J.R. 1990. Spectral gain hole-burning at 1.53 μm in erbium-doped fiber amplifiers. *IEEE Photon. Technol. Lett.* 2 (4):246–248.
- 31. Walker, G.R. 1991. Gain and noise characterisation of erbium-doped fiber amplifiers. *Electron. Lett.* 27 (9):744–745.
- 32. Srivastava, A.K., Zyskind, J.L., Sulhoff, J.W., Evankow, J.D. Jr., and Mills, M.A. 1996. Room temperature spectral hole-burning in erbium-doped fiber amplifiers. In *OFC'96 Technical Di*-

References

- gest, Optical Fiber Communication Conference, Technical Digest Series Vol. 2 (Optical Society of America, Washington, DC, 1996):33-34.
- 33. Hansen, S.L., Andreasen, S.B., Thorsen, P., and Dybdal, K. 1993. Experimental verification of new EDFA gain-tilt distortion theory. *IEEE Photon. Technol. Lett.* 5 (12):1433-1435.
- 34. Olsson, N.A. 1989. Lightwave systems with optical amplifers. J. Lightwave Technol. 7 (7):1071-1082.
- 35. Baney, D.M. and Sorin, W.V. 1995. Broadband frequency characterization of optical receivers using intensity noise. *Hewlett-Packard J.* 46(1):6–12.
- 36. Bonnedal, D. 1993. Single-setup characterization of optical fiber amplifiers. *IEEE Photon. Technol. Lett.* 5 (10):1193-1195.
- 37. Chou, H. and Stimple, J. 1995. Inhomogeneous gain saturation of erbium-doped fiber amplifiers. In *Optical Amplifiers and their Applications*, Technical Digest Series Vol. 8 (Optical Society of America, Washington, DC, 1995):92–95.
- 38. Poole, S. 1994. Noise figure measurement in optical fibre amplifiers. In NIST Technical Digest—Symposium on optical fiber measurements, Boulder, CO. NIST special publication 864: 1-6.
- 39. Baney, D.M., and Dupre, J. 1992. Pulsed-source technique for optical amplifier noise figure measurement. European Conference on Communications. Paper WeP2.11. Berlin.
- 40. Bertilsson, K., Andrekson, P.A., and Olsson, B.E. 1994. Noise figure of erbium-doped fiber amplifiers in the saturated regime. *IEEE Photon. Technol. Lett.* 6(10):199-201.
- 41. Onaka, H., Miyata, H., Ishikawa, G., Otsuka, K., Ooi, H., Kai, Y., Kinoshita, S., Seino, M., Nishimoto, H., and Chikama, T. 1996. 1.1 Tb/s WDM transmission over a 150 km 1.3 μm zero-dispersion singlemode fiber. In *Optical Fiber Communication Conference*, Technical Digest Series Vol. 2 (Washington, DC: *Optical Society of America*, 1996) PD 19.
- 42. Baney, D.M. and Stimple, J. 1996. WDM EDFA gain characterization with a reduced set of saturating channels. *IEEE Photon. Technol. Lett.* 8(12):1615-1617.
- 43. Baney, D.M. and Jungerman, R.L. 1997. Optical Noise Standard for the Electrical Method of Optical Amplifier Noise Figure Measurement" in Optical Amplifiers and Their Applications, Technical Digest Series Vol. 2 (Optical Society of America: Washington, DC) paper MB3.
- 44. Willems, F.W., van der Plaats, Hentschel, D., and Leckel, E. 1994. Optical amplifier noise figure determination by signal RIN subtraction. In NIST Technical Digest—Symposium on optical fiber measurements, Boulder, CO: NIST Special publication 864:7-9.
- 45. Smart, R.G., Hanna, D.C., Tropper, A.C., Davey, S.T., Carter, S.F., and Szebesta, D. 1991. CW room temperature upconversion lasing at blue, green and red wavelengths in infrared-pumped Pr<sup>3+</sup>-doped fluoride fibre. *Electron. Lett.* 27:1307-1309.
- 46. Piehler, D., Craven, D., Kwong, N.K., and Zarem, H. 1993. Laser-diode-pumped red and green upconversion fibre lasers. *Electron. Lett.* 29:1857-1858.
- 47. Baney, D.M., Rankin, G., and Chang, K.W. 1996. Simultaneous blue and green upconversion lasing in a laser-diode-pumped Pr<sup>3+</sup>/Yb3+doped fluoride fiber laser. *Appl. Phys. Lett.* 69(12):1662-1664.
- 48. Baney, D.M., Rankin, G., and Chang, K.W. 1996. Blue Pr<sup>3+</sup>-doped ZBLAN fiber upconversion laser. *Optics Lett.* 21(17):1372-1374.
- 49. Petreski, B.P., Murphy, M.M., Collins, S.F., and Booth, D.J. 1993. Amplification in Pr<sup>3+</sup>-doped fluorozirconate optical fibre at 632.8 μm. *Electron. Lett.* 29:1421-1423.
- 50. Durteste, Y., Monerie, M., Allain, J.Y., Poignant, H. 1991. Amplification and lasing at 1.3 μm in praseodymium-doped fluorozirconate fibres. *Electron. Lett.* 27(8):626–628.

- 51. Miyajima, Y., Sugawa, T., and Fukasaku, Y. 1991. 38.2 dB amplification at 1.31 μm and possibility of 0.98 μm pumping in Pr<sup>3+</sup>–doped fluoride fibre. *Electron. Lett.* 27(19):626–628.
- 52. Miyajima, Y., Sugawa, T., Fukasaku, Y. 1992. Noise characteristics of Pr<sup>3+</sup>-doped fluoride fibre amplifier. *Electron. Lett.* 28(3):246-247.
- 53. Whitley, T.J., Wyatt, R., Szebesta, D., and Davey, S.T. 1993. Towards a practical 1.3 μm optical fibre amplifier. *BT Technol. J.* 11(2):115–127.
- 54. Yamada, M. et al. 1995. Low-noise and high-power PR<sup>3+</sup>-doped fluoride fiber amplifier. *IEEE Photon. Technol. Lett.* 7(8):868–871.
- 55. Dye, S., Fake, M., and Simmons, T.J. 1994. Practical praseodymium power amplifier with a saturated output power of +18 dBm, in Conference on *Optical Fiber Communications, Technical Digest Series*, Vol. 4 (Optical Society of America, Washington DC, 1994):200.
- 56. Payne, A.S., Wilke, G.D., Smith, L.K., and Krupke, F. 1994. Auger upconversion losses in Nd-doped laser glasses. *Optics. Comm.* 111:263-268.
- 57. Page, R., Schaffers, K.I., Wilke, G.D., Waide, P., A., Tassano, J.B., Beach, R.J., Payne, S.A., and Krupke, W.F. 1996. Observation of 1300 nm gain in dysprosium-doped chloride crystals in *Optical Fiber Communication Conference, Technical Digest Series*, Vol. 2 (Optical Society of America, Washington DC, 1996).
- 58. Samson, B.N., Medeiros, J.A., Neto, R.I., Laming, R.I., and Hewak, D.W. 1994. Dyprosium doped Ga:La:S glass for a efficient optical fibre amplifier operating at 1.3 μm. *Electron. Lett.* 30(19):1617–1619.
- 59. Komukai, T., Yamamoto, T., Sugawa, T., and Miyajima, Y. 1993. 1.47 μm band Tm<sup>3+</sup> doped fluoride fibre amplifier using a 1.064 μm upconversion pumping scheme. *Electron. Lett.* 29(1):110–112.
- 60. Dye, S.P., Fake, M., and Simmons, T.J. 1995. Fully engineered 800 nm thulium-doped fluoride-fiber amplifier. In *Optical Fiber Communications, Technical Digest Series*, Vol. 8 (Optical Society of America, Washington DC, 1995):110.
- 61. Spirit, D.M., Blank, L.C., Davey, S.T., and Williams, D.L. 1990. System apects of Raman fibre amplifiers. *IEE Proc.* 137, Pt. J. (4):221–224.
- 62. Stolen, R.H. and Ippen, E.P. 1973. Raman gain in glass optical waveguides. *Appl. Phys. Lett.* 22(6):276–278.
- 63. Aoki, Y. 1988. Properties of fiber Raman amplifiers and their applicability to digital optical communications systems. *J. Lightwave Technol.* 6(7):1225–1239.
- 64. da Silva, V.L. 1994. Comparison of Raman efficiencies in optical fibers. In *Conference on Optical Fiber Communications, Technical Digest Series,* Vol. 4 (Optical Society of America, Washington, DC, 1994):136–137.
- 65. Tiemeijer, L.F., Thijs, P.J.A., and Binsma, J.J.M. 1994. Progress in 1.3 μm polarization insensitive multiple quantum well laser amplifiers. In *Optical Fiber Communications, Technical Digest Series*, Vol. 17 (Optical Society of America, Washington, DC, 1994):234–236.
- 66. Doussiere, P. 1996. Recent advances in conventional and gain clamped semiconductor optical amplifiers. In *Optical Fiber Communications, Technical Digest Series,* Vol. 19 (Optical Society of America, Washington DC, 1994):220–223.
- 67. Koren, U., Miller, B.I., Young, M.G., Chien, M., Raybon, G., Brenner, T., Ben-Michael, R., Dreyer, K., and Capik, R.J. 1996. Polarization insensitive semiconductor optical amplifier with integrated electroabsorption modulators. *Electron. Lett.* 32(2):111–112.
- 68. Leckel, E., Sang, J., Muller, R., Ruck, C., and Hentschel, C. 1995. Erbium-doped fiber amplifier test system. *Hewlett-Packard J.* 46(1):13–19.